UNIVERSITÀ DEGLI STUDI DI PADOVA

DIPARTIMENTO DI ASTRONOMIA

DOTTORATO DI RICERCA IN ASTRONOMIA
CICLO XVIII

SINEO:

SPECTROSCOPIC INVESTIGATION OF NEAR EARTH OBJECTS

Coordinatore:
prof. GIAMPAOLO PIOTTO
Supervisori:
dott. MONICA LAZZARIN
Dipartimento di Astronomia, Università di Padova
Ch.mo prof. CESARE BARBIERI
Dipartimento di Astronomia, Università di Padova
Ch.mo prof. SERGIO ORTOLANI
Dipartimento di Astronomia, Università di Padova

Dottorando: SARA MAGRIN

2 Gennaio 2006

PADOVA UNIVERSITY

ASTRONOMY DEPARTMENT

PhD in ASTRONOMY
CYCLE XVIII

SINEO:

SPECTROSCOPIC INVESTIGATION OF NEAR EARTH OBJECTS

PhD Coordinator:
prof. GIAMPAOLO PIOTTO
Supervisors:
dr. MONICA LAZZARIN
Astronomy Department, Padova University
prof. CESARE BARBIERI
Astronomy Department, Padova University
prof. SERGIO ORTOLANI
Astronomy Department, Padova University

External Supervisor:
dr. MARIO DI MARTINO
Torino Astronomical Observatory

PhD Student: SARA MAGRIN

January 2nd, 2006

Contents

List of Figures

List of Tables

Riassunto

In questo lavoro di tesi descrivo il progetto SINEO (*Spectroscopic Investigation of Near Earth Objects* - Studio Spettroscopico di Near Earth Objects), discuto tutti i risultati ottenuti finora e presento i lavori attualmente in svolgimento e i progetti futuri. SINEO è una campagna di osservazioni spettroscopiche di asteroidi *Near Earth* (vicini alla Terra) nel visibile e nel vicino infrarosso (attorno a 0.40-2.50 μm) iniziata nel 2000 dal nostro gruppo di ricerca a Padova.

Gli oggetti *Near Earth* (NEO) rappresentano una delle più peculiari ed eterogenee popolazioni del Sistema Solare. Solo negli ultimi anni, inoltre, è stata seriamente presa in considerazione la possibilità di un impatto sulla Terra da parte di un NEO.

Questi oggetti sono per definizione asteroidi e nuclei di comete aventi orbite con perielio q$<$1.3 UA. Essi avvicinano o intersecano l'orbita della Terra e si ritiene orbitino nelle stesse traiettorie che portano le meteoriti a cadere su di essa. Se un asteroide di circa un chilometro di diametro collidesse con il nostro pianeta porrebbe a serio rischio la vita sulla Terra. La ricerca di NEO e lo studio dettagliato delle loro principali proprietà risultano quindi essenziali anche per lo sviluppo di strategie di difesa efficienti.

L'importanza dello studio dei NEO è stata riconosciuta a livello internazionale e una grande mole di risorse è stata utilizzata a riguardo. Molti programmi spaziali (ad esempio NEAR e DS1) sono state indirizzate allo studio di NEO, atterrando anche su uno di essi, e molti altri sono previsti. Anche il nostro gruppo di ricerca è coinvolto in questi progetti. Le sonde spaziali, però, possono essere dedicate solo allo studio di un numero molto limitato di oggetti. Un quadro generale della popolazione NEO e uno studio delle loro proprietà generali e delle loro differenze possono essere ottenuti solo compiendo osservazioni da terra di un gran numero di essi.

I dati disponibili finora indicano che i NEO mostrano una natura molto differen-

ziata: sono presenti oggetti con forme molto varie, sistemi binari, oggetti con una complessa rotazione (*tumbling asteroids*) e altri con periodi di rotazione particolarmente lunghi, difficilmente spiegabili dagli attuali modelli dinamici e collisionali. La differenziazione dei NEO è anche evidenziata dai differenti tipi tassonomici presenti nella popolazione (Lazzarin et al. 2004; Lazzarin et al. 2005; Binzel et al. 2002).

Un altro interessante argomento è la possibile relazione tra i NEO e le meteoriti, in particolare le Condriti Ordinarie (OC), che sono ritenute avere una composizione molto simile a quella del disco protoplanetario, avendo subito minime evoluzioni termiche nell'arco della vita del Sistema Solare (Binzel et al. 1996; Lazzarin et al. 1997; Binzel et al. 2001; Binzel et al. 2002; Lazzarin et al. 2004; Lazzarin et al. 2005).

L'origine dei NEO è ancora dibattuta. Sappiamo che i NEO presenti oggi hanno tempi di vita tipicamente attorno a 10-100 milioni di anni (molto minore dell'età del Sistema Solare) e che in questi tempi scala essi possono essere espulsi dal Sistema Solare oppure possono collidere con il Sole o con un pianeta. Lo studio della craterizzazione della Luna, poi, sembra indicare che il numero di NEO sia stata praticamente costante negli ultimi 2 miliardi di anni. Questo implica che la loro popolazione deve continuamente essere rifornita di oggetti da altre sorgenti. La prima è la *Fascia Principale* di asteroidi, dove le perturbazioni gravitazionali dei pianeti giganti producono risonanze dinamiche che fungono da vere e proprie vie di fuga per gli oggetti al loro interno. La seconda è rappresentata dalle comete estinte (oggetti originariamente provenienti dalla Fascia di Kuiper e dalla Nube di Oort). Un esempio di questo è dato dall'asteroide 4015 che corrisponde alla cometa Wilson-Harrington. Non sono ancora del tutto chiare le efficienze dei vari meccanismi che potrebbero condurre questi oggetti nella zona dei NEO come non è conosciuta perfettamente la percentuale di NEO che può aver avuto origine dall'una o dall'altra sorgente.

Un modo di avere informazioni su questi ed altri argomenti è di caratterizzare i NEO spettroscopicamente, per studiare la loro mineralogia e per poterli classificare tassonomicamente. Data la loro differenziazione risulta necessario condurre un'ampia campagna osservativa, per essere in grado di campionare il maggior numero possibile di NEO.

In questo contesto abbiamo iniziato una osservazione sistematica di Near Earth Objects: "SINEO". Negli ultimi cinque anni ci sono state assegnate complessiva-

mente 28 notti al telescopio ESO-NTT (*New Technology Telescope*, La Silla, Cile) e al TNG (*Telescopio Nazionale Galileo*, Isole Canarie) in otto periodi osservativi. Abbiamo ottenuto un totale di 117 spettri di asteroidi, di cui 63 sia nel visibile che nel vicino infrarosso (Lazzarin et al. 2004; Lazzarin et al. 2005).

Abbiamo classificato tassonomicamente questi oggetti per mezzo di un confronto con i tipi spettrali medi definiti da Bus (1999) sugli spettri osservati dal progetto SMASSII. Un secondo metodo applicato allo scopo è stata l'Analisi delle Componenti Principali (*Principal Component Analysis*, PCA), con la quale abbiamo ottenuto quasi tutte le classi spettrali individuate nella fascia principale. Entrambi questi metodi utilizzano la parte visibile dello spettro. I dati nel vicino infrarosso, quando disponibili, si sono rivelati essenziali per discriminare tra sottoclassi aventi simili caratteristiche nel visibile.

In particolare abbiamo classificato degli oggetti peculiari. Abbiamo osservato quattro tipi V e un tipo R (raro nella Fascia Principale e, se confermato, unico tra in NEO) e abbiamo avanzato delle ipotesi preliminari su un loro possibile legame genetico con dei corpi "genitori" come Vesta e Dembowska, rispettivamente (Marchi et al. 2004; Marchi et al. 2005). Abbiamo anche osservato due oggetti le cui orbite suggeriscono un'origine cometaria. I loro spettri mostrano una composizione primitiva consistente con un'origine di questo tipo (Lazzarin et al. 2005). In tutti questi casi la spettroscopia è in grado di dare suggerimenti importanti alla dinamica.

Per capire meglio la mineralogia degli asteroidi abbiamo effettuato un confronto con le meteoriti. Abbiamo selezionato una serie di più di 800 spettri di meteoriti dal catalogo RELAB, disponibile in rete. Per ogni oggetto SINEO abbiamo cercato il miglior analogo meteorico, trovando nella maggior parte dei casi una buon soluzione. In alcuni casi, comunque, in particolare nel caso di asteroidi di tipo S particolarmente rossi, non è stato possibile trovare alcun analogo. Questo dato può in parte essere spiegato considerando gli effetti di invecchiamento subiti dalle superfici asteroidali esposte all'ambiente spaziale (*space weathering*).

Abbiamo quindi cominciato ad approfondire lo studio di questo effetto innanzi tutto analizzando le pendenze degli spettri di meteoriti, di NEO e di oggetti appartenenti alla Fascia Principale. Abbiamo iniziato una collaborazione con il prof. Strazzulla e il dott. Brunetto (Osservatorio di Catania) che hanno effettuato esperimenti in laboratorio di bombardamento ionico di condriti ordinarie. Questo esperimento è in grado di simulare gli effetti dello *space weathering* dovuto al vento solare. Attraverso il confronto degli spettri dei NEO di tipo S da noi osservati con gli spettri di laboratorio abbiamo ottenuto importanti suggerimenti sull'efficienza di questo

effetto di invecchiamento su diversi composti (Marchi et al. 2005).

Con il prof. Paolicchi (Università di Pisa) e il prof. Morbidelli (Osservatorio di Nizza) abbiamo confrontato le età degli oggetti dedotta dallo *space weathering* con quella calcolata dalla dinamica (età collisionali). Abbiamo iniziato ad esaminare possibili implicazioni sull'evoluzione degli asteroidi, trovando una relazione generale e unica, valida sia per i NEO che per gli oggetti della Fascia Principale (Marchi et al. 2006).

Tutti i risultati ottenuti finora ci hanno spinto ad approfondire ulteriori aspetti degli argomenti analizzati. In particolare stiamo collaborando ora con il dott. Nesvorný (SwRI, Boulder, Colorado), la dott. Moroz (DLR, Berlino), il dott. Folco (Università di Siena) e nuovamente con l'Osservatorio di Catania.

Assieme al dott. Nesvorný ci stiamo concentrando sullo studio della distribuzione in funzione del perielio di NEO e Mars Crosser di tipo S che mostrino o meno segni di invecchiamento superficiale. I primi risultati mostrano che il numero di oggetti di tipo Q (con superficie più giovane) rispetto al numero di oggetti dell'intero complesso S cresce al diminuire del perielio: la popolazione di NEO sembra, in media, più giovane all'aumentare del numero di intersezioni dell'orbita con le orbite dei pianeti interni. Questo ci ha portato a studiare la possibililità di un effetto di ringiovanimento superficiale degli asteroidi dovuto ad avvicinamenti più o meno stretti con i pianeti interni. Sono comunque necessari ulteriori studi sugli effetti mareali necessari per un processo di questo tipo.

Il dott. Folco ci ha aiutato a selezionare dal Museo Nazionale dell'Antartide (Siena) una lista di campioni meteorici appartenenti alle condriti carbonacee (CC), alle enstatiti (EC), alle acondriti (AC) e meteoriti ferrose. Il dott. Brunetto sta ora eseguendo esperimenti di bombardamento ionico su questi campioni.

Con la dott. Moroz stiamo analizzando la possibilità di effetti di *space weathering* visibili anche su composti primitivi, su asteroidi del complesso C e del complesso X.

Il nostro gruppo sta inoltre acquisendo abilità nell'analisi di spettri meteorici e asteroidali attraverso il *Modified Gaussian Model* (MGM). Questo metodo è in grado di decomporre gli spettri in due contributi: continuo e bande di assorbimento. Il suo utilizzo dovrebbe aiutarci a comprendere meglio sia la composizione superficiale che il grado di *space weathering* dei corpi osservati.

Abstract

In this thesis I describe the SINEO (*Spectroscopic Investigation of Near Earth Objects*) project and I discuss all ongoing results and future works. SINEO is a spectroscopic survey of Near Earth Asteroids (NEOs) in the visible and near infrared (about 0.40-2.50 μm) started in 2000 by our group in Padova.

Near-Earth Objects (NEOs) represent one of the most peculiar and heterogeneous population of the Solar System. It is only in recent years that the threat to Earth from Near Earth Objects (NEOs) has been recognised.

These objects, by definition asteroids and comet nuclei on orbits with perihelion distances q$<$1.3 AU, periodically approach or intersect the orbit of the Earth and are believed to be on the same dynamical routes which deliver meteorites to the Earth. Moreover, because impact of a km-sized asteroid with our planet poses a significant risk to life on Earth the exploration of NEOs is particularly important. In fact, to be able to develop effective strategies requires detailed knowledge of the gross properties, structure and composition of these objects.

The importance of studying NEOs has been recognised worldwide, and a great deal of resources are being used for this task; several space programs (e.g. NEAR and DS1) have targeted NEOs landing also on one of them and other missions are in program to investigate NEOs. Our group is also involved in these studies. However, space probes can, by necessity, only visit a very limited number of objects. So if we want a picture of the whole NEO population, to study their global properties and their diversity, we must observe NEOs from ground-based observatories.

Available data indicate that NEOs population is very diverse in nature (objects with unusual shapes, binary systems, objects with a complex, non–principal axis rotation state (*tumbling* asteroids), some others with very long rotational periods, which are not easily explained by the current dynamical and collisional models, etc.). NEO diversity is also reflected by the different taxonomic types present in the population (Lazzarin et al. 2004; Lazzarin et al. 2005; Binzel et al. 2002).

Another interesting issue is the relationship between NEO and meteorites, in particular the Ordinary Chondrites (OC), that are thought to represent samples of the primitive solar nebula that have undergone modest thermal evolution over the age of the Solar System (Binzel et al. 1996; Lazzarin et al. 1997; Binzel et al. 2001; Binzel et al. 2002; Lazzarin et al. 2004; Lazzarin et al. 2005).

The question of NEO origin is also not well understood. We know that the present NEOs have typical life-times of 10-100 My (much shorter than the age of the Solar System), and that over these time scales NEOs are ejected from the Solar System or collide with the Sun or a planet. Because the cratering record on the Moon suggests a fairly constant NEO population during past 2 billion years, new NEOs must be continuously supplied by some sources in order to maintain the present steady state. The principal one is the Main Belt, where gravitational perturbations by the major planets cause dynamical resonances which provide escape routes. The second source is represented by extinct comets (objects coming from the Kuiper Belt and the Oort Cloud). An example is the asteroid Apollo 4015 which was the comet Wilson Harrington in 1949. It is not clear, however, what the efficiency of the delivery mechanisms is, and what percentage of the NEOs we observe today comes from the one or from the other source. One way of addressing many issues related to NEOs is to characterise them spectroscopically in order to derive their mineralogy and to classify them taxonomically. Owing to their heterogeneity it is evident the importance to carry on a large survey in order to investigate the physical properties of an as large as possible sample of NEOs.

In this contest we started a spectroscopic survey of Near Earth Objects (SINEO) and my thesis describe all analysis done till now, ongoing projects and future works we are going to carry on.

In the last five years observational time was allocated both at ESO-NTT (*New Technology Telescope*, La Silla, Chile) and at TNG (*Telescopio Nazionale Galileo*, Canary Islands) in eight observing runs. We have obtained until now a total of 117 asteroid spectra of which 63 have both visible and NIR range (Lazzarin et al. 2004; Lazzarin et al. 2005).

We performed a first taxonomic classification for most of them, principally by means of a best fit with mean taxonomic types defined by Bus (1999) on SMASSII spectra and through the *Principal Component Analysis* (PCA), obtaining all the classes defined by main belt asteroids. Both these methods refer to the visible part of the spectra. Where available near infrared data have revealed essential to dis-

criminate between subclasses with similar visible features.

In particular we classified some peculiar objects. We observed four V-type and an R-type, rare in the Main Belt and even more rare in the NEO space, and we gave some preliminary hypothesis on their possible genetic link with Vesta and Dembowska, respectively (Marchi et al. 2004; Marchi et al. 2005). We also observed two bodies whose orbits suggest a cometary origin. Their spectra showed a primitive composition also consistent with that origin (Lazzarin et al. 2005). These are cases where spectroscopy can give important hints on dynamics.

To better understand asteroids mineralogy we compared them with meteorites. So we selected a set of more than 800 meteorite spectra from the RELAB catalogue and we performed a best fit for every SINEO object observed finding in many cases good agreements. However in some cases, in particular on reddish S-type asteroids, we could not find any meteorite analogue. This can be in part explained considering the *space weathering* effect.

We therefore started a deep study of this effect principally by analysing the spectral slope of meteorites, NEOs and Main Belt Objects. We started a collaboration with Prof. Strazzulla and Dr. Brunetto (Observatory of Catania) who made laboratory experiments of ion bombardment on Ordinary Chondrites, able to simulate the effect of space weathering due to solar wind. Through the comparison of our S-type NEOs' spectra with laboratory ones we obtained important hints on space weathering time scale on different compounds (Marchi et al. 2005).

With Prof. Paolicchi (Pisa University) and Prof. Morbidelli (Nice Observatory) we also started to examine possible implication on asteroid history, mainly by comparing age deduced from space weathering with age deduced by dynamics (computed from asteroid collisional lifetime) and finding a unique general relationship valid both for NEOs and MBOs (Marchi et al. 2006).

All results obtained till now led us to deepen some other aspects of the topics studied. In particular we are now collaborating with Dr. Nesvorný (SwRI, Boulder, Colorado), with Dr. Moroz (DLR, Berlin), with Dr. Folco (Siena University) and again with Observatory of Catania.

With Dr. Nesvorný we are concentrating on the distribution of weathered and non weathered S-type NEOs and Mars Crossers as a function of their perihelion distance. First results showed that the fraction of Q-type (fresh surface) above the whole S-complex increases as perihelion become shorter: the NEO population looks younger, in average, as the number of intersection with inner planets orbit

increases. This led us to study the efficiency of a possible resurfacing effect due to close and/or very close encounters of asteroids with one or more inner planet. A more quantitative assessment of the (tidal) effect of a close encounter to remove the space weathered surface layers of a typical km-sized asteroid is required.

Dr. Folco helped us to select from the "Museo Nazionale dell'Antartide" a list of meteorite samples comprising some Carbocaneous Chondrites (CC), Enstatite Chondrites (EC), Achondrites (AC) and Iron meteorite. Dr. Brunetto is now applying laboratory experiments of ion bombardment on these samples. With Dr. Moroz, we are working on the analysis of possible optical effect of space weathering on primitive compounds, on C-complex and on X-complex Near Earth and Main Belt asteroids.

We are also acquiring abilities in analysing meteorite and asteroid spectra through the Modified Gaussian Model (MGM). The method is in principle able to decompose spectra in continuum part plus absorption bands so that it can help us to better understand mineralogy, surface composition and space weathering degree of minor bodies observed.

Introduction

In this thesis I will describe the SINEO (*Spectroscopic Investigation of Near Earth Objects*) project and I will discuss all ongoing results and future works. SINEO is a spectroscopic survey of Near Earth Asteroids (NEOs) in the visible and near infrared started in 2000 by our group in Padova.

Near-Earth Objects (NEOs) represent one of the most peculiar and heterogeneous population of the Solar System. These objects, by definition composed by asteroids and comet nuclei on orbits with perihelion distances q$<$1.3 AU, periodically approach or intersect the orbit of the Earth and are believed to be on the same dynamical routes which deliver meteorites to the Earth.

The importance of studying NEOs has been recognised worldwide, and a great deal of resources are being used for this task; several space programs (i.e. NEAR and DS1) have targeted NEOs landing also on one of them, but other missions are in program to investigate NEOs. Our group is also involved in these studies. However, space probes can, by necessity, only visit a very limited number of objects. If we want a picture of the whole NEO population, to study their global properties and their diversity, we must observe NEOs from ground-based observatories. Available data indicate that NEOs population is very diverse in nature (they can be objects with unusual shapes, or in binary systems, or sometimes with a complex, non–principal axis rotation state (*tumbling* asteroids), some others with very long rotational periods, which are not easily explained by the current dynamical and collisional models, ...). NEO diversity is also reflected by the different taxonomic types present in the population (Lazzarin et al. (2004); Lazzarin et al. (2005); Binzel et al. (2002); see also chapter 2 and 4 in this thesis).

Another interesting issue is the relationship between NEO and meteorites, in particular the Ordinary Chondrites (OC), that are thought to represent samples of the primitive solar nebula that have undergone modest thermal evolution over the age of the Solar System (Binzel et al. 1996; Lazzarin et al. 1997; Binzel et al. 2001;

Binzel et al. 2002; Lazzarin et al. 2004; Lazzarin et al. 2005).

The question of NEOs origin is also not well understood. We know that the present NEOs have typical life-times of 10-100 My (much shorter than the age of the Solar System), and that over these time scales NEOs can fall into the Sun, or collide with inner planets or the Moon, or they can be scattered in a hyperbolic orbit and escape from Solar System. Because the cratering record on the Moon suggests a fairly constant NEO population during past 2 billion years, new NEOs must be continuously supplied by some sources in order to maintain the present steady state.

The principal one (maybe for about 80% of NEOs) is the Main Belt, where gravitational perturbations by the major planets cause dynamical resonances (both mean motion and secular resonances) which provide escape routes. The second source (probably for less than 20% NEOs) is represented by extinct comets (objects coming from the Kuiper Belt and the Oort Cloud). An example is the Apollo NEO 4015 which was the comet Wilson Harrington in 1949. It is not clear, however, what the efficiency of the delivery mechanisms is, and what percentage of the NEOs we observe today comes from the one or from the other source (about the NEO-comets relations and probabilities see for example Weissman et al. (2002); Wetherill (1988); Rabinowitz (1997); Cochran & Barker (1984)). One way of addressing many issues related to NEOs is to characterise these objects spectroscopically. These objects are usually faint, so the use of medium to large-sized telescopes is necessary.

In this contest in 2000 we started a spectroscopic survey of Near Earth Objects in visible and near infrared (NIR) wavelengths. Our observations were performed at European Southern Observatory with New Technology Telescope (ESO-NTT) at La Silla, Chile and at Telescopio Nazionale Galileo (TNG) in Canary Islands in the spectral range of about 0.40-2.50 μm. In chapter 3 all our observations are described in detail.

We have obtained until now a total of 117 asteroid spectra of which 63 have both visible and NIR range. The observed objects were almost all unclassified and the classification of the reduced data has been performed by means of Principal Component Analysis (PCA), a best fit with Bus' mean taxonomic types (Bus 1999) and a comparison with Tholen taxonomy definitions (Tholen (1984) and followings). The infrared data have revealed essential for the taxonomic classification since in some cases (for example in some higher noise spectra) different classes can share similar features in the visible but different characteristics at longer wavelengths. With NEOs we have obtained almost all the taxonomic classes and with PCA we

obtained that our data distribute in the same cluster defined by SMASSII data (Bus 1999).

An interesting result obtained from the survey is the classification of some peculiar objects. In particular we have obtained the spectra of four V-type objects very similar to Vesta, the spectrum of a NEO probably belonging to the rare R-class and two objects of primitive composition that could be, according to their orbital elements, of cometary origin.

We have also performed a comparison with meteorites (a set of more than 800 spectra) finding interesting results from the comparison with the OC and other meteorites. From the analysis of the NIR we got also indications about the effects of space weathering on NEOs' spectra.

We have also recently started other analysis connected with NEOs dynamics and the space weathering process (i.e. the alteration of optical properties of asteroid surfaces due to space environment). For the dynamics we started a new collaboration with Nice Observatory and Pisa University (prof. Morbidelli and prof. Paolicchi; see Marchi et al. (2006)); while together with the Observatory of Catania we are studying the space weathering with new dedicated experiments (prof. Strazzulla and coll., see Marchi et al. (2005)). Both approaches are providing new important results, but more data are needed. In particular, regarding space weathering, it is now evident the importance of investigating small objects, which generally means younger bodies: they are too faint to be observed in the Main Belt, but more easily detectable in the Near Earth space. For this reason NEO spectroscopic investigation provides a unique possibility of studying such physical processes.

Chapter 1

Solar System Minor Planets

Physical evidences relating to the period of first 200 million years of the Solar System history are not preserved on Earth nor on other planets because of the geologic processes that took place in these large bodies: investigation of the oldest terrestrial and lunar rocks provide information on the early planetary evolution of these objects, but a substantial part of the earliest evolutionary period has been erased by erosion, metamorphism and remelting.

Asteroids and meteorites are well-preserved samples from the first post-accretionally period of the Solar System, being residual rocky inner planetesimals or fragments of the bodies accreted from that population.

Plausible models describe the general nature of the major stages of the Solar System formation. A major purpose of meteorite and asteroid studies is to provide the physical database to check and constrain such models.

1.1 The discovery of first asteroids

Johann Daniel Titius in 1766 noted a regularity in the spacings between planets. The sequence of the distances from the Sun of the seven known planets could fit with a geometric progression, published by Johann Elert Bode in 1772. The modern formulation of the *Titius-Bode* law is:

$$r_n = 0.4 + 0.3 \cdot 2^n \tag{1.1}$$

where r_n is the distance (in astronomical units) of the n^{th} planet, once we identify Mercury with $n = -\infty$, Venus with $n = 0$, the Earth with $n = 1$, Mars with $n = 2$, Jupiter with $n = 4$ and Saturn with $n = 5$, skipping the $n = 3$ value.

This regularity in planetary location was considered to be an important primary feature of the Solar System, especially after the discovery, made by Sir William Herschel in 1781, of the planet Uranus at a solar distance close to the solution obtainable with $n = 6$. With this the hunt for the "missing planet" ($n = 3$) began.

In 1801, the abbot Giuseppe Piazzi discovered the small body *Ceres*, at just the right distance. In 1802 Heinrich Olbers discovered another body, *Pallas*, at the same orbital distance. They both were too small to be classified like planets, but the gap was finally filled. [1]

At that epoch only comets were known to be small objects with an independent orbit about the Sun, but their main characteristic is to appear like diffuse objects. In 1802, Herschel coined for these new objects the word *asteroid* (from Greek *asteroeides*) that means "star-like", to underline their different appearance (they were unresolved point sources) from the aspect of comets (which show extended comas when present in the warmer inner Solar System).

In following years other asteroids were discovered at about the same solar distance. With the number of these new findings the hypothesis that they could be fragments of an exploded planet grew. This idea became very popular and remained so for a long time. In the middle of the 20^{th} century Otto Johannes Schmidt proposed that asteroids represented an arrested stage of planet formation and have never been assembled into a large body. This is now the most accredited hypothesis.

1.2 General Properties of Minor Planets

Since now more than 285 000 asteroids are known at different distances from the Sun. Most of them have orbits between Mars and Jupiter and form what is called the *Main Belt* (from about 2.0 to about 3.3AU).

Many other groups of asteroids are present at different distances from the Sun. In Tab. 1.1 the dynamical definitions of the main asteroid groups and families are summarised.

In the following we will describe the principal characteristics of most important ones. Their definitions are often related to the resonance with Jupiter and with Neptune, while other groups (i.e. *Near Earth Objects* and *Mars Crossers*) definitions refer to the intersection of their orbits with the orbit of a planet (in this case Earth

[1] Neptune (discovered in Johann Galle in 1846) and Pluto (discovered by Clyde Tombaugh in 1930) do not fit the law very well. In fact, Pluto fits the spot where Neptune should be.

or Mars respectively).

1.2.1 Resonances

Figure 1.1 shows the distribution of known asteroids as a function of the semi-major axis (in the range between 1 and 6 *AU*).

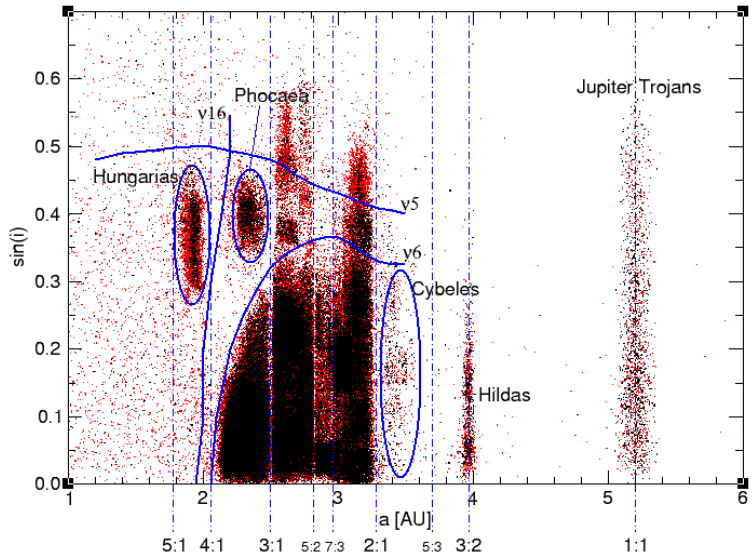

Figure 1.1: Distribution of asteroids (sine of the inclination *vs.* semi-major axis), from 1 to 6 *AU*. Data reported comes from *The Asteroid Orbital Elements Database*, updated 2005/07/18 (*Dr. Edward Bowell - Lowell Observatory*). Resonances reported (both *mean* and *secular*) are related to Jupiter's orbit. Secular resonances are also a function of eccentricity. Curves plotted here refer to $e = 0.05$ (Gaffey et al. 1993).

The general structure of the asteroid distribution is related to orbital resonances with a major planet. These resonances are mainly divided in two major classes: *mean motion* and *secular* resonances, but other exist.

Mean Motion resonances: Mean motion resonances take place at solar distances where the orbital periods are some small integer fraction of a planet period. This occur mainly with Jupiter's one, especially in the inner solar system. In the asteroid Main Belt many of these resonances are present. They are also called *Kirkwood Gaps*, in honour of Daniel Kirkwood who first recognised them in 1874. In the outer solar system mean motion resonances are mainly related with Neptune orbit (see Tab. 1.1 for further details).

Secular resonances: *Secular* resonances are due to relations between the asteroid and the major planet frequencies of precessions and to relations between asteroid and planet frequencies of variation of eccentricity and inclination. In Fig. 1.1 there are reported the three major secular resonances (ν_5, ν_6 and ν_{16}, see Williams & Faulkner (1981)). They refer to Jupiter and Saturn and define some important asteroid boundaries.

Diffusive resonances: In addition to the few wide mean motion resonances with Jupiter described above, the main belt is also crisscrossed by hundreds of thin resonances: high-order mean motion resonances with Jupiter (where the orbital frequencies are in a ratio of large integer numbers), three-body resonances with Jupiter and Saturn (where an integer combination of the orbital frequencies of the asteroid, Jupiter, and Saturn is equal to zero) and mean motion resonances with Mars. The typical width of each of these resonances is of the order of a few $10^{-4} - 10^{-3} AU$. Because of these resonances many main belt asteroids are chaotic. The effect of this chaoticity is very weak, with an asteroid eccentricity and inclination slowly changing over time. The time required to reach a planet-crossing orbit (Mars-crossing in the inner belt, Jupiter-crossing in the outer belt) ranges from several 10^7 years to billions of years, depending on the resonances and the starting eccentricity.

Since asteroids in resonant positions experience close encounters with a major planet more often than the other asteroids in random location, they feel the attraction of this planet powerful gravity more frequently. Therefore resonances provide potential escape route for most of the flux of asteroids and meteorites. In Fig. 1.1 shows that the main belt population is split in different groups by ν_6 resonance besides mean motion resonances; therefore, for example, Hungaria and Phocaea groups are well defined among ν_{16}, ν_5 and ν_6 secular resonance and 5:1, 4:1, 3:1 mean motion resonance.

Wetherill (1985), Wetherill (1987) and Wetherill (1988) have argued that the terrestrial meteorite flux and *NEA* population will contain contribution mainly from objects near the 3:1 resonance and then from objects near the ν_6 resonance.

1.2.2 The Yarkovsky Effect

The Yarkovsky effect is a force felt by a body caused by the anisotropic emission of thermal photons, which carry momentum. It is usually considered in relation to

meteoroids or small asteroids (about 10 cm to 10 km in diameter), as its influence is most significant for these bodies.

The effect was discovered by Ivan Osipovich Yarkovsky (1844-1902). Yarkovsky noted that the diurnal heating of a rotating object in space would cause a small force on the object that could lead to large long-term effects in its orbits. This would affect especially meteoroids and small asteroids. Yarkovsky's idea was then recalled by Ernst J. Öpik (1893-1985) who discussed the possible importance of the Yarkovsky effect for moving meteoroids about the solar system (1951).

The Yarkovsky effect is a consequence of the thermal inertia (time needed for the surface to warm up or cool down). In general there are two components to the effect:

Diurnal effect. On a rotating body (e.g. an asteroid) illuminated by the Sun, as on the Earth, the surface is warmer in the afternoon and early night, than in the morning and late night. The result is that more heat is radiated on the evening side than the morning side, leading to a net force due to radiation pressure in the direction opposite to "evening" one. For prograde rotators, this is in the direction of motion on their orbit, and causes their semi-major axis to steadily increase, spiraling away from the Sun. Retrograde rotators spiral inward (see fig. 1.2 left panel).

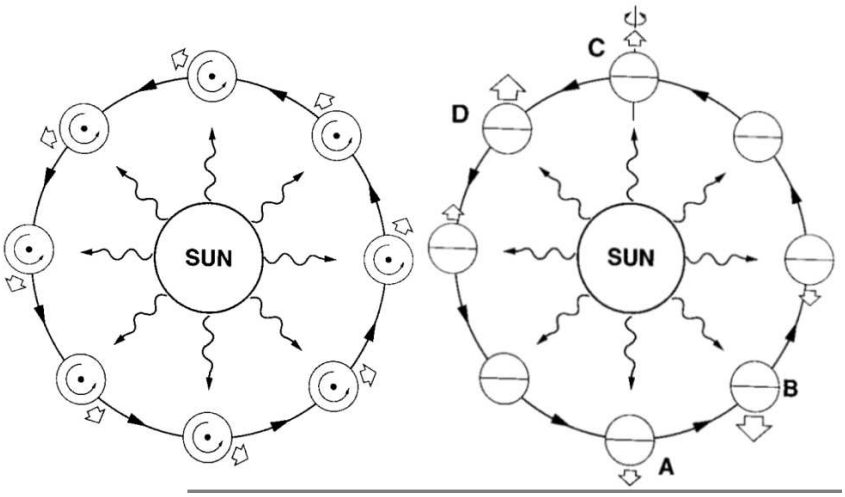

Figure 1.2: The Yarkovsky effect: diurnal (left panel) and seasonal (right panel).

Seasonal effect. This is easiest to understand for non-rotating bodies orbiting the Sun, for which each year consists of exactly one day. As it travels around its orbit, the evening hemisphere which has been heated over a long preceding time period is in the direction of orbital motion. The excess of thermal radiation in this direction causes a braking force which always causes spiraling inward toward the Sun (see fig. 1.2 right panel).

For rotating bodies, this seasonal effect increases with the axial tilt. It dominates only if the diurnal effect is small enough. This may occur because of:

- very fast rotation (no time to cool off on the night side, hence an almost uniform longitudinal temperature distribution);
- small size (the whole body is heated throughout) or
- an axial tilt close to 90.

The seasonal effect is more important for smaller asteroid fragments (from a few metres up to about 100 m), provided their surfaces are not covered by an insulating regolith layer and they do not have exceedingly slow rotations. Additionally, on very long timescales over which the spin axis of the body may be repeatedly changed due to collisions (and hence also the direction of the diurnal effect changes), the seasonal effect will also tend to dominate.

The above details can become more complicated for bodies in strongly eccentric orbits.

The effect was first measured in 1991-2003 on the asteroid (6489) Golevka. The asteroid drifted 15 km from its predicted position over 12 years (the orbit was established with great precision by a series of radar observations in 1991, 1995 and 1999).

In general, the effect is size dependent, and will affect the semi-major axis of smaller asteroids, while leaving large asteroids practically unaffected. For kilometre-sized asteroids the Yarkovsky effect is very small over short periods: (6489) Golevka is estimated to be subjected to a force of about 0.25 *Newton*, for a net acceleration of $10^{-10} m/s^2$. But it is steady so that over millions of years an asteroid's orbit can be perturbed enough to transport it from the main belt to the inner solar system.

For a specific asteroid, it is very hard to predict the exact impact of the Yarkovsky effect on its orbit. This is because its magnitude depends on many variables that are hard to determine from the limited observational information that is available. These include the exact shape of the asteroid, its orientation, and its albedo, along

with its variations over the surface and with wavelength. Calculations are further complicated by the effects of shadowing and thermal "reillumination", whether caused by local craters or a possible overall concave shape. The Yarkovsky effect also competes with radiation pressure whose net effect may cause similar small long-term forces for bodies with albedo variations and/or non-spherical shapes.

As an example, even for the simple case of the pure seasonal Yarkovsky effect on a spherical body in a circular orbit with 90 obliquity, semi-major axis changes could differ by as much as a factor of two between the case of a uniform albedo and the case of a strong north/south albedo asymmetry. Depending on the orbit and spin axis, the Yarkovsky semi-major axis change may be reversed simply by changing from a spherical to a non-spherical shape.

The YORP Effect The Yarkovsky-O'Keefe-Radzievskii-Paddack effect, or YORP effect for short, is a second-order variation on the Yarkovsky effect which causes a small body (such as an asteroid) to spin up or down. The term was coined by Dr. David P. Rubincam in 2000.

Imagine a rotating spherical asteroid with two wedges attached to its equator. The reaction force from photons departing from any given surface element of the sphere will be normal to the surface, such that no torque is produced. Energy reradiated from the wedges, however, can produce a torque because the wedge faces are not parallel to the sphere's surface. An object with some asymmetry can therefore be subjected to small torque forces that will tend to spin it up or down as well as make its axis of rotation precess. Note that the YORP effect is zero for a rotating ellipsoid.

In the long term, the object's changing obliquity and rotation rate may wander randomly, chaotically or regularly, depending on many factors.

Observations show that asteroids larger than 125 km have rotation rates that follow a Maxwellian frequency distribution, while smaller asteroids (in the 50 to 125 km size range) show a small excess of fast rotators. The smallest asteroids (size less than 50 km) show a clear excess of very fast and slow rotators, and this becomes even more pronounced as smaller populations are measured. These results suggest that one or more size-dependent mechanisms are depopulating the centre of the spin rate distribution in favour of the extremes. The YORP effect is a prime candidate. It is not capable of significantly modifying the spin rates of large asteroids by itself, however, so a different explanation must be thought for large asteroids.

1.2.3 Minor Planet distribution and dynamical classification

In this paragraph we will expose asteroid classification into groups and families. This classification is also summarised in Tab. 1.1.

Minor planets are divided into groups and families based on their orbital characteristics. It is common use to name a group of asteroids after the first member of that group to be discovered (generally the largest). *Groups* are relatively loose dynamical associations, whereas *families* are tighter and result most probably from the catastrophic breakup of a large parent asteroid sometime in the past. They were first recognised by Kiyotsugu Hirayama in 1918 and are often called Hirayama families in his honour.

To better understand what reported in the following we recall here the analytic definition of *aphelion* and *perihelion* of an orbit:

$$\begin{cases} Q = a(1+e) & \textit{aphelion} \\ q = a(1-e) & \textit{perihelion} \end{cases} \tag{1.2}$$

where a and e are respectively the semi-major axis and the eccentricity of the orbit.

Near Earth Objects

Here we list just few characteristics of this minor planet group. In the following there will be a more complete description of the dynamical and physical characteristics of these objects.

Near Earth Objects (in the following *NEOs*) are asteroids (*NEAs*) and comets (*NECs*) moving in orbits whose perihelion is smaller than Mars': $q < 1.3\,AU$.

According to the relation between their orbit and the Earth one they are catalogued in different sub-groups: *Atens* and *Apollos* are Earth Crossers while *Amors* approach the Earth but never intersect its orbit. Atens have a semi-major axis smaller than the Earth one ($a < 1\,AU$) while Apollos have $a > 1\,AU$.

There is also one another class of Near Earth Objects: the *Inner Earth Objects* or *Interior to the Earth Orbits* (*IEOs*). They are asteroids with an orbit completely inside the Earth one (asteroid aphelion is smaller than Earth perihelion). The *Jet Propulsion Laboratory* considers this as a separate class and enumerates four asteroids (see Tab. 1.2). The *Minor Planet Center* classified them as *Aten*.

Up to now (August 2005) there are 3443 NEAs (288 Atens, 1673 Apollos, 1482 Amors) and 74 NECs known.

population	a	q	Q	comments
NEAs				
IEOs	< 1		< 0.983	
Atens	< 1		$\geqq 0.983$	Earth crossers
Apollos	> 1	$\leqq 1.017$		Earth crossers
Amors	> 1	$]1.017, 1.3[$		
Mars Crossers		$[1.3, 1.666]$		

population	a	e	i	resonances
Hungarias	$[1.78, 2.06]$	< 0.18	$[16, 34]$	$[5:1, 4:1]$
MBAs	$[2.06, 3.28]$			$[4:1, 2:1]$
Inner MB	$[2.06, 2.50]$			$[4:1, 3:1]$
Phocaeas	$[2.25, 2.50]$	> 0.1	$[18, 32]$	
Middle MB	$[2.50, 2.82]$			$[3:1, 5:2]$
Outer MB	$[2.82, 3.28]$			$[5:2, 2:1]$
Koronis	$[2.82, 2.94]$	< 0.12	< 3.5	$[5:2, 7:3]$
Eos	$[2.99, 3.05]$	< 0.13	$[8, 12]$	$[7:3, 9:4]$
Themis	$[3.05, 3.22]$	< 0.22	< 3	$[9:4, 2:1]$
Cybeles	$[3.28, 3.70]$	< 0.3	< 25	$[2:1, 5:3]$
Hildas	~ 3.97	> 0.07	< 20	$3:2$
Jupiter Trojans	~ 5.20			$1:1$
Centaurs	$[5.4, 30]$			
Neptune Trojans	~ 30			1 : 1 Nep
TNOs (or KBOs)	> 32			
	~ 35			4 : 5 Nep
	~ 39			2 : 3 Nep
	~ 42			3 : 5 Nep
	~ 48			1 : 2 Nep

Table 1.1: List and definition of main groups and families of asteroids. Semi-major axis, perihelion and aphelion are expressed in *AU*, inclination is in degrees. Where not specified mean resonances refer to Jupiter orbit. In last five cases, as reported, they refer to Neptune.

Mars Crossers

Mars Crossers are objects that cross Mars orbit (bodies whose perihelions are included between Mars perihelion and aphelion).

Object	*a*	*e*	*i*	*q*	*Q*	*P*	*H*
1998 DK36	0.69	0.416	2.0	0.404	0.98	0.58	25.01
2003 CP20	0.74	0.322	25.6	0.502	0.98	0.64	16.41
2004 JG6	0.64	0.532	18.9	0.298	0.97	0.51	18.96
2004 XZ130	0.62	0.455	3.0	0.337	0.90	0.49	20.12

Table 1.2: This table provides J2000 heliocentric ecliptic orbital elements for the 4 known IEOs (*Interior Earth Object*) sorted by object number/name. The semi-major axis *a*, the perihelion *q* and the aphelion *Q* are expressed in *AU*, the inclination *i* is in degrees. *e* is the eccentricity of the orbit, *P* is the orbital period in Julian years and *H* is the absolute V-magnitude. Updated August 2005.

In this group we list also 6 asteroids once thought to be *Mars Trojans*[2]. The lists of Trojans are extracted by the *Minor Planet Center* (MPC) using cuts in osculating element space. This technique works very well for Jupiter and Neptune Trojans, but it has been known to be problematic for Martian Trojans. The list of Martian Trojans is then removed from the MPC web site with the intention to list only those that are confirmed (by long-term integration of good orbits) to be Trojans. At this time this list is not available yet.

It has been shown that the population of asteroids on Mars-crossing orbits, which is roughly four times the size of the NEO population, is predominately re-supplied by diffusive resonances in the main belt (Migliorini et al. 1998; Morbidelli & Nesvorny 1999; Michel et al. 2000; Bottke et al. 2002). This region is called the "intermediate-source Mars-crossing region", or IMC for short. The IMC is bracketed by the main belt, the NEA population, the ν_6 resonance and $2.0 < a < 2.8AU$, while they are split in two sub-population ("inner" and "outer" regions) by the 3:1 mean motion resonance gap (see next paragraph for further details).

IMC asteroids can escape the main belt via mean-motion resonances with Mars, three-body mean-motion resonances (i.e. Jupiter-Saturn-asteroid) and the ν_6 resonance.

Main Belt Asteroids

Asteroids are located mostly between the orbits of Mars and Jupiter. Figure 1.1 shows the distribution of known asteroids in the $a, \sin(i)$ space (semimajor axis versus sine of the inclination). The strong concentration of asteroids are located

[2]For more information on *Trojan asteroid* definition see paragraph at page 24 about *Jupiter and Neptune Trojans*

between 2.0 and 3.3 *AU* (between 4:1 and 2:1 mean motion resonances): this is the *Main Asteroid Belt*.

Jupiter's gravitational influence, through orbital resonance, clears Kirkwood gaps in the asteroid belt. As a result of these gaps the asteroids in this region are divided into a large number of groups, sub-groups and families. Here we describe only the larger.

Hungaria asteroids have a semimajor axis between 1.78 AU and 2.06 AU, an eccentricity less than 0.18, and inclination between 16° and 34°. Named after 434 Hungaria, these are just outside Mars orbit, and are possibly attracted by the 2:9 resonance.

Inner Main Belt asteroids have a semimajor axis between 2.06 AU and 2.50 AU. These bound are defined by the 4:1 and the 3:1 mean motion resonances. Inside this group: *Phocaea* asteroids have a semimajor axis between 2.25 AU and 2.50 AU, an eccentricity greater than 0.1, and inclination between 18° and 32°. Named after 25 Phocaea.

Middle Main Belt asteroids have a semimajor axis between 2.50 AU and 2.82 AU. These bound are defined by the 3:1 and the 5:2 mean motion resonances.

Outer Main Belt asteroids have a semimajor axis between 2.82 AU and 3.28 AU. These bound are defined by the 5:2 and the 2:1 mean motion resonances. Inside the group: *Koronis*, *Eos* and *Themis* are families, each derived from a common ancestor object, 158 Koronis, 221 Eos and 24 Themis, respectively.

Cybele asteroids have a mean orbital radius between 3.28 AU and 3.70 AU, an eccentricity less than 0.3, and an inclination less than 25°. This group appears to cluster around the 4:7 resonance with Jupiter. Named after 65 Cybele.

Hilda asteroids have a mean orbital radius between 3.7 AU and 4.2 AU, an eccentricity greater than 0.07, and an inclination less than 20°. These asteroids are in a 3:2 resonance with Jupiter. Named after 153 Hilda.

Asteroid *families* are an important additional aspect of the main belt. They are dynamical associations which origin as fragments of a collision af a parent body. When family members have compositions which are consistent with a common origin these associations are called *Genetic Families*. The study of these genetic families provide constraints on collisional disruption of large bodies, on the collisional lifetime of asteroids as function of size and on the internal composition of their parent bodies.

Jupiter and Neptune Trojans

Another very interesting class of bodies are those lying around the $L4$ and $L5$ lagrangian points of a planet, i.e. placed 60 deg ahead and behind the planet, on the same orbit. About Jupiter these regions were called the Greek and Trojan nodes respectively; objects in each node are named for members of that side of the conflict (actually there are some misplacements: 617 Patroclus is in the Trojan node and 624 Hektor is in the Greek one). Altogether they are now called "Jupiter Trojans".

Although the existence of trojan-like asteroids is not a dynamical prerogative of Jupiter (every single planet of the Solar System could have sable zones around their $L4$ and $L5$ lagrangian points), for a long time no other planets were observed to have objects like these.

Finally in 1990 the first Mars Trojan was found, (5261) Eureka (from the greek, meaning: "I have found it"). Other five asteroids were found and thought to be Mars trojans. As reported in previous paragraph they are now considered as simple Mars Crossers, since the orbit solutions and perturbations on them still have to be studied in detail. However in 2001 the first Neptune Trojan was also found 2001 QR322 and since then other 3 Neptune trojans were found, so that at present searches for trojans of other planets are in progress. Our group was also involved with these searches.

Jupiter Family Comets

Comets are usually categorised into two groups: the long period comets and short period comets.

The short period comets have orbital periods < 20 years and low inclination. They also have $2 < T_J < 3$, being T_J the *Tisserand Invariant*:

$$T_J = \frac{a_J}{a} + 2\cos(i)\left[\frac{a}{a_J}(1-e^2)\right]^{1/2} \tag{1.3}$$

where a and a_J are the object and Jupiter orbit semimajor axis respectively and e is the orbit eccentricity of the object.

Since their orbits are controlled by Jupiter they are also called Jupiter Family comets (JFCs). The short period comets are believed to originate from the Kuiper Belt, the large reservoir of small icy bodies just beyond Neptune. These Kuiper Belt objects also have very low inclinations. From collisions or gravitational perturbations some Kuiper Belt objects escape the Kuiper Belt and fall towards the

Sun. Because the orbit crosses that of Jupiter, the comet may have gravitational interactions with it. The orbital evolution of Jupiter-family comets (JFCs) under the gravitational influence of planets can lead these objects to get typical asteroid orbits. JFCs can get NEO orbits more often than typical asteroid orbits.

The probability of a collision of one of such objects, which move for millions of years inside Jupiter's orbit, with a terrestrial planet can be greater than analogous total probability for thousands other objects. The obtained results show that during the accumulation of the giant planets the total mass of icy bodies delivered to the Earth could be about the mass of water in Earth's oceans.

Centaurs

The Centaurs are bodies orbiting between Jupiter and Neptune (i.e. $5.4 \leq a \leq 30$), but with not yet a clear definition from a dynamical point of view. Dynamical studies of their orbits indicate that centaurs are probably an intermediate orbital state of objects transitioning from the Kuiper Belt to the Jupiter Family comets. Objects may be perturbed from the Kuiper Belt so that they become Neptune-crossing and interact gravitationally with that planet. They then become centaurs, but their orbits are chaotic, evolving relatively rapidly (lifetimes of the order of 10^7 yr) as the centaur makes repeated close approaches to one or more of the outer planets. Some centaurs will evolve into Jupiter-crossing orbits and then their perihelia may become reduced into the inner solar system. They are probably much closer to comets than asteroids, and one of these (Chiron) has shown a little cometary activity.

Trans Neptunian Objects

Objects with $a \geq 30$ (more than 900 objects, up to now) are broadly defined as Trans-Neptunian Objects (TNOs) which are divided dynamically in the following groups.

Kuiper Belt Objects: include objects between 41 and 47 AU, having nearly circular orbits and low inclinations. The outer boundary of the Kuiper belt is not defined arbitrarily: there appears to be a real and fairly sharp drop in objects beyond a certain distance.

Plutinos objects are in (3:2) resonance with Neptune, just like Pluto. They have a semi-major axis of about 39.4 AU, eccentricities up to 0.34 and high inclination.

A few objects are trapped in (2:1) and (5:3) resonances, and just one (2000 CQ104) in (4:3) resonance.

Cubewanos are Kuiper belt object, orbiting beyond about 41 AU and not controlled by resonances with the outer planets. The odd name is derived from the first trans-Neptunian object found, (15760) 1992 QB1. Later objects were called "QB1-os", or cubewanos. They are also known as classical KBOs.

Scattered-Disk Objects (SDOs): these objects generally have very large orbits with a ranging from 50 to 675 AU. They are assumed to be objects that encountered Neptune and were "scattered" into long-period, very elliptical ($0.34 \leq e \leq 0.94$) orbits with perihelia that are still not too far from Neptune's orbit.

Oort Cloud Objects (OCOs): The Oort cloud is a postulated spherical cloud of comets situated about 50 000 to 100 000 AU from the Sun. According to the hypothesis, the Oort cloud contains millions of comet nuclei, which are stable because the Sun radiation is very weak at their distance. The cloud provides a continual supply of new comets, replacing those that are destroyed.

1.2.4 Asteroid brightness and size constraints

Asteroid brightness, in the 0.40-2.50 μm spectral range, is entirely due to reflected solar light. Asteroid apparent magnitude depends from Earth-object distance, Sun-object distance and from body physical and optical properties, such as its size and albedo. After that we have to consider the phase angle, since from the Earth in general we see only a part of its irradiated surface.

The *apparent magnitude* m_V of the object in the visible spectrum can thus be expressed with:

$$m_V = m_{V\odot} - 2.5 \log \left(\frac{p_V \left(\frac{D}{2}\right)^2 \Phi(\alpha)}{2.24 \cdot 10^{16} R^2 \Delta^2} \right) \tag{1.4}$$

where $m_{V\odot}$ is the Sun V apparent magnitude, p_V is the V geometric albedo, D is the asteroid diameter (expressed in km), $\Phi(\alpha)$ a function of the angle phase and R and Δ are Sun-object and Earth-object distances respectively (expressed in AU, thanks to the $2.24 \cdot 10^{16}$ factor).

Asteroid *absolute magnitude* H is defined for distances $R = \Delta = 1\ AU$ and phase angle $\alpha = 0$ (visible face completely illuminated[3]).

[3]This definition is obviously only analytical, since no geometrical point can satisfy at the same

From astrometric and photometric observations of asteroids we can find H, being:

$$H = m_V + 2.5 \log\left(\frac{\Phi(\alpha)}{R^2\Delta^2}\right) \tag{1.5}$$

with R and Δ expressed in AU. Once we know H we can compute:

$$\log\left(p_V D^2\right) = 6.259 - 0.4H \tag{1.6}$$

with D expressed in km. Notice that with photometry only the product $p_V D^2$ can be determined, it is not possible to know the two variables indipendently.

1.3 Near Earth Asteroids

Near-Earth Objects (NEOs) represent an heterogeneous population which comprises asteroids and extinct comet nuclei in orbits with perihelion distances q <1.3 which periodically approach or intersect the orbit of the Earth. Given their vicinity to the Earth, NEOs are believed to be a source for most meteorites which arrive on our planet.

The importance of studying NEOs has been recognised worldwide, and a great deal of resources are being used for this task, both for ground-based facilities and space missions.

Available data indicate that NEOs population is very diverse in nature (objects with unusual shapes, binary systems, objects with a complex, non–principal axis rotation state (*tumbling* asteroids), some others with very long rotational periods, which are not easily explained by the current dynamical and collisional models, etc.).

The question of NEO origin is also not well understood. We know that the present NEOs have typical life-times of 10-100 My (much shorter than the age of the Solar System), and that over these time scales NEOs are ejected from the Solar System or collide with the Sun or a planet. Because the cratering record on the Moon suggests a fairly constant NEO population during past 2 billion years, new NEOs must be continuously supplied by some sources in order to maintain the present steady state.

The principal one is the Main Belt, where gravitational perturbations by the major planets cause dynamical resonances which provide escape routes (i.e. mean

time the three conditions.

motion, secular and diffuse resonances). The second source is represented by dead or dormant comets (objects originally coming from the Kuiper Belt and the Oort Cloud) that is devolatilised cometary nuclei and/or comets whose icy surface is covered by a subtle non volatile crust which inhibits possible gas emissions. An example is the apollo asteroid 4015 which at the time of discovery, in 1949, was the comet named Wilson-Harrington.

It is not clear, however, what the efficiency of the delivery mechanisms is, and what percentage of the NEOs we observe today comes from the one or from the other source. Although this global picture of NEOs origin is now widely accepted, a detailed knowledge of their physical properties has been obtained only for less than 10% of them.

One way of addressing many issues related to NEOs is to characterise them spectroscopically in order to derive their mineralogy and to classify them taxonomically. Owing to their heterogeneity it is evident the importance to carry on a large survey in order to investigate the physical properties of an as large as possible sample of NEOs.

The different nature of these bodies is particularly evident from their taxonomy (Lazzarin et al. 2004; Lazzarin et al. 2005; Binzel et al. 2002). In fact almost all taxonomic classes identified among MB asteroids have been also found among NEOs, including the C, P and D classes that are typical of outer MB asteroids. The most common taxonomic class among NEOs is however the S-type.

Besides a possible selection effect (being this class dominated by high albedo objects), this could indicate that Near Earth Asteroids derive mostly by the inner MB, via the ν_6 resonance, where S-types are the most common asteroids. However, other sources have been proposed like the 3:1 resonance (see for example Morbidelli et al. (2002) and Bottke et al. (2002)), which is surrounded by C- and S-type asteroids in almost equal quantity.

Other sources of Near Earth asteroids can be the Mars-Crossers Asteroid population through the Intermediate Source Mars-Crossers (IMC) and the Outer Main Belt (OB) population, while other secondary contributors to the NEA population can be the evolved Mars-crosser population, Mars-crosser asteroids derived from Hungaria population and from Phocaeas population and Mars-crossers with $a > 2.5AU$ and high i (above the ν_6 resonance, see Fig. 1.1).

Finally, another interesting issue is the now evident relationship between NEOs and meteorites: understanding the sources of NEOs means also to understand the origin locations for most meteorites.

1.4 Meteorites

A *meteoroid* is a natural small object orbiting in space. A *meteor* is the visual phenomenon associated with the passage of a meteoroid through the Earth's atmosphere. A *meteorite* is a recovered remnant of a meteoroid that has survived to the transit through the Earth's atmosphere.

At the beginning of their study meteorites were thought to be atmospheric phenomena or volcanic ejecta. Ernst Chladni in 1794 argued for the first time that meteorites were from extraterrestrial origin.

Iron meteorites consist almost entirely of nickel-iron metal alloys, whereas *stony meteorites* are composed mostly of silicate and oxide minerals. *Stony-iron meteorites* have nearly equal proportion of metals and silicates.

Stones can be divided in two categories: chondrites and achondrites. A *chondrite* is an agglomeration of early solar system materials with little, if any, chemical change since its formation. An *achondrite* is an igneous rock, the product of partial melting, changes in composition and crystallisation.

The proportion of iron and stony-iron *falls* are very small, only 5% and 1% of the total. The ratio between irons to stones *finds* is much larger, because irons better survive terrestrial weathering processes and are more recognisable as something unusual on the Earth surface.

The meteorites represent fragments chipped from surface parts on bodies in the present solar system. In particular the presence of iron meteorites requires a disruption large enough to expose core material. Also small asteroid are probably fragments of bigger parent bodies. Studies of the surface of small bodies can provide information on internal layers and on the evolution of the parent bodies and on the processes which broke them.

The best direct information on asteroid collisional processes is probably the study of asteroid genetic families (i.e. Eos, Koronis, Themis families).

Chapter 2

Asteroid Spectroscopy

2.1 Introduction

The study of the surface mineralogy of individual asteroids and groups of asteroids can provide the data base for improving our understanding of their origin and evolution. Asteroid surface can be studied by the interpretation of observable properties to determine presence, abundance and, where possible, the mineralogical composition.

Visible and near-infrared reflectance spectroscopy has been widely used to determine asteroid composition since it can characterise the surface composition of most asteroid types. Diagnostic features in reflectance spectra that come from electronic and vibrational transitions within minerals or molecules are detectable in the (0.35-2.50) μm range.

Most important mineral species present in asteroid spectra are: olivine, pyroxene (clino- and ortho-pyroxene), Iron-Nickel ($Fe-Ni$) metal, spinel, feldspar and hydrated phyllosilicates and organic compounds. Since they are characterised by unique composition or limited compositional differences, each of them produces a characteristic reflectance spectrum with, in some cases, particular spectral features.

Most asteroids are composed of mixture of these minerals. Since the spectral parameters of the different absorption features (i.e. band position and the ratio between band areas) are related to a specific composition of the individual mineral, spectral analysis of the asteroid surface is able in most cases to detect mineralogical signatures characteristic of a particular species.

So it is possible to establish the *presence* of specific mineral phases such those listed before. The possibility of revealing a feature depends on the abundance of

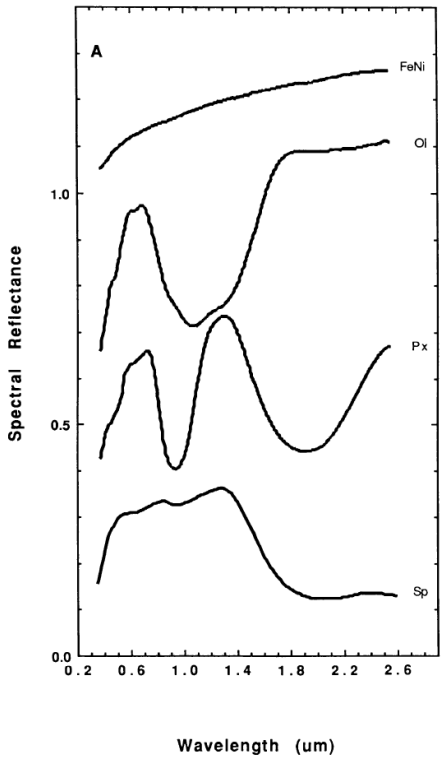

Figure 2.1: Spectral reflectance of most important mineral species: olivine (Ol), pyroxene (Px), Iron-nickel metal (Fe-Ni) and spinel (Sp).

the particular species so that the strength of the feature can be detected over the spectrum noise.

In some high quality spectra of some simple mineral mixtures the average *composition* and *relative abundances* can be also determined (several procedures by many authors have been developed to extract these information).

Therefore the analysis of reflectance spectra can provide a variety of compositional data on asteroid surface materials.

2.1.1 Asteroid Spectrum

The incident flux arriving on an asteroid surface (function of the heliocentric distance) is split in two contributions: the reflected and the absorbed part, whose ratio depends on the surface albedo. The absorbed part warms the body surface. It therefore emits black-body radiation at the reached temperature. So the Earth receives both the “solar” flux reflected from the body surface and its black-body emission.

In asteroid spectra, reflected sunlight dominates the flux from the ultraviolet to

the near-infrared (0.35-2.50 μm), while at longer wavelength (2.5-5.0 μm, depending on the surface temperature) the contribution due to the asteroid black-body emission becames detectable.

2.2 Photometric and Spectroscopic Surveys of asteroids

2.2.1 ECAS and 52-Color Photometry

The two most notable surveys in the 1980s to measure the spectral characteristics of a large number of asteroids were the Eight-Color Asteroid Survey (ECAS, Zellner et al. (1985)) and the 52-color survey (Bell et al. 1988). ECAS observed 589 objects in the visible while the 52-color survey measured 120 objects in the near-infrared (0.9 to 2.5 μm).

ECAS data are the basis for the asteroid taxonomy (Tholen (1984), see paragraph 2.3.1) that is still used today. The 52-color survey focused on S asteroids, which later allowed Gaffey et al. (1993) to divide the S class into a number of subclasses with interpreted surface compositions that varied from olivine-dominated to olivine/pyroxene mixtures to pyroxene-dominated. The mineralogical characterisation of these objects was made using the band centre of the 1 μm feature and the ratio of the areas of the 1 and 2 μm features.

However, both surveys could only make measurements of main belt asteroids with diameters greater than 20 km. The low number of objects that have been observed in this wavelength region is due primarily to the fact that very few observatories are at altitudes high enough for these observations.

2.2.2 SMASS: Small Main-Belt Asteroid Spectroscopic Survey

SMASS I and II

Between 1991 and 1993, the first phase of the Small Main-belt Asteroid Spectroscopic Survey (SMASSI) was carried out, resulting in spectral measurements for 316 different asteroids (Xu et al. 1995). The goal of SMASSI was to measure the spectral properties for a large sample of small- to medium-sized asteroids (mainly with diameters < 20 km), primarily focusing on those objects located in the inner

main belt (< 2.6 AU), as a means of addressing questions about the interrelationships between meteorites and asteroids.

Significant results from this survey include the discovery of objects in the Vesta family and between Vesta and the 3:1 resonance with Vesta-like spectra (Binzel & Xu 1993).

The second phase of the Small Main-belt Asteroid Spectroscopic Survey (SMASSII, see Bus & Binzel (2002b) and Bus & Binzel (2002a)) focused on producing an even larger, internally consistent data set, with the spectral observations and reductions being carried out in the most uniform manner possible.

The primary observational goals of SMASSII were to classify each new observed asteroid within the Tholen taxonomy, the sampling of planet-crossing asteroids (both near-Earth asteroids and Mars-crossing asteroids), the continued study of dynamical families, with particular emphasis on the Vesta family, and an in-depth study of several families located in the middle of the main belt between 2.7 and 2.8 *AU* (Bus 1999).

The significant differences between the SMASSII and the ECAS data sets, lead the authors of SMASSII to explore new options for classifying asteroids (Bus (1999), see paragraph 2.3.3). Mainly the differences regard the spectral coverage: SMASSII spectra cover a narrower wavelength range then ECAS. On the other hand, the greater spectral resolution obtained with CCD spectroscopy reveals subtle details like faint features, which are hardly identified with ECAS measurements.

They obtained the visible-wavelength spectra for 1341 main-belt asteroids (objects with perihelia greater than 1.3 AU). A list of observed SMASS I and II objects may be found at http://web.mit.edu/thb/www/smass/smass.html.

SMASSIR

To complement SMASS and to better characterise the mineralogies of asteroids, the Small Main-Belt Asteroid Spectroscopic Survey in the near-infrared (SMASSIR) was initiated at the IRTF, the NASA Infrared Telescope Facility (IRTF) on Mauna Kea on the island of Hawaii.

Results for main belt asteroids and for near-Earth objects are discussed in Burbine et al. (002a) and Binzel et al. (2001) respectively.

SMASSIR has a wavelength coverage from ~ 0.9 to ~ 1.65 μm and focuses on asteroids thought to have interesting surface compositions based on their visible spectra. These objects included olivine-dominated asteroids, objects with V (or J)

designations, and proposed meteoritic spectral analogs.

Compared to the 52-color survey, the advantage of SMASSIR is that much fainter main-belt objects (with estimated diameters as small as a few kilometres) can be observed, being the predicted V- magnitude limit 17.5. The disadvantage of SMASSIR is that reflectance data can only be obtained out to $\sim 1.65\ \mu m$, compared to 2.5 μm for 52-color, allowing only part of the 2 μm feature due to pyroxene to be characterised. The SMASSIR spectral wavelength coverage allows full characterisation of the 1 μm feature of olivine and pyroxene. However, the quantitative mineralogical determination of the relative abundances of pyroxene and olivine (Cloutis et al. 1986) and the composition of the pyroxene (Adams 1974) requires full measurement of the 2 μm feature.

2.2.3 S3OS2: Small Solar System Objects Spectroscopic Survey

The purpose of the Small Solar System Objects Spectroscopic Survey - S3OS2, was to contribute to increase the database of known superficial composition of asteroids in the visible range.

The S3OS2 was performed at the European Southern Observatory (La Silla, Chile) under the agreement with the Observatorio Nacional of Brasil, using the 1.52-m telescope equipped with a Boller & Chivens Spectrograph and a CCD. The survey was carried on from November 1996 up to September 2001 and visible spectra, in the range 4900-9200 Å, were obtained for 843 asteroids. All these spectra are available at the page http://www.daf.on.br/ lazzaro/S3OS2-Pub/s3os2.htm of the Observatorio Nacional. The taxonomic classification of all the sample is also available at the same site.

The spatial distribution of S3OS2 range from the Near Earth region, around 1.5 *AU*, up to the Trojan region, around 5.2 *AU*. Several families have been studied as well as several groups, all of which have been object of specific papers (see for example Florczak et al. (1998), Florczak et al. (1999), Lazzaro et al. (1999), Carvano et al. (2001), Michtchenko et al. (2002), Angeli & Lazzaro (2002) and Florczak et al. (2002)).

2.3 Taxonomic types

Taxonomy is the classification of objects into categories defined by some characterising parameters. Since 1970s many authors defined different taxonomic classes

on the basis of some observable properties. The principal aim is to identify groups of asteroids that share similar surface composition and thermal histories. In the following we shall name just the principal of them.

The most widely used taxonomy was made by Tholen (1984), Tholen & Barucci (1989), Tholen (1989), who used a minimal tree clustering algorithm on a set of more than 400 spectra from the Eight-Color Asteroid Survey (ECAS) in the 0.3-1.1 μm range (Zellner et al. 1985). The peak position of the eight ECAS broad band filter is: 0.31, 0.32, 0.43, 0.54, 0.70, 0.86, 0.95 and 1.0 μm.

Eleven of these classes (A, B, C, D, F, G, Q, R, S, T and V) could be distinguished by ECAS spectra. Other three classes (E, M and P) had degenerate ECAS spectra and could only be separated by using albedos. When albedo information was not available, the E, M and P-type were grouped into a generic X-type.

After that Barucci et al. (1987) used seven spectrophotometric colours plus the albedos from IRAS. In this way nine broad classes were obtained, and for each one fine subclasses were identified according to the detailed structure of the spectra. Moreover, we mention the Tedesco (Tedesco et al. 1989) taxonomy done with the help of the Johnson U-V colour, the ECAS colour v-x and the IRAS albedos.

Finally, we cite the new taxonomy proposed by Bus derived from recent spectrophotometric data (see Bus & Binzel (2002b), Bus & Binzel (2002a)). We will analyse in detail Tholen's, Barucci's and Bus' taxonomy in next paragraphs.

2.3.1 Tholen taxonomy

Each of previous mentioned taxonomies separates asteroids into different classes whose members have similar reflectivity and visual albedos. Although no specific mineralogical criteria were used in defining the classes, taxonomy can be used to derive mineralogical characterisations for individual asteroids in each class.

In the following, we shall briefly describe the main characteristics for each Tholen's class and their relationships with meteorites. In the next sections, a more detailed analysis of spectra information and the latest results in terms of asteroid classification will be given (taken mainly from Gaffey et al. (1993) and McSween (1999)).

Taxonomic class A

A-asteroids exhibit a strong decrease in reflectance shortward of 0.7 μm, related to metal compounds, and a strong broad absorption feature centred near 1 μm with no

significant 2 μm absorption (characteristic of pyroxene). Although the spectrum of olivine is unambiguous, it is difficult to specify exactly how much metal is present in these bodies. Among the asteroids classified as A-type, there is a spreading of a factor 3 in the albedo distribution. If the albedo range is real, the differences may be a function of metal abundance, with higher metal content resulting in a darker surface material. Regarding the origins, these asteroids are assemblages of either mono-mineral olivine or olivine-metal from the mantles or core-mantle regions of differentiated parent bodies.

The meteorite analogues of the A-type objects would be olivine achondrites and/or pallasites.

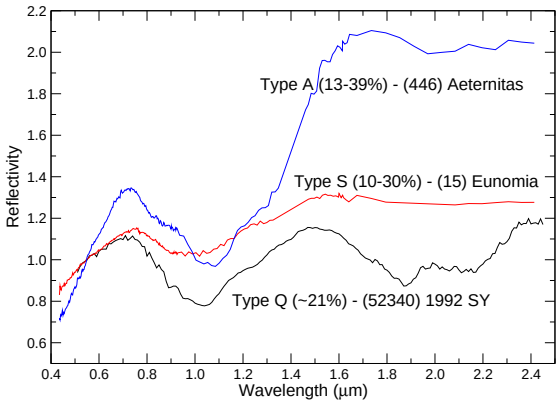

Figure 2.2: Examples of Q, S and A-type asteroids. Reflectance spectra are normalised at 0.55 μm. In parentheses the albedo range is reported in percentage for each class.

Taxonomic class S

The S-class constitutes the second most abundant asteroid class, and is characterised by spectra with moderate to steep reddish slopes shortward of 0.7 μm and weak to moderate absorption features near 1 and 2 μm. The absorption bands are weaker than those of V and R-class. The IRAS albedos vary from 0.1 to 0.3. The typical S-asteroids spectrum indicates the presence of some mixture of olivine, pyroxene and Fe-Ni metal.

However, it has long been recognised that S-class includes a very diverse group of objects. For example, Gaffey et al. (1993) carried out a quantitative spectral

analysis of 52-channel survey set (Bell et al. 1985). As a result, seven mineralogical subtypes (designed S(I)-S(VII)) were identified based upon compositions derived from the spectral analysis. These subclasses correspond to mineralogically distinct subtypes produced by different degree of melting, igneous differentiation, and may include some unmelted objects.

Although the spectral analysis performed by studying Band I and II is useful to identify asteroid counterparts of meteorites, it should be noted that this do not imply a strict similarity among the asteroids spectra and the meteorites ones. For example the spectra of the Main Belt asteroid 6 Hebe, suggested as possible parent body for the OCs, has a spectra less curvaceous and more highly reflective (reddened) that those of OCs. A number of possible explanations have been offered, but the most likely one seems to be space weathering (see, for example, Pieters et al. (2000), Gaffey (2001), Ueda et al. (2002b) and Ueda et al. (2002a)). When an asteroid's surface live in the space environment for millions of years, it undergoes chemical and physical changes as a result of bombardment by meteoroids and interaction with the solar wind. A direct evidence of the activity of these processes has been shown by the spacecraft Galileo. In fact, it found on the surface of asteroid 243 Ida reddened material except in the vicinity of younger craters, that have excavated materials that have not been exposed on the surface for very long time.

Taxonomic class Q

The problem connected with this class is the scarcity of Q-asteroids in the Main Belt. In fact, till now, only few objects have been proposed to belong to the Q-class (all NEOs, none belonging to the Main Belt). On the other hand, it has long been recognised that Q-type spectra are similar to those of OCs, and Q-asteroids could be thought of as parent bodies for at least part of those meteorites.

This class is well represented by the NEO 1862 Apollo. Its spectrum is strongly reddened shortward of 0.7 μm and has a strong 1 μm absorption feature characteristic of a mixture of olivine and pyroxene, and NIR data imply a low-Ca pyroxene.

Among the other classes of the Main Belt, the S(IV) provide the better spectral match to OCs. Moreover, this relationship seems to be indicated also by the orbital distribution of S(IV)-objects, because of their relative concentration adjacent to the (3:1) orbital resonance at 2.5 AU.

In this respect, it is of particular importance to analyse the NEOs, in order to find out the abundance of Q and S(IV)-type within them. Although the spectral

information of NEOs is still too poor to make a detailed statistical analysis of their taxonomic types, it results clear (Binzel et al. 2001) that they possess spectral properties to fill the gap between the OCs and the S(IV). NEOs have been found with spectra ranging from OC-like objects to S-class passing through the Q-class. As a consequence, a natural process able to produce continuous transition, such as space weathering, has been invoked to explain the spectral distribution of such NEOs. On this topic we shall return later on.

Taxonomic class R

This class was firstly proposed with the sole member 349 Dembowska. Its reflectance spectrum exhibits strong 1 and 2 μm absorption features similar to those of Vesta. Dembowska, differently from Vesta, has features broadened toward longer wavelength while the 2 μm feature is narrower and centred at shorter wavelength. The spectrum of Dembowska indicates a pyroxene-olivine assemblage (in approximately equal part) with little or no metal.

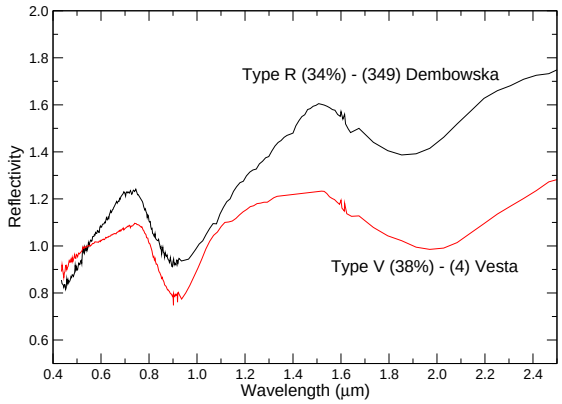

Figure 2.3: Examples of R and V-type asteroids. Reflectance spectra are normalised at 0.55 μm. In parentheses the albedo range is reported in percentage for each class.

Taxonomic class V

This class was proposed for the asteroid 4 Vesta. Its spectrum is characterised by two strong symmetric absorption features centred near 1 and 2 μm, with a weaker feature near 1.2-1.3 μm. The 1 and 2 μm features are due to pyroxene, and their

positions indicate a predominantly iron-bearing low calcium pyroxene or piogenite. The weaker feature is probably due to plagioclase feldspar.

As discussed previously, the spectra of eucrites have characteristics that compare favourably with the spectrum of Vesta, although the surface of this 530 km diameter body shows differences in composition. A detailed study of its surface, both photometrically and spectroscopically, has been performed with the HST (Binzel et al. 1997; Thomas et al. 1997; Cellino et al. 1987). It results that Vesta's surface is covered with eucritic basalts. Moreover, two large areas, having spectra similar to those of diogenites or olivine-rich ultramafic rocks, have been identified: they are apparently underlying rocks exposed in the floors of large craters.

For a long time Vesta was the only asteroid with such kind of spectrum, but now we know other analogs, the so-called Vesta chips (or Vestoids). These are small asteroids near Vesta, the (3:1) and ν_6 resonances. Notice that in spite of the large known sample of Main Belt asteroids' spectra (more than 1400 objects), all Vesta-like objects found are in the vicinity of Vesta, with the only exception of 1459 Magnya detected in the outer Main Belt (Michtchenko et al. 2002).

It seems likely therefore that the Vesta chips are effectively fragments delivered by Vesta itself. Regarding 1459 Magnya, Michtchenko et al. (2002) had shown how it could be an highly perturbed Vesta chip (by means of high-order two-body and three-body mean motion resonances and nonlinear secular resonances). Among NEOs, bodies having spectra similar to that of Vesta have also been identified, confirming the efficiency of the delivery mechanisms from the Main Belt.

Taxonomic class C (B, F, G and P)

In literature usually the authors refer to the C-group as a wide set of asteroid spectra, representing dark and primitive objects. The C-class asteroids have nearly featureless ECAS spectra longward of 0.4 μm, but have different UV absorption intensity. Within this set, several subclasses have been distinguished, namely C, B, F, G and P.

The P-class has no UV absorption feature (and also a reddish spectrum, see in the following), the F-class has a weak one, the B- and C-classes have a slightly stronger one, and the G-class has the strongest UV absorption edge of the C-group. The B-class has flat to slightly bluish ECAS spectra while the C- class has flat to slightly reddish spectra. The B-class also tends to have higher albedos than the C one. Bell et al. (1989) proposed a model for understanding the diversity in the

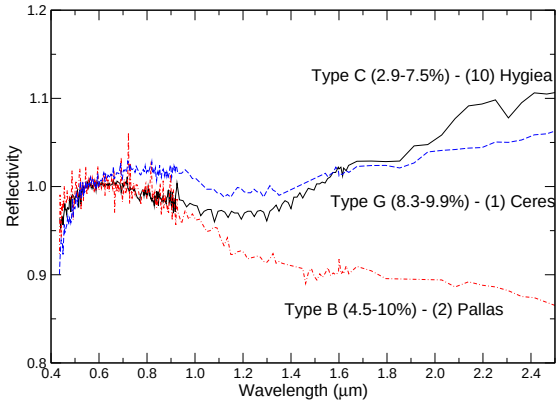

Figure 2.4: Example of C, B and G-type asteroids. Reflectance spectra are normalised at 0.55 μm. The vertical plot scale is amplified to better show differences among classes. In parentheses the albedo range is reported in percentage for each class.

C-group by means of metamorphic evolution: the classes B, F and G would be the result of such alteration from C-class parent material. The P-class, which are mainly located in the outer part of the belt, is believed to be primitive material that contains a large amount of organics, and may be a transitional class between the C-class and the very primitive D-class.

About two-thirds of C-group appear hydrated as result of analysis around 3 μm and in the visible region, probably indicating that they were heated to the point that liquid water became in contact with surrounding minerals. On the other hand, the dry C-type asteroids may never have had liquid water through them, or may have been heated so much that any hydrated mineral reverted or metamorphosed, or may never have contained much water to produce observable features.

More in detail, as suggested by Feierberg et al. (1985), there seems to be a correlation with the strength of the UV absorption feature and the presence of the hydrated minerals. The G-class, which has the strongest UV feature, exhibits the 3 μm hydration feature. C and F asteroids with moderate UV features include both hydrated and non-hydrated bodies. Among the P-class, which lack UV absorption features, the 3 μm hydration band is absent.

Another important feature observed is the absorption at ~ 0.7 μm similar to features present in the spectra of CI and CM meteorites. These features appear to be due to iron oxides or to oxidised iron in phyllosilicates produced by aqueous

alteration processes. However, it has been shown (Bus & Binzel 2002a) that the correlation among asteroid with 3 μm band (associate with water) and those with 0.7 μm feature is not perfect. For this reason we cannot conclude that an object without the 0.7 μm feature is dry. These features are common in the C, G and B objects but rare in the F and P ones.

The general C-group thus includes a variety of assemblages which overlap with the CI and CM meteorites, and some C-type objects seem to be equivalent to those meteorites, namely those with absorption band due to hydrated minerals (especially G and B-types). Other C-objects, like 2 Pallas, have spectra that closely resemble that of CR chondrites, suggesting that it might be the parent body for this chondrite group. The F and P classes appear to have experienced only minor or no aqueous alteration, and may represent ice-depleted samples of the parent assemblages.

Taxonomic class D

The spectra of the D-asteroids are generally featureless with neutral to slightly red spectra shortward of 0.55 μm, and very red spectra longward of 0.55 μm. They also have very low IRAS albedo (≤ 0.05) and are found predominantly in the outer part of the Main Belt. For these reasons D-asteroids (as well as the Cs and Ps) are believed to be composed of some complex mixture of organic materials and regolith[1]. This organics are usually referred to as kerogen-like, but also other materials are used for comparison. Nikolaeva et al. (1991) proposed to use the continuous series of the natural carbonaceous materials ranging from oil, passing by asphaltite, to anthraxolite. A spectroscopic analysis of such material showed that they may be used as spectral analogs of extraterrestrial organics.

The D-asteroids dominate the trojan asteroids comprising more than 60% of the classified objects in that area. (Vilas & Smith 1985) did spectral observations of D and P asteroids in the visible range and concluded that there seems to be a gradual reddening in the spectra slope with heliocentric distance, which implies varying composition and/or thermal histories with increasing distance from the Sun. This fact can be interpreted, from laboratory analysis, as a consequence of a gradual changes in H/C content and in the relative content of aliphatic and aromatic components of the organic compounds. It should be emphasised that the presence of both aliphatic and aromatic groups seems to be needed to provide the red spectra of

[1]The regolith is the layer of fragmental incoherent rocky debris that nearly everywhere in the Solar System forms the surface terrain.

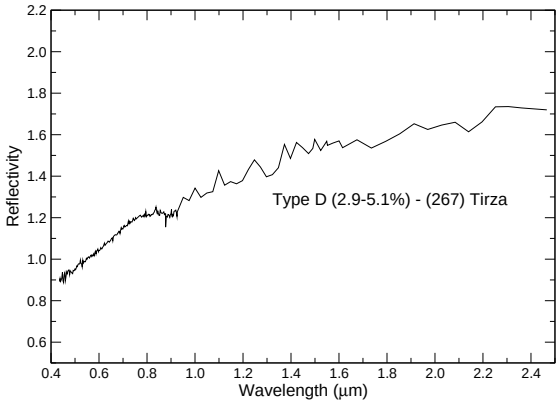

Figure 2.5: Example of D-type asteroid. Reflectance spectrum is normalised at 0.55 μm. In parentheses the albedo range is reported in percentage.

this type of asteroids, being the first with high H content responsible for the high IR reflectance; while the PAH's yield red slope in the NIR. The suggested change of organic materials with solar distance could result from a gradient of temperature in the solar nebula and/or as a result of a subsequent evolution[2].

We discussed about the fact that the meteorites are believed to come from asteroids, except for known lunar and martian meteorites. However, there are several spectral types of asteroids whose meteorite counterparts have not been found. Among them there were for a long period the P and D asteroids, until the fall of the so called Tagish Lake (Canada) meteorite in 2000. The spectral analysis of the two chips found (Hiroi et al. 2001), reveals a typical trend similar to those of D and P type; among them, the spectrum of the asteroid 368 Haidea is the better fit to the Tagish Lake one, although the albedo of the Tagish Lake (2.1%) is somewhat lower that 368 Haidea (3.2%). This discrepancy may either mean that the surface regolith of 368 Haidea is more fine grained than this Tagish Lake sample, or that the asteroid surface returned more specular reflection (or, simply, one albedo is wrong).

The asteroid 368 Haidea is located at about 0.2 *AU* inside a huge asteroid vacancy at the (2:1) mean motion resonance with Jupiter, and it is possible that frag-

[2]Let us note that the laboratory ion irradiation of various organic targets indicates that the increase of ion flux causes the darkening and the reduction of the spectral slope in VIS-NIR region due to carbonisation. Therefore, the bombardment of the asteroids surface by solar fast ions (wind and flares) could be in part responsible of such behaviour.

ments of it have been injected in the resonance (like for Vesta and Vestoids, see below), and after that they acquired orbits colliding with the Earth. On the other side, we did not find NEOs in our sample with the spectral property neither of P nor D-class, and the problem of the origin of the Tagish Lake meteorite is still open.

Taxonomic class E

E-asteroids exhibit featureless or very weakly featured flat to slightly reddish spectra, and have high albedo (mean ~ 0.44), which distinguishes them from the M and P type. The nearly absence of absorption features indicates the presence of very iron-poor or iron-free silicate (e.g. enstatite, forsterite or feldspar). This asteroid class has been identified as probable parent bodies of the enstatite achondrites or aubrites (Zellner et al. 1977). At least one of the E asteroids (44 Nysa) also has a weak 0.85-0.90 μm pyroxene feature consistent with low- iron enstatite seen in some meteorites (Gaffey et al. 1989). Moreover, 3 μm observations of 44 Nysa showed the presence on hydrated silicates on this asteroid, making its composition closer to that of C-class. Another interesting issue related to the E-type is the presence of an absorption band centred at 0.5 μm shown by some asteroids belonging to this group (see, for instance, Fornasier & Lazzarin (2001)).

The Hungaria asteroid region, which is located between 1.79 *AU* and 1.98 is dominated by E-type asteroids and contains about half of all E-types known in the Main Belt. From a general point of view, we can state that the composition of Hungaria asteroids is consistent with the predicted composition of the protoplanetary disk at roughly 2 *AU* from the Sun.

In the NEOs group, the E-types are rare, the first discovered one was 3103 Eger (roughly 1.5 km size), which was thought to be the parent body for, or at least connected with, the aubrites. The orbit of 3103 Eger has the aphelion distance of 1.905 *AU* (within the Hungaria zone), and this fact appears to indicate that Eger was most probably derived from that region. These results could represent the first plausible link between a meteorite group and a particular source region (Burbine & Bell 1993).

As we shall discuss in the next chapter, in our sample of observed NEOs at least another E-type body has been found.

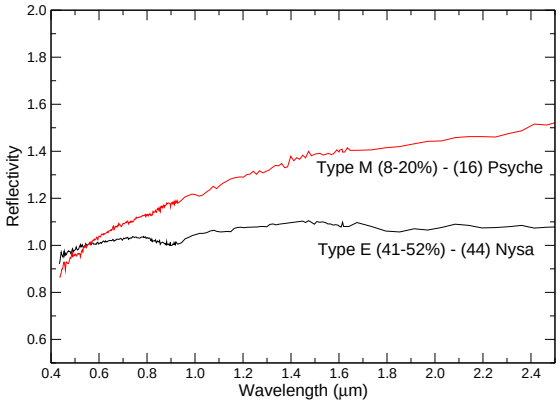

Figure 2.6: Example of E and M-type asteroids. Reflectance spectra are normalised at 0.55 μm. In parentheses the albedo range is reported in percentage for both classes.

Taxonomic class M

The M-type asteroids have reddened and weakly featured spectral reflectance curves, similar in shape to those of the E and P-asteroids, but have albedos intermediate between the E and P-classes. All the data concerning the M-class are consistent with Fe-Ni metals, so that these asteroids have generally been thought to be exposed metallic cores of differentiated parent bodies which suffered catastrophic disruption. For these reasons they are related to iron meteorites. Some M-asteroids show a 3 μm absorption feature, suggesting the presence of clays, which is in partial contrast with a metallic composition. They could have been generated by incompletely denuded parent bodies and/or from rubble pile asteroids.

The diversity within the M-class derives from a weakness of the classification system, because the objects which are classified as M-type do not exhibit strong features in the spectral interval used in the taxonomic classification. As a result, objects with different composition can be grouped together. Moreover, the featureless spectrum of iron metal makes quantitative estimation of metal content impossible. Radar imagery offers a more definitive analysis for metal objects, but it is applicable only for large objects or in near Earth orbits.

Taxonomic class T

T-asteroids have low albedos (≤ 0.10) with spectra that are slightly red shortward of 0.85 μm. They are interpreted as made by highly altered (either thermally or aqueously) carbonaceous material and also as physical mixture of S and C-type material.

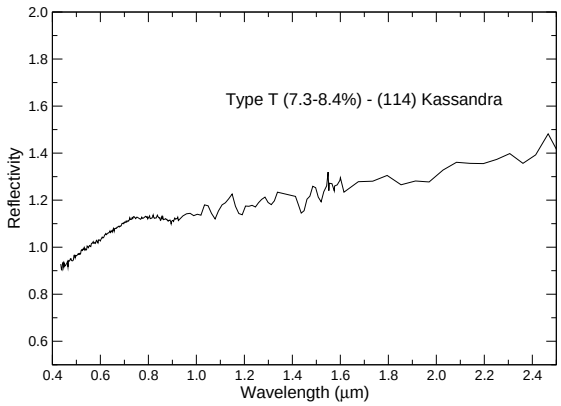

Figure 2.7: Example of T-type asteroid. Reflectance spectrum is normalised at 0.55 μm. In parentheses the albedo range is reported in percentage.

Britt et al. (1992) noted the similarity of the spectrum of troilite (FeS) and the spectra of some T-asteroids. As we discussed, troilite is a common meteoritic mineral found in almost all iron meteorites, with abundances reaching 60%. It has been suggested that troilite-rich regions should be present in the interiors of differentiated asteroids. Since M and T class asteroids have similar heliocentric distributions, Britt et al. (1992) suggested that T-asteroids may be collisionally evolved differentiated asteroids.

Summary of Tholen's Taxonomy

A Extremely reddish shortward of 0.7 μm; strong absorption feature longward of 0.7 μm, centred near the 1.05 μm. Albedo: moderately high.

B Higher albedo variant of C class with a tendency toward lower reflectivities at the red end of the spectrum. Albedo: moderately low.

C UV absorption feature shortward of 0.4 μm, generally flat to slightly reddish longward of 0.4 μm. Albedo: low.

D Generally featureless spectrum; neutral to slightly reddish shortward of 0.55 μm, very red longward of 0.55 μm. Albedo: low.

E Featureless spectrum; flat to slightly reddish over entire 0.3 to 1.1 μm range; differs from the spectrally identical M and P classes in albedo only. Albedo: high.

F Featureless spectrum; flat to slightly bluish over entire 0.3 to 1.1 μm range; differs from the C class in the weakness of the UV absorption feature. Albedo: low.

G Very strong UV absorption feature shortward of 0.4 μm, flat longward of 0.4 μm; differs from the C in the strength of the UV absorption feature. Albedo: low.

M Featureless spectrum; flat to slightly reddish over entire 0.3 to 1.1 μm range; differs from the spectrally identical E and P classes in albedo only. Albedo: moderate.

P Featureless spectrum; flat to slightly reddish over entire 0.3 to 1.1 μm range; spectra are intermediate between C and D classes. Albedo: low.

Q Strong absorption features shortward and longward of 0.7 μm; band centred between those of A and V classes (1862 Apollo is the type example). Albedo: moderately high.

R Strong absorption features shortward and longward of 0.7 μm; band centre between those of A and V classes (349 Dembowska is the type example). Albedo: moderately high.

S Moderate to strong absorption feature shortward of 0.7 μm, and moderate to nonexistent absorption feature longward of 0.7 μm. Albedo: moderate.

T Moderate absorption feature shortward of 0.85 μm and generally flat longward of 0.85 μm. Albedo: low.

V Strong absorption feature shortward of 0.7 μm and strong absorption feature longward of 0.7 μm, centred near 0.95 μm. Albedo: moderately high.

I Used for inconsistent data (e.g. a low albedo but an A-type spectrum).

K This letter has been reserved to represent a class of objects similar to 221 Eos.

U Appended to the classifications of those objects that fall far from the cluster centre,indicating an unusual spectrum for that class.

X The class for the degenerate E, M and P classes when albedos are not available.

2.3.2 Barucci taxonomy

A revised version of the G-mode multivariate statistics (Coradini et al. 1977) has been used to classify the 438 asteroids for which the ECAS data and IRAS albedo are available.

The G-mode classification technique separates a sample of N objects into J homogeneous classes containing N_j objects. Each object is described by M variables i. Initial data are arranged in a $N \times M$ matrix and for each variable i the mean value, the variance $(\overline{x_i}, \sigma_i)$ and the correlation matrix are computed. The method is iterative: a sample is considered to belong to a particular class if some conditions on mean, variance and correlation matrix are verified and a particular class is defined by its component.

The only *a priori* choice of the method is the definition of the confidence level in the determination of the taxonomic classes. At a confidence level of 99.7%, seven taxonomic units of asteroids are separated by the method, while with higher values of the confidence level no separation occurs in the adopted sample. Decreasing the confidence level (i.e. accepting a higher probability of a wrong decision in classifying the asteroids), Barucci et al. (1987) obtain a more detailed grouping, which results in a successive subdivision of the first units found.

They therefore found that the asteroid population separates into nine major taxonomic classes (C, S, M, D, B, G, E, A, V) and that three of these (S, D, B) can be further subdivided into subclasses. In total, 18 groups of objects can be distinguished, showing small deviations from the trend of the original groups. The method gives a quantitative estimate of the significance of the variables used. A comparison with the results obtained by Tholen (1984) shows that the nine principal units coincide with the Tholen's homonym classes. They finally interpret the obtained results in terms of natural processes which characterised the history of asteroid population.

2.3.3 Bus taxonomy

The SMASSII data provided a basis for developing a new asteroid taxonomy. Bus & Binzel (2002b) and Bus & Binzel (2002a) constructed a classification system based on the robust framework provided by existing asteroid taxonomies. In particular, they defined three major groupings (the S-, C-, and X-complexes) that adhere to the classical definitions of the S-, C-, and X-type asteroids. A total of 26 classes are defined, based on the presence or absence of specific spectral features. Defini-

tions and boundary parameters are provided for each class, allowing new spectral observations to be placed in this system. Of these 26 classes, 12 bear familiar single-letter designations that follow previous conventions: A, B, C, D, K, O, Q, R, S, T, V, and X. A new L-class is introduced to describe objects with spectra having a steep UV slope shortward of 0.75 μm, but which are relatively flat longward of 0.75 μm. Asteroids with intermediate spectral characteristics are assigned multi-letter designations: Cb, Cg, Cgh, Ch, Ld, Sa, Sk, Sl, Sq, Sr, Xc, Xe, and Xk. Members of the Cgh- and Ch-classes have spectra containing a 0.7-μm feature that is generally attributed to hydration.

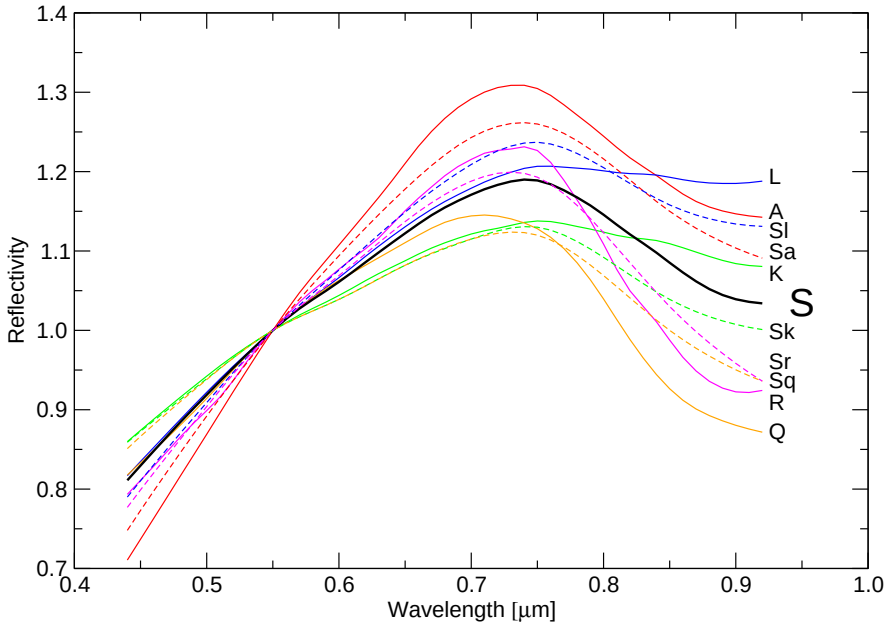

Figure 2.8: Bus' mean types belonging to the S-complex. Spectra are normalised at $\lambda = 0.55 \mu m$.

S-complex

A Very steep to extremely steep UV slope shortward of 0.75 μm, and a moderately deep absorption feature, longward of 0.75 μm. The shape of the reflectance maximum around 0.75 μm can either be sharply peaked or can be quite broad,

with the shape of the peak possibly being tied to the shape and roundness of the 1 μm feature. A subtle absorption feature is often present around 0.63 μm;

K Moderately steep UV slope shortward of 0.75 μm, reaching a maximum relative reflectance of about 1.15. The spectral slope becomes flat to slightly negative (blue) longward of 0.75 μm, showing little or no concave-up curvature in the 1 μm absorption band;

L Very steep UV slope shortward of 0.75 μm, becoming approximately flat, with a relative reflectance of about 1.2 longward of 0.75 μm;

Q Moderately steep UV slope shortward of 0.7 μm, and a deep, rounded 1 μm absorption band that reaches a minimum reflectance level of about 0.9. Reflectance maximum is relatively broad, with an average peak value of about 1.12;

R Very steep UV slope shortward of 0.7 μm, and a deep absorption feature longward of 0.75 μm. The shape of the spectrum, near maximum reflectance, is more sharply peaked than is typical for S-type spectra and is somewhat skewed due to the strength of the 1 μm absorption band that reaches a minimum at roughly 0.9 μm with a relative reflectance level of 0.9. An additional small absorption feature can be seen centred near 0.52 μm;

S Moderately steep UV slope shortward of 0.7 μm and a moderate to deep absorption band longward of 0.75 μm. Average S-type spectrum has a peak reflectance of about 1.2 at 0.73. The spectral slope is almost always slightly steeper over the wavelength interval from 0.44 to 0.55 μm than it is from 0.55 to 0.7 μm, and often there is a broad, but shallow absorption feature centred near 0.63 μm;

Sa Spectrum intermediate between S and A-types. Very steep UV slope shortward of 0.7 μm. The reflectance peak is typically broader than it is in A-type spectrum;

Sk Intermediate between S and K-type spectra. Absorption feature longward of 0.75 μm shows moderate concave-up curvature, as compared to the K-types, where the spectrum over this interval tends to be approximately linear. Compared with other S-types, the 0.63 μm feature can be strong;

Sl Intermediate between S and L-type spectra. Absorption feature longward of 0.75 is shallow to moderately deep, as compared to L-types, where this spectral interval is essentially flat;

Sq Spectrum intermediate between S and Q-types. Compared with other S-types, these spectra can contain a relatively strong 0.63 μm feature;

Sr Intermediate between S and R-type spectra. Very steep UV slope shortward of 0.7 μm and a deep absorption feature longward of 0.75 μm. Reflectance peak is broader and more symmetric in shape than it is in R-type spectra;

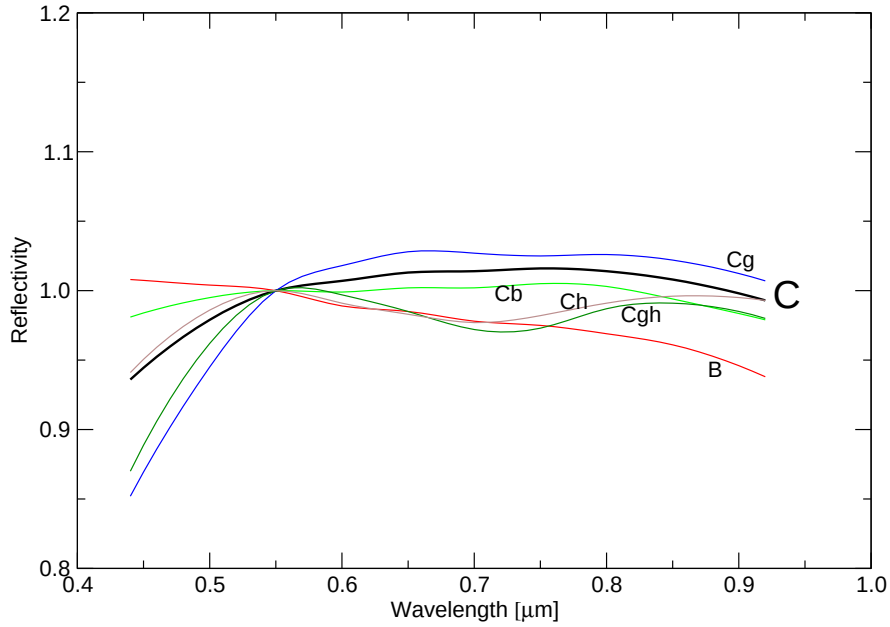

Figure 2.9: Bus' mean types belonging to the C-complex. Spectra are normalised at $\lambda = 0.55 \mu m$.

C-complex

B Linear, featureless spectrum over the interval from 0.44 to 0.92 μm, with negative (blue) to flat slope;

C Weak to medium UV absorption shortward of 0.55 μm, generally flat to slightly red and featureless longward of 0.55 μm;

Cb Generally linear, featureless spectrum over the interval from 0.44 to 0.92 μm, with a flat to slightly red slope;

Cg Strong UV absorption shortward of 0.55 μm and generally flat to slightly reddish slope longward of 0.55 μm. Occasionally a shallow absorption feature is seen longward of 0.85 μm;

Cgh Similar to Cg spectrum with addition of a broad, moderately shallow absorption band centred near 0.7 μm;

Ch Similar to C spectrum with addition of a broad, relatively shallow absorption band centred near 0.7 μm;

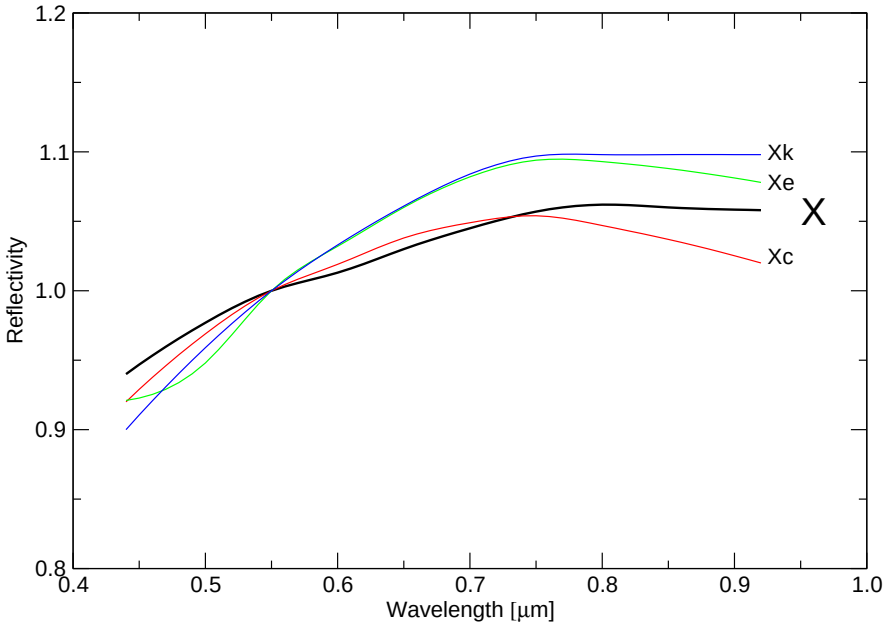

Figure 2.10: Bus' mean types belonging to the X-complex. Spectra are normalised at $\lambda = 0.55 \mu m$.

X-complex

X A generally featureless spectrum, with slight to moderately reddish slope. A subtle UV absorption feature, shortward of 0.55 μm, can be present, as well as an occasional shallow absorption feature longward of 0.85 μm;

Xc A slightly reddish spectrum, generally featureless except for a gentle convex curvature over the middle and red portions of the spectrum;

Xe Overall slope that is slightly to moderately red, with a series of subtle absorption shortward of 0.55 μm. This feature exhibits a concave-up curvature, most visible in the spectrum of 64 Angelina, where the band centre is located at about 0.49 μm;

Xk Moderately red slope, shortward of about 0.75 μm, and generally flat longward of 0.75 μm with a peak relative reflectance of roughly 1.2, the change in slope occurring very gradually. Similar in spectral shape to Xc, but redder in overall slope.

Other Classes

D Relatively featureless spectrum with very steep slope. A slight decrease in spectral slope (less reddened) is often seen longward of 0.75 μm;

Ld Very steep UV slope shortward of 0.7 μm, becoming essentially flat, with a relative reflectance of about 1.3 longward of 0.75 μm;

O Moderately steep UV slope from 0.44 to 0.54 μm, becoming less steep over the interval from 0.54 to 0.7 μm, and reaching peak relative reflectance of 1.05. Deep absorption feature longward of 0.75 μm;

T Moderately steep UV slope shortward of 0.75 μm, becoming flat with a relative reflectance between 1.15 and 1.2 longward of 0.85 μm. The change in spectral slope occurs very gradually;

V moderate to very steep UV slope shortward of 0.7 μm with a sharp, extremely deep absorption band longward of 0.75 μm that usually reaches a minimum relative reflectance level between 0.7 and 0.8. The spectral slope between 0.44 and 0.55 μm is usually steeper than that over the interval from 0.55 to 0.7 μm. An additional small absorption feature, centred near 0.52 μm, is occasionally seen. The largest member (4 Vesta) is anomalous in that its slope and band depth is less extreme than for other members of this class;

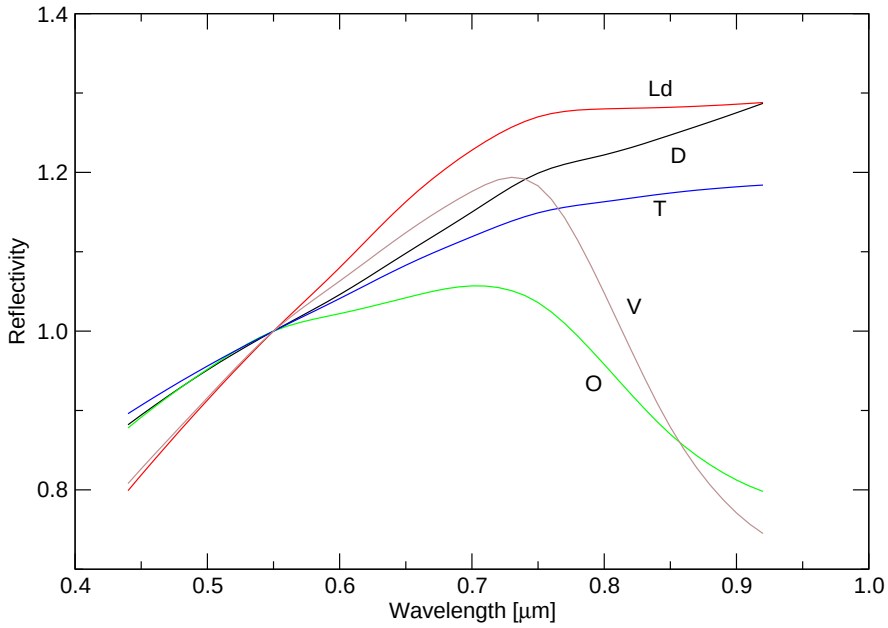

Figure 2.11: Bus' mean types not belonging to any complex. Spectra are normalised at $\lambda = 0.55\mu m$.

Although at the beginning taxonomy was created with data coming from Main Belt asteroids, it is natural to extend it to the NEOs population, with the main purpose of obtaining information on their origins. In fact, we can reasonably expect that if the NEOs originate in the Main Belt they should belong to the groups which are common in this region (e.g. S, C, V, M), while a membership to the D or P primitive groups would be highly suggestive of a cometary origin (or outer MB too). Unfortunately, not enough visible plus near infrared spectral information has been gathered about these objects, especially in the near infrared, because their faintness calls for the use of medium to large-sized telescopes, which normally are not systematically devoted to this type of research. However, these measurements are fundamental to address the origin of these objects and their relations with comets, Main Belt asteroids and meteorites. A recommendation for the necessity of physical and chemical characterisation of NEOs has been issued and addressed to the world governments and to the international agencies and organisations involved in space and astronom-

ical research. In order to contribute to the investigation of these objects, we started in 2000 a visible and near infrared spectroscopic investigation of NEOs. The aims of this work are both to improve the background knowledges and to look for a link with NEOs, MBAs, extinct cometary nucleus and meteorites. In the next chapter we shall present our data.

2.4 Principal Component Analysis

Principal Component Analysis (in the following: PCA) is a powerful instrument, widely used for problems related to taxonomy, and it is worthwhile to briefly describe how it works.

2.4.1 Statistical Method

PCA is a classical statistical method, based on the statistical representation of a random variable.

Suppose we have a random vector population $\vec{x}$ of n variables:

$$\vec{x} = (x_1, \ldots, x_n)^T \tag{2.1}$$

and the *mean* of that population is:

$$\mu_{\vec{x}} = E\{\vec{x}\}. \tag{2.2}$$

The *covariance matrix* (symmetric) of the same data set is:

$$C_x = E\left\{(\vec{x} - \mu_{\vec{x}})(\vec{x} - \mu_{\vec{x}})^T\right\} \tag{2.3}$$

The components $c_{ij} = c_{ji}$ of C_x represent the covariances between the random variable components x_i and x_j, while c_{ii} is the *variance* of the component x_i (the spread of the component values around its mean value). If two components x_i and x_j are uncorrelated, their covariance is zero:

$$c_{ij} = c_{ji} = 0 \tag{2.4}$$

Suppose to make many measurements of the variables. So we have a sample of vectors $\vec{x_1}, \ldots, \vec{x_m}$. We can calculate the sample *mean* and the sample *covariance matrix*.

From that $(n \times n)$ symmetric matrix we can transform the matrix in a diagonal one (A) with simple linear combinations of the original variables: we can thus calculate an orthogonal basis by finding its *eigenvectors* ($e_i,\ i = 0,\ldots,n$) and *eigenvalues* ($a_{ii} = a_i,\ i = 0,\ldots,n$). This means that we computed some *uncorrelated* components e_i, each one with the variance a_i.

By ordering the eigenvectors in order of descending eigenvalues (largest first), one can create an ordered orthogonal basis with the first eigenvector having the direction of the largest variance of the data. In this way we can find directions in which the data set has the most significant amount of *energy* (dispersion).

Instead of using all the eigenvectors of the covariance matrix, we may *summarise* the data set in representing it in terms of only a few basis vectors of the orthogonal basis. The number of eigenvectors considered is a compromise between simplify the problem and preserve as much as possible of the original information content.

So, PCA is a mathematical technique which describes a multivariate set of data using derived variables. The derived variables are formulated using specific linear combination of the original variables. The derived variables are uncorrelated and are computed in decreasing order of importance: the first variable (first principal component: PC1) accounts for as much as possible of the variation in the original data, the second variable (PC2) accounts for the second largest portion of the variation in the original data, and so on (PC3,...,PCn). PCA attempts to construct a small set of derived variables which summarise the original data, reducing the dimensionality of the original data and losing as little information as possible.

2.4.2 Application to Taxonomy

Principal component analysis is a commonly used method for spectral parametrisation. PCA was used by Tholen (1984) to visualise the distribution of taxonomic classes he had assigned to the ECAS asteroids. SMASSII data were also analysed by means of this technique (Bus & Binzel 2002b).

In applying this method to spectra, the different samples are the observed asteroids and the variables correspond to the values of reflectivity taken at given wavelengths (named channels). The choice of the displacement between two adjacent channels is arbitrary. The PCA applied on SMASSII data (Bus & Binzel 2002b) refer to 49 channels covering the wavelength range from 0.44 to 0.92 μm at steps of 0.01 μm.

Because of the noise on the asteroid spectra, the sampling must be done on a cubic spline of the original spectra. To ensure the normalisation, the fitted spectra were renormalised, so each spectrum has reflectivity of 1.00 at 0.55 μm.

Since the power of principal component analysis lies in its ability to parametrise the gross characteristics of a data set, it is often advantageous to first fit and remove the primary features of the data (if known) and use PCA to parametrise any residual characteristics. For asteroid spectra, it has long been recognised that the average spectral slope is strongly correlated with the first principal component.

Based on these considerations, it is now common to calculate and remove the average slope from each spectrum before applying PCA. To do that, for each spectrum, the least squares fit to the equation

$$R = 1.0 + slope \cdot (\lambda - 0.55) \tag{2.5}$$

is found, where R is the reflectivity, λ is the wavelength of the channels in micron and *slope* is the slope of the fitted line, forced to unity at 0.55 μm. To remove the slope, each spectrum is divided by its best fit line, producing the residual spectrum, whose value at 0.55 μm is still 1.00, with a mean value over all channels approximately 1.0. The value of *slope* is recorded as a spectral parameter, replacing the first principal component (PC1) in describing the spectrum.

Finally, all the residual spectra are parametrised using PCA, getting PC2′ and PC3′ as first two principal components[3].

Notice that the results of the PCA strongly depend on the original dataset. This mean that if we have to compare different spectra we cannot use previously computed principal components: we have to create a new matrix with all the samples (asteroids) data and compute a new PCA.

A deep inspection of the method reveals that the second spectral component PC2′ is most sensitive to the presence (or absence) of a 1 μm absorption band. In fact, the spectra distribution on the (*slope*, PC2′) plane clearly shows a broad bimodal distribution, being the most part of the asteroids clustered into two regions. One of these is called the S-complex, and the other has been divided into two regions for which the terms C-complex and X-complex have been introduced. Of course, the C and S-complex include the previous C and S-type asteroids; while the X-complex is representative of those objects with spectra similar to E and M-classes

[3]This nomenclature was made to minimise confusion, since the variables PC1, PC2, and PC3 refer to the more traditional principal components computed in the manner described by Tholen (1984), where no slope was removed prior to the application of PCA.

that, without any albedos information, are degenerate (see Fig. 2.12). Notice that PC2′ and PC3′ have been standardised, i.e. with mean and standard deviation equal to 1.

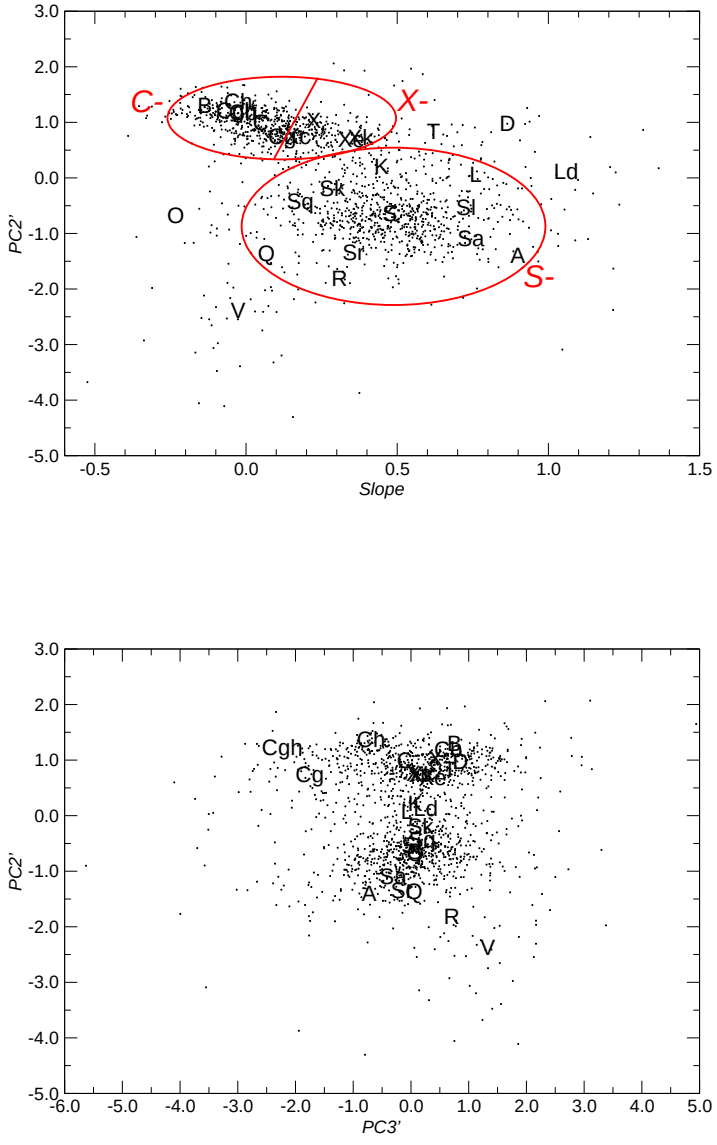

Figure 2.12: PCA on SMASSII data in the 0.44-0.92 μm spectral range. Upper panel: *slope* vs. PC2′. Lower panel: PC3′ vs. PC3′. In both plots positions of Bus' mean types are reported and in the first panel clusters defined by taxonomic complexes are put in evidence.

The third spectral component PC3′ is more complex, indicating it is sensitive to higher order variations in the spectra. Bus & Binzel (2002b) found that PC3′ is especially useful in isolating those asteroids whose spectra contain either a strong UV absorption band shortward of 0.55 μm or a 0.7 μm phyllosilicate feature.

The three major complexes are only the first product of the Bus taxonomy, since many objects lie outside of the nominal ranges defined for the C, X and S- complexes. These objects are mostly clustered in two opposite regions. The first of these region is located in the lower left-hand with respect to the S- complex. Many objects belongs to this region: Vesta and Vesta-like objects plus four bodies that have visible spectra consistent with that of L6 and LL6 ordinary chondrites. For them the V and O-class are used, respectively.

The second region lies in the upper right-hand with respect to the S- complex. Those objects defined by Tholen as T and D-type belong to this region. Moreover, a new class (Ld-type) has been introduced for those bodies having spectra similar to L-types (see later on) but with much steeper UV slopes, like D-types.

Concerning the S-complex, it contains asteroids having spectra similar to Tholen S-type. However, with the help of the large SMASSII data set, it has been possible to identify many subclasses. The task of dividing the S-complex into smaller classes was accomplished by targeting objects that appear to be around the perimeter of the complex. Among these objects some classified as A, Q and R-type by Tholen have been found: for them the previous class name has been retained. For others, placed at the upper perimeter of the S-complex, the new K and L-type have been introduced.

Also for the C-complex some subclasses have been introduced. For the analysis of the C-complex, Bus and Binzel found that the (PC3',PC2') plot can be useful. In fact, in this plot the variation of some distinct spectral features produces linear trends. The principal features are a significant UV absorption versus linear spectra and the depth of the 0.7 μm feature. Asteroids which do not show the absorption at 0.7 μm and have a slight convex curvature in the middle of the spectrum are still called C-types. Around these, the classes Cg, Cgh, Ch, B and Cb have been introduced.

Finally, subclasses also for the X-complex have been introduced. However in this case, owing to the subtle nature of the features observed in these spectra, the boundaries of X-complex do not identify well defined classes. The main feature for a subdivision is the presence of a absorption band around 0.49 μm, probably due to troilite: these objects are indicated by Xe. The other characteristic used in dividing

the X-complex is a broad, convex curvature that extends from roughly 0.55 to 0.8 μm. Those exhibiting the curvature are grouped into Xk and Xc depending on their slope. The remaining asteroids (having linear spectra) are posed in the X-class.

2.5 Link with meteorites

Meteorites are (by definition of their orbital intersection) near-Earth objects prior to their arrival, thus correlations between NEOs and meteorites represent the most direct link for achieving an understanding of asteroid-meteorite relationships.

Investigation of asteroid compositions can identify potential parent bodies of specific meteorite types. While mineralogical and petrological properties of meteorites can define the original condition of the Solar System, asteroid actual orbits can sometimes lead to the knowledge of their formation zone. So the link among meteorites and their asteroidal or planetary parent bodies can provide the basis to better understand the early Solar System history.

2.5.1 Stony Meteorites - Chondrites

The only records of the origin and the early evolution of the Sun and planets are the chondrites. This name derive from the ancient Greek *chondros*, meaning grain or seed, a reference to the appearance produced by numerous small, rounded inclusions called *chondrules*. Those chondrules are small droplets of olivine and pyroxene condensed and crystallised from the hot primordial solar nebula in form of small spheres. They accreted with other material that condensed from the solar nebula forming a matrix.

The chemical composition of the Solar System is often referred to as the *cosmic abundance* of the elements. The Solar System composition is really equivalent to the chemistry of the Sun, since it contains most of the mass (more than 99%) of the whole System. So, since the solar abundances are known and, on the other hand, chondrites composition are studied from 18^{th} century (the first publication was made by Antoine Lavoisier), a chemical comparison can be made.

The abundances of different elements vary over many orders of magnitude, but the correspondence between the Sun and chondrites is very good. No kind of terrestrial rock would show such an agreement because the chemistry of rocks changes every time they have geologic processing. By the way they have some discrepancies involving the lightest elements (hydrogen, helium, carbon, nitrogen and oxygen):

under most conditions these so-called *volatiles elements* exist primarily as gases and are more abundant in the Sun. Other elements, like lithium and boron, are more abundant in chondrites than in the Sun. This can be explained by the fact that these elements are utilised in fusion reaction by the Sun so that their solar abundance have been reduced. This mean that chondrites actually record the original chemistry of the Sun (and of the Solar System) even better than the present-day Sun does (except for volatiles).

However minor concentration differences are present within chondrites so that they are classified in *groups* (probably formed from the same parent body) and *clans* (sets of groups with common properties, inferred to have formed in the same region of the Solar System).

Principal clans are: *ordinary chondrites* so named because they are the most abundant clan; the *carbonaceous chondrites* actually misnamed when they were believed to have much higher carbon contents than other chondrites; *enstatite chondrites* named for their high abundances of enstatite, a magnesium silicate mineral. Each of last two clans are formed by a single group: *Rumuruti* and *Kakangari chondrites* are named from the only meteorite fall of that type.

Different clans also have different degrees of oxidation state. Increased oxidation is reflected, for example, in an increase in the relative proportions of olivine over pyroxene. Olivine is more abundant in carbonaceous chondrites (the most highly oxidised clan) and in Rumuruti. Ordinary chondrites are moderately oxidised and have twice as much olivine as pyroxene and less metal. Kakangari is intermediate between ordinary chondrites and enstatite chondrites (least oxidised and mostly pyroxene with abundant iron metal).

Within enstatite and ordinary chondrites clans different degrees of oxidation are generally specified by different letters: *H* as high, *L* as low and, for ordinary chondrites, *LL* as very low. Among carbonaceous chondrites groups refers to some geographic localities in which some falls were found.

Because rocks are poor conductors of heat, the original heat generated inside a chondritic planetesimal could not readily escape. Increased temperatures in the interior caused *metamorphism*, the adjustment of the minerals in chondrites to hotter conditions.

Different levels of metamorphism (*petrologic types*) have been distinguished with numbers from 1 to 6. The least metamorphosed chondrites of any group is type 3. From 4 to 6 the metamorphic grade increases that is reflected in an increasing

alteration of the chondrules. It is important to say that the thermal metamorphism that creates petrologic types 4 to 6 doesn't involve any melting. Recrystallisation takes place in the solid state.

Type 1 and 2 are represented only by some groups of carbonaceous chondrites that experienced a processing called *aqueous alteration* with the result that type 1 chondrites don't show any chondrules (they are virtually absent even though the meteorite is of chondritic composition and certainly contained chondrules in its early history).

Table 2.1: Chondrite classification: grid of meteorite clans, groups (identified by letters) and petrologic types (identified by numbers).

	Petrologic Types					
	1	2	3	4	5	6
Carbonaceous	CI1					
		CM2				
		CR2				
			CV3			
			CO3			
				CK4		
Rumuruti			R3			
Ordinary			H3	H4	H5	H6
			L3	L4	L5	L6
			LL3	LL4	LL5	LL6
Kakangari			K3			
Enstatite			EH3	EH4	EH5	EH6
			EL3	EL4	EL5	EL6

Carbonaceous Chondrites have composition that most closely match that of the Sun, and the *CI* group is commonly taken as the best approximation of cosmic element abundances.

An important chemical component of chondrites is *organic matter*. These are complex materials composed mostly of carbon, with hydrogen, oxygen, nitrogen or sulphur. Such materials occur in all chondrites, but have been studied particularly on carbonaceous chondrites. It is a complex mixture of straight to slightly branching hydrocarbon chains (alkanes), rings (aromatic hydrocarbons) and carbocyclic and amino acids.

Table 2.2: Asteroid taxonomic types with possible meteorite analogues.

Class	Possible Meteorite Analogues
A	Olivine Achondrites
	Pallasides
	Olivine-metal partial melt residues
B	CI1-type assemblages
C	CI1 and CM2 Chondrites
D	Tagish Lake meteorite
	Organic-olivine cosmic dust particles
E	Enstatite Achondrites
	Iron-bearing Enstatite
	Fe-bearing Aubrites
F	CI1 and CM2 assemblages (organic-rich)
G	Highly leached CI1-type assemblages
K	CV3 and CO3 Chondrites
M	Iron meteorites
	Enstatite Chondrites
P	Organic-olivine cosmic dust particles
Q	Ordinary Chondrites
R	Olivine-pyroxene cumulates
S	Ordinary Chondrites
	Pallasites with accessory py.
	Olivine-dominated stony-Iron
T	Troilite-rich iron
V	Howardites
	Eucrites
	Diogenites

S-types and Ordinary Chondrites

The spectra of S-type asteroids provide the closest link to the ordinary chondrites, with some differences. Gaffey et al. (1993) and Gaffey et al. (1993) have carried out a systematic analysis of the spectra of S-type asteroids. They found that only a small part of this class show an evident correlation is actually chondritic. Only one class, S(IV), out of six provides a match with ordinary chondrites. Other classes do not show any meteorite analog, or seem to be related to achondrites.

A number of possible hypothesis have been proposed to explain this discrepancy, but the most likely seems to be the *space weathering*. See paragraph 2.6 for further details.

C-types and Carbonaceous Chondrites

C-type objects (together with G, B and F-types) have nearly featureless spectra from 0.4 to 2.6 μm, but most of them show a prominent absorption band near 3 μm, indicating the presence of hydrated minerals such as phyllosilicates. Some C-type asteroids also exhibit other weak absorptions caused by iron in phyllosilicates and possibly by organic matter. All these spectral features and the composition they suggest are similar to those of carbonaceous chondrites, especially the CI and CM chondrites that have suffered aqueous alteration.

2.5.2 Stony Meteorites - Achondrites

The word *achondrite* is used to describe a stony meteorite without chondrules, and this lack of chondrules is the primary characteristic used to distinguish the two major stony groups. Within the process of accretion and differentiation of larger asteroids and planets, this primordial chondritic matter was melted in magma and recrystallised to form achondrites. The igneous origin of these rocks imply a partial or total melting of small inclusions such as chondrules. Meteorites that are residues of the partial melting are termed *primitive achondrites*.

Primitive achondrites are nearly chondritic in composition with an age similar to the primordial chondrites. They are the residues from partial melting that took place on small parent bodies having chondritic compositions. Following an initial heating phase, they were quickly cooled to become geologically inactive.

Igneous processes are the primary means by which planetary body evolve. Igneous activity also means planetary and asteroid resurfacing and transport of material from the interior. So igneous rocks potentially give information of the composition of their internal source region and the internal global characteristics.

Howardite, Eucrite, Diogenite Achondrites

The howardite-eucrite-diogenite (HED) association is the most abundant class of achondrites. It represent a collection of rocks formed from basaltic magmas. Even

if terrestrial basalts contain minor amounts of hydrated minerals HED achondrites contain no water.

The crystallisation ages of HED meteorites are very old (4.4-4.5 Gyr), indicating that the parent body had a relatively short but quick igneous history.

Eucrite. The plagioclase in eucrites is rich in calcium, poor in sodium; the common pyroxene is pigeonite (an iron-magnesium silicate with very little calcium).

Diogenite. The diogenites are composed mostly of magnesium-rich, calcium-poor orthopyroxene and only small amounts of olivine or plagioclase

Howardite. Most eucrites and some diogenites are actually breccias (clasts of rock cemented by pulverised mineral grains). Large impacts into a parent body, able to excavate inner material, can mix eucrite and diogenite fragments. Achondrites breccias containing both eucrite and diogenite clasts are called howardites.

Aubrites

The aubrites are achondrites composed primarily of nearly iron-free magnesium pyroxene (enstatite), in contrast to the pyroxene composition in other igneous meteorites. They also contain small but variable amount of iron-nickel metal, olivine and troilite all formed in extremely reducing conditions. Most of them are breccias with clasts commonly composed of enormous enstatite crystals.

Other Achondrites

There are other achondrites. Here we just list some of them, without going in detail about their composition and aspect.

Shergottite-Nakhlite-Chassignite (SNC) meteorites. All these meteorites define a common oxygen isotope fractional line and they also share other geochemical characteristics that indicate they could come from the same parent body.

Detailed modelling of their structure indicates that SNC could have been produced by several generation of melting and crystallisation and that their parent body must have been large and geologically complex. This also means that they are relatively young (compare with HED): various radiogenic isotope systems define age varying between 1.3 and 0.2 Gyr.

Achondrites of the SNC group are believed to have their origin on the planet Mars. These meteorites represent highly evolved rocks and resemble terrestrial rocks more than any of the other achondrites.

Lunar Meteorites. The cratered face of the Moon indicates that it has been repeatedly target of massive impacts. Lunar rocks can be ejected by such collision and a tiny fraction of that can reach the Earth.

An example is ALH81005, the first lunar meteorites found in 1982 near Allan Hills, Antarctica. To confirm its origin, this meteorite have been compared with lunar rocks collected by Apollo missions (i.e. the manganese to iron ratios of in ALH81005 resemble those in lunar rocks and are significantly different from terrestrial basalts and other achondrites).

The meteorite presents some white clasts of igneous rock (anorthosites, composed almost wholly of calcium-rich plagioclase with only minor of olivine and pyroxene) and some dark clasts of basalt.

Other lunar meteorites have been found since 1982. Most of them are breccias composed of materials rich in anorthosite.

Acapulcoites and Lodranites. They form a coherent group with continuously varying characteristics. They are primitive achondrites, with achondritic textures but with nearly chondritic compositions. They are largely composed of olivine, pyroxene, with minor plagioclase, iron-nickel metal and troilite.

Ureilites This is the second largest group of achondrites. They consist principally of the minerals olivine and pyroxene in a matrix of graphite or diamond, iron-nickel metal and troilite. They seem to be formed in the deep interior of their parent bodies and they are probably unmelted residues left behind after a partial melt was extracted.

The presence of diamonds indicate that they have experienced variable but typically intense shock metamorphism. This shock can also disturb the isotopic clocks in ureilites: the olivine and pyroxene assemblage appears to have formed 4.5 Gyr ago, but some radiogenic isotopes were redistributed at 4.0 Gyr.

2.5.3 Iron and Stony-Iron Meteorites

Iron Meteorites

Prior to the modern meteorite hunting in deserts and their robotic recovery in the ice fields of Antarctica, most meteorite finds were irons. Due to their metallic composition and their extraordinary weight they are easily recognised as foreign intruders. Moreover, most iron meteorites are quite resistant to terrestrial weathering, permitting them to be preserved much longer than any other type of meteorite. Finally, irons are usually much larger than stony or stony-iron meteorites. Irons rarely are fragmented upon entering the atmosphere and suffer much less from the effects of ablation during their passage through the atmosphere.

All iron meteorites taken together represent approximately 89.3% of the entire mass of all meteorites known. Despite these facts, iron meteorites are rare since they represent just 5.7% of all witnessed falls.

Iron meteorites are composed largely of nickel-iron metal, and most contain only minor accessory minerals. These accessory minerals often occur in rounded nodules that consist of the iron-sulfide troilite or graphite, often surrounded by the iron-phosphide schreibersite and the iron-carbide cohenite.

Stony-Iron Meteorites

This category comprises several chemically and genetically unrelated classes of meteorites that are composed of approximately equal parts of nickel-iron metal and different types of stony components. Several groups of chondrites and achondrites would fit into this definition and several silicated irons could be regarded as true stony-irons too. However, modern meteoritics assigns just two groups to this heterogeneous class, the pallasites and the mesosiderites.

Stony-iron meteorites are less abundant than their stony and iron cousins are. Taken together, all pallasites and mesosiderites comprise a total known weight of about 10 tons, representing approximately 1.8% of the entire mass of all meteorites known. This low abundance is also reflected by their fall-ratio; when compared to the other major types of meteorites, stony-irons are exceptionally rare, representing just 1.5% of all witnessed falls.

2.6 Space weathering

It is now widely accepted that space environment alters the optical properties of airless bodies' surfaces. A number of physical processes have been proposed to be relevant in this context (e.g. micrometeoroid impacts, solar wind bombardment, etc.). The result of all these effects on airless bodies is known as *space weathering*.

Space weathering effects were initially studied on lunar soils; indeed it was found that lunar soils returned from Apollo missions had optical properties that differed significantly from those of pristine lunar rocks (Conel & Nash 1970). The presence of metallic iron particle coatings on lunar soils was suggested by Cassidy & Hapke (1975); these coatings should be produced by deposition of atoms sputtered by solar wind particles and deposition of gaseous species produced by micro-meteoritic impacts. More recently, Pieters et al. (2000) analysed the products of space weathering of lunar soils, and demonstrated that nanophase reduced iron is produced on the surface of grains by a combination of vapour deposition and irradiation effects.

Since '80s space weathering effects were suggested to be present also on other bodies, like asteroids (as well as on planets, like Mercury), e.g. see the detailed review by Chapman (2004). This idea was due to a mismatch between laboratory spectra of freshly cut ordinary chondrites (OCs) and remote sensing spectra of S-type asteroids, which were thought to represent their parent bodies.

Recently, thanks to an increasing number of high quality asteroid spectra, along with dedicated laboratory experiments, new insights arose. The importance of laboratory experiments to simulate space weathering processes on asteroid-like materials is widely established. Experiments have been performed simulating solar wind and cosmic ion irradiation by keV-MeV ion irradiation, and assuming that micrometeorite bombardment can be simulated by laser ablation.

The first experiments simulating space weathering of OCs were performed by Moroz et al. (1996); they used micro-pulsed laser irradiation and the effect was to redden and darken reflectance spectra, and produced also a shift of the peak position of the 1 μm absorption band. Other laser ablation experiments were performed by Yamada et al. (1999) and Sasaki et al. (2001): they assumed that micrometeoroid impacts could be simulated by using a nanosecond pulsed Nd-YAG laser (1064 nm) on pellets of pressed silicate powder. Such experiments showed progressive (with increasing shots number) darkening and reddening of the UV-Vis-NIR silicate spectra. They attributed the observed spectral weathering to formation of coating

enriched in vapour-deposited nanophase iron (Sasaki et al. 2001).

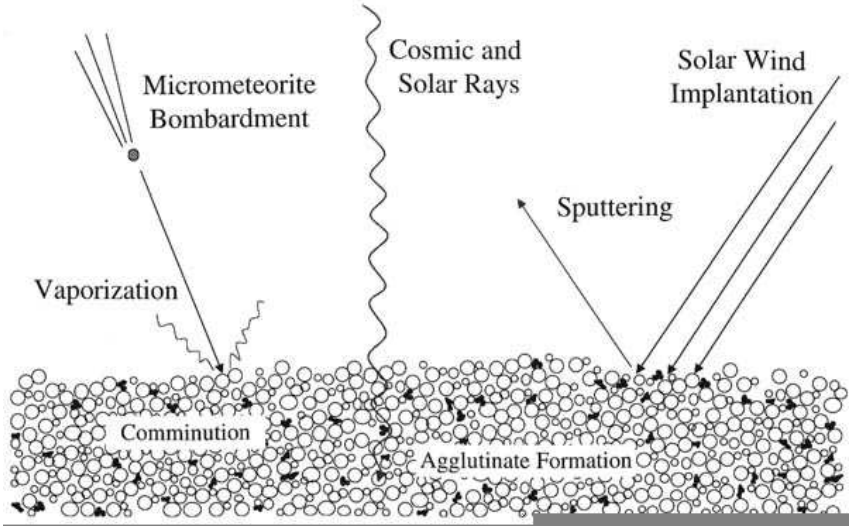

Figure 2.13: Different ways in which space weathering affects the visible and near-infrared spectra of soil. Space weathering processes alters the properties of the soil that covers the surface of all bodies which are not protected by an atmosphere.

On the other hand, ion irradiation using H^+ and He^+ ions (Dukes et al. 1999; Hapke 2001), and high energy (MeV) proton implantation (Yamada et al. 1999) produced only small changes in the spectra. A different result was obtained by Strazzulla et al. (2005), who performed ion irradiation of ordinary chondrite Epinal (H5) with Ar^{++} 60 keV, that produced strong darkening and reddening of the Vis-NIR spectra. A plausible explanation of this discrepancy is that irradiation effects are much more efficient with high mass ions than low mass.

Consequently, Brunetto & Strazzulla (2005) have performed ion irradiation experiments of bulk silicates, using different ions (H^+, He^+, Ar^+, Ar^{++}) with different energies (60-400 keV). They found an increasing of the 1 μm band spectral slope, which turned out to be strongly related with the number of displacements caused by colliding ions inside the sample, i.e. the elastic collisions with the target nuclei.

One point to be underlined is that solar wind irradiation can redden reflectance spectra by two processes: creation of displacements (Brunetto & Strazzulla 2005) and sputtering of iron from silicates and the deposition of nanophase neutral Fe on adjacent grains (Hapke 2001). These two processes take place at very different ion fluences: creation of displacements acts as main process for fluence lower than 10^{17}

ions/cm^2, while sputtering of iron is relevant for fluence higher than 10^{18} ions/cm^2.

Chapter 3

Visible and Near Infrared spectroscopy of NEOs

3.1 Introduction

As already discussed in paragraph 1.3, NEOs have a short lifetime after which they can collide with inner planets or with the Sun or they can be perturbed in hyperbolic orbits and thus escape from the Solar System. So, since their number is almost constant, it is now accepted that they have to be replenished from other sources, mainly from comets and the Main Belt. Moreover, given their vicinity to the Earth, they are believed to be a source for most meteorites which arrive on Earth.

So their study is essential to obtain information on the other minor bodies and the Solar System origin and evolution.

Spectroscopy gives the possibility to study the asteroid surface composition and mineralogy and so the taxonomic classification and the link among different dynamic groups of Solar System minor bodies. This can give hints in particular on NEOs origin and on the formation, dynamic and evolution of the whole Solar System.

3.2 SINEO: Spectroscopic Investigation of Near Earth Objects

In this contest, in 2000, we started a spectroscopic investigation of Near Earth Objects (*SINEO*). Here we present the results obtained until now from our long term

survey in the visible and Near Infrared Region (NIR).

Up to now we have obtained a data set of 113 spectra of which 106 in the visible range (0.40-0.95 μm) and 70 in the near infrared region (most of them in the whole 0.40-2.5 μm range). In the following we will present the results of a taxonomic classification of the objects, their linkage with meteorites and the influence of space weathering.

3.2.1 Observations and data reduction

The observations, both in the visible and in the near infrared spectral range, have been performed with the ESO-NTT in Chile (4 runs) and the Telescopio Nazionale Galileo (TNG) at the Canary Islands (4 runs).

Telescopio Nazionale Galileo

47 spectra have been recorded with the TNG in the course of four runs performed in December 2002, July 2003, May 2004 and June 2005 for a total of 12 nights, 6 in the visible and 6 in the NIR.

In the visible we used the *Low Resolution Spectrograph (LRS)* with the LR-R Grism which provides a resolving power of about 300, in the 0.50-0.95 μm range. We used a slit aperture of $5''$ in order to minimise effects due to atmosphere differential refraction. For the same reason the slit was oriented along the parallactic angle, for both asteroids and solar analogues.

In the near-infrared (NIR) we used *NICS (Near Infrared Camera Spectrometer)* equipped with the AMICI prism, which provides a resolving power of about 50 almost constant through out the range 0.8-2.5 μm. In the NIR we used a $2''$ slit width. As the influence of the differential refraction is less relevant in the NIR, we oriented the slit along the direction of the motion of every asteroid and along the parallactic angle for solar analogues.

For both visible and NIR, to minimise the possibility of losing objects, we decided to check the position of each moving target on the slit every 15-20 minutes, depending on the velocity of the asteroid. Longer exposures, needed on fainter objects, have been split in shorter ones, repeated as many times as needed to reach the required S/N ratio.

ESO - New Technology Telescope

70 spectra have been recorded with the ESO-NTT during four runs in October 2000, November 2001, May 2003 and December 2004, for a total of 16 nights, 6 in the visible and 10 in the NIR.

For the visible observations the NTT was equipped with *EMMI (ESO Multi–Mode Instrument)* in low resolution spectroscopy mode. The disperser element was the Grism #1 which gives a dispersion of 0.59 nm/pix, and the spectra obtained are in the range 0.38–1.0 μm with a resolution of 270 (for a slit of $1''$). As for TNG+LRS we used a slit aperture of $5''$. We oriented the slit along the parallactic angle for all objects, for both asteroids and solar analogues.

In the NIR we used NTT equipped with *SOFI (Son OF Isaac)* in the low resolution mode with two different dispersers: the Grism Blue that in the range 0.95–1.64 μm gives a resolution of 1000 with a slit of $0.6''$; the Grism Red for the range 1.53–2.52 μm, with the same resolution. As for TNG+NICS we used a $2''$ slit width for all objects. We oriented the slit along the direction of the motion for every asteroid observed and along the parallactic angle for solar analogues.

Data Reduction

For the data reduction we used the software ESO-MIDAS, applying the general procedures that can be described in the following steps: subtraction of the electronic background signal for each row frame, correction for the non uniformity of the images, cosmic rays removal and sky subtraction.

At this point the two dimensional spectra were collapsed to one–dimension and then calibrated in wavelength. The latter procedure was done using spectra of calibration lamps, namely *He, Th, Ne, Ar* lamps. The resulting uncertainty in the wavelength position is less than 4 Å.

Particular care has been paid to the correction for atmospheric extinction. To do that several Landolt G stars (Landolt 1973) and Hyades 64 were observed during the nights at different airmasses. As proof of the accuracy of our method we computed the ratio between the solar analogues' spectra, obtaining a low noise, almost constant curve with a maximum deviation of 5% around 1[1]. The ratio between stars shows a P–Cygni profile around 0.76 μm, due to the atmospheric O_2, but this ar-

[1]They were also observed in previous runs together with the solar analogue star P330E (Colina & Bohlin 1997) and they present similar spectra in the infrared region, so we used them as solar analogues for both visible and NIR.

tificial feature is restricted to a narrow wavelength interval and does not affect the behaviour at other wavelengths.

Finally, we obtained the reflectivity by dividing the asteroid spectrum by the solar analogue's. The uncertainty on the reflectivity introduced by the division of the asteroid's spectra by analogues' spectra is estimated to be of the order of 5% at most.

In the NIR image owing to the high luminosity and variability of the sky, special precautions were used. During the acquisition the telescope was moved by few arcmin in order to obtain a sequence of spectra located at different positions on the array. Let A and B be the images corresponding to the two different positions of the telescope. To reduce rapid sky variations, every image at position A is the result of the average of many consecutive subframes made automatically by the instrument. The telescope then moves to position B and repeats the same procedure, completing a cycle. Then a new cycle $A-B$ starts and so on, until the total exposure time is reached. At the end of the acquisition a sequence of images $A_1, B_1, A_2, B_2 \ldots$ is produced. The frequency of switching between the position A and B was typically of few minutes.

The reduction has been performed by using the MIDAS package. Basically, the reduction consists of a complex sequence of addition, subtraction and alignment of all the frames A_i, B_i. The resulting spectrum corresponds to that with the required total exposure time, and at this stage the presence of the sky (including the random fluctuations) is almost completely removed. This is because the sky and the random fluctuations cancel each other when enough images are added. The resulting uncertainty due to the sky is estimated to be of the order of 1–2%. At this point, the collapse of the spectra and the wavelength calibration proceed as in the visible, resulting in an uncertainty in the wavelength position less than 4 Å. On the contrary, the atmospheric extinction in the NIR cannot be done as in the visible, owing to the rapid changes of the atmospheric absorption. The strategy we followed to reduce the effect of the atmosphere was to observe solar analogues as close as possible (in term of airmass) to the asteroids. Finally, the spectra of the asteroids were divided by the solar analogue ones to get the reflectivity. By comparison of the solar analogues taken for each night, we estimated an uncertainty of the order of 6–8% introduced by this division. More precisely:

- The bias subtraction is performed by $D_i = A_i - B_i$, for each pair of the sequence. As a consequence, also the sky is at the same time subtracted. However, due to the rapid variation of the sky, its subtraction is always not perfect

at this stage;

- The images D_i contain two spectra (one positive and one negative, corresponding to the A_i and B_i respectively), so the next step is to algebraically add them all. In practice, this is done by subtracting to the images D_i a shifted D_i, that we call $D_{i,sh}$. The shift has to be done in such a way to exactly superimpose the positive spectra of the D_i with the negative one of the $D_{i,sh}$: $S_i = D_i - D_{i,sh}$. At this point the mean level of the sky around the spectra is almost zero, except for the random fluctuations. The resulting uncertainty due to the sky is estimated to be of the order of 1–2%;

- All the spectra in the images S_i have been added: $S = \sum_i S_i$, after their alignment. The resulting spectrum corresponds to one with the total exposure time required and at this stage the presence of the sky (also the random fluctuations) is almost completely removed. This is because the random fluctuations cancel each other when enough images are added;

- Collapsing the two dimensional spectra to one–dimension: the same as in the visible;

- The wavelength calibration proceeds as in the visible, resulting in an uncertainty in the wavelength position less than 4Å. On the contrary, the atmospheric extinction in the NIR cannot be done, owing to the rapid changing of the atmospheric absorption. The strategy we followed to reduce the effect of the atmosphere was to observe solar analogues as near as possible (in term of airmass) to the asteroids;

- Division of the asteroid spectrum by the solar analogue one to get the reflectivity. By comparison of the solar analogues taken for each night, we estimated an uncertainty of the order of 6–8% introduced by this division.

All the spectra have been smoothed with a median filter calculating the average over a 3 pixels window around each pixel, and replacing the original value by the average value only if the average differs more than 1/10th of the original intensity. The resulting small reduction in resolution does not affect our interpretation of the asteroids' spectral behaviour. The visible, NIR blue and NIR red spectra have not been acquired simultaneously (intervals of about one day), so we implicitly assume that the surface of the objects is homogeneous.

3.2.2 The spectra

Table 3.1: SINEO objects observed.

num	name	Spec. range	Telescope
(719)	Albert	0.41 - 2.45	NTT
(1916)	Boreas	0.41 - 0.97	NTT
(2063)	Bacchus	0.41 - 0.94	NTT
(3102)	Krok	0.41 - 2.45	NTT
(3103)	Eger	0.41 - 0.98	NTT
(3122)	Florence	0.41 - 0.94	NTT
(3362)	Khufu	0.41 - 0.98	NTT
(3553)	Mera	0.76 - 2.49	TNG
(3753)	Cruithne	0.41 - 2.53	NTT
(4587)	Rees	0.50 - 2.47	TNG
(4660)	Nereus	0.41 - 1.65	NTT
(5143)	Heracles	0.41 - 0.94	NTT
(5645)	1990SP	0.43 - 0.93	NTT
(5751)	Zao	0.41 - 1.61	NTT
(6489)	Golevka	0.41 - 2.52	NTT
(6491)	1991OA	0.41 - 0.94	NTT
(7336)	Saunders	0.51 - 1.03	TNG
(7341)	1991VK	0.41 - 2.50	NTT
(8013)	Gordonmoore	0.50 - 2.45	TNG
(8567)	1996HW1	0.51 - 2.49	TNG
(11054)	1991FA	0.41 - 2.49	NTT
(25330)	1999KV4	0.41 - 1.34	NTT
(26379)	1999HZ1	0.41 - 0.93	NTT
(31210)	1998BX7	0.41 - 0.97	NTT
(33342)	1998WT24	0.41 - 2.36	NTT
(35107)	1991VH	0.51 - 2.49	TNG
(35396)	1997XF11	0.51 - 2.49	TNG
(48603)	1995BC2	0.51 - 2.49	TNG
(52340)	1992SY	0.51 - 2.49	TNG
(54071)	2000GQ146	0.41 - 2.49	NTT+TNG
(54789)	2001MZ7	0.76 - 2.49	TNG
(65674)	1988SM	0.41 - 1.65	NTT
(65996)	1998MX5	0.51 - 2.47	TNG
(66251)	1999GJ2	0.50 - 2.49	TNG
(68346)	2001KZ66	0.50 - 2.45	TNG
(68372)	2001PM9	0.51 - 2.43	TNG

continued on next page

Table 3.1 – continued from previous page

num	name	Spec. range	Telescope
(68548)	2001XR31	0.40 - 1.65	NTT
(85989)	1999JD6	0.52 - 2.47	TNG
(86667)	2000FO10	0.76 - 2.49	TNG
(87024)	2000JS66	0.52 - 2.49	TNG
(87684)	2000SY2	0.41 - 1.50	NTT
(88710)	2001SL9	0.41 - 2.48	NTT+TNG
(98943)	2001CC21	0.51 - 2.49	TNG
(99935)	2002AV4	0.41 - 2.52	NTT
	1991BN	0.76 - 2.49	TNG
	1993FS	0.41 - 0.93	NTT
	1997UH9	0.41 - 0.97	NTT
	1998KG3	0.41 - 0.93	NTT
	2000EZ148	0.41 - 2.48	NTT
	2000QN130	0.41 - 2.42	NTT
	2000RL77	0.41 - 0.98	NTT
	2000RS11	0.41 - 0.95	NTT
	2000SA10	0.41 - 2.39	NTT
	2001CL42	0.41 - 1.65	NTT
	2001FZ6	0.41 - 1.65	NTT
	2001LF	0.41 - 1.65	NTT
	2001RB18	0.41 - 2.53	NTT
	2002AL14	0.51 - 2.47	TNG
	2002DB4	0.76 - 2.49	TNG
	2002NX18	0.51 - 2.49	TNG
	2002QE15	0.51 - 2.49	TNG
	2002TB9	0.50 - 0.99	TNG
	2002TD60	0.51 - 2.49	TNG
	2002TP69	0.51 - 2.49	TNG
	2002TS67	0.51 - 2.49	TNG
	2002TX68	0.51 - 0.92	TNG
	2002UN	0.51 - 2.49	TNG
	2002VP69	0.41 - 2.49	NTT+TNG
	2002VX17	0.76 - 2.49	TNG
	2002XK4	0.76 - 2.49	TNG
	2002YB12	0.51 - 2.48	TNG
	2003AJ73	0.41 - 0.94	NTT
	2003BT47	0.41 - 0.94	NTT
	2003DP13	0.41 - 0.94	NTT
	2003EG	0.41 - 1.65	NTT

continued on next page

Table 3.1 – continued from previous page

num	name	Spec. range	Telescope
	2003FH1	0.41 - 0.94	NTT
	2003FS2	0.51 - 1.03	TNG
	2003FT3	0.41 - 2.49	NTT
	2003FU3	0.41 - 0.94	NTT
	2003GA	0.41 - 1.65	NTT
	2003GJ21	0.41 - 0.94	NTT
	2003KR18	0.50 - 2.46	TNG

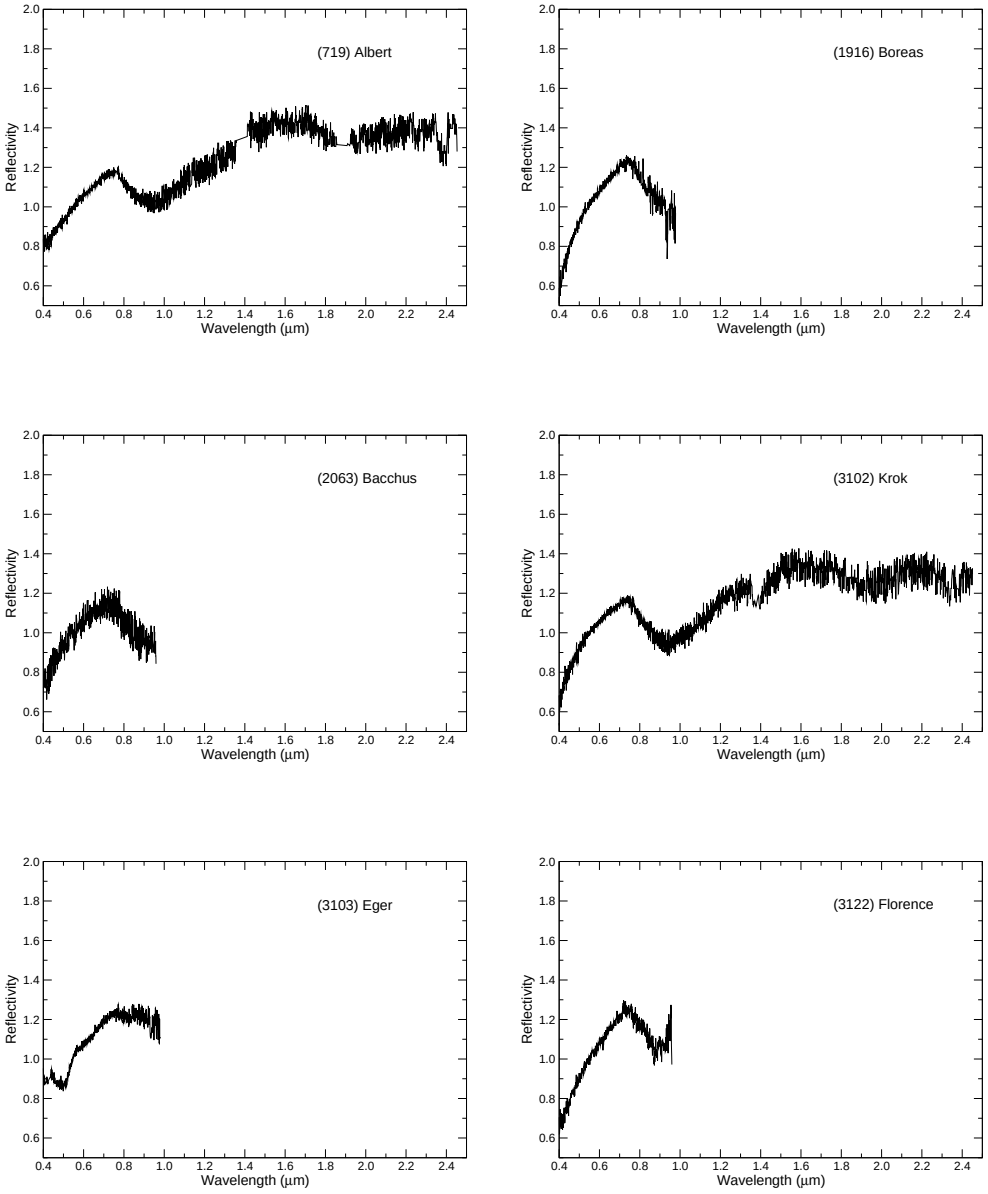

Figure 3.1: SINEO spectra.

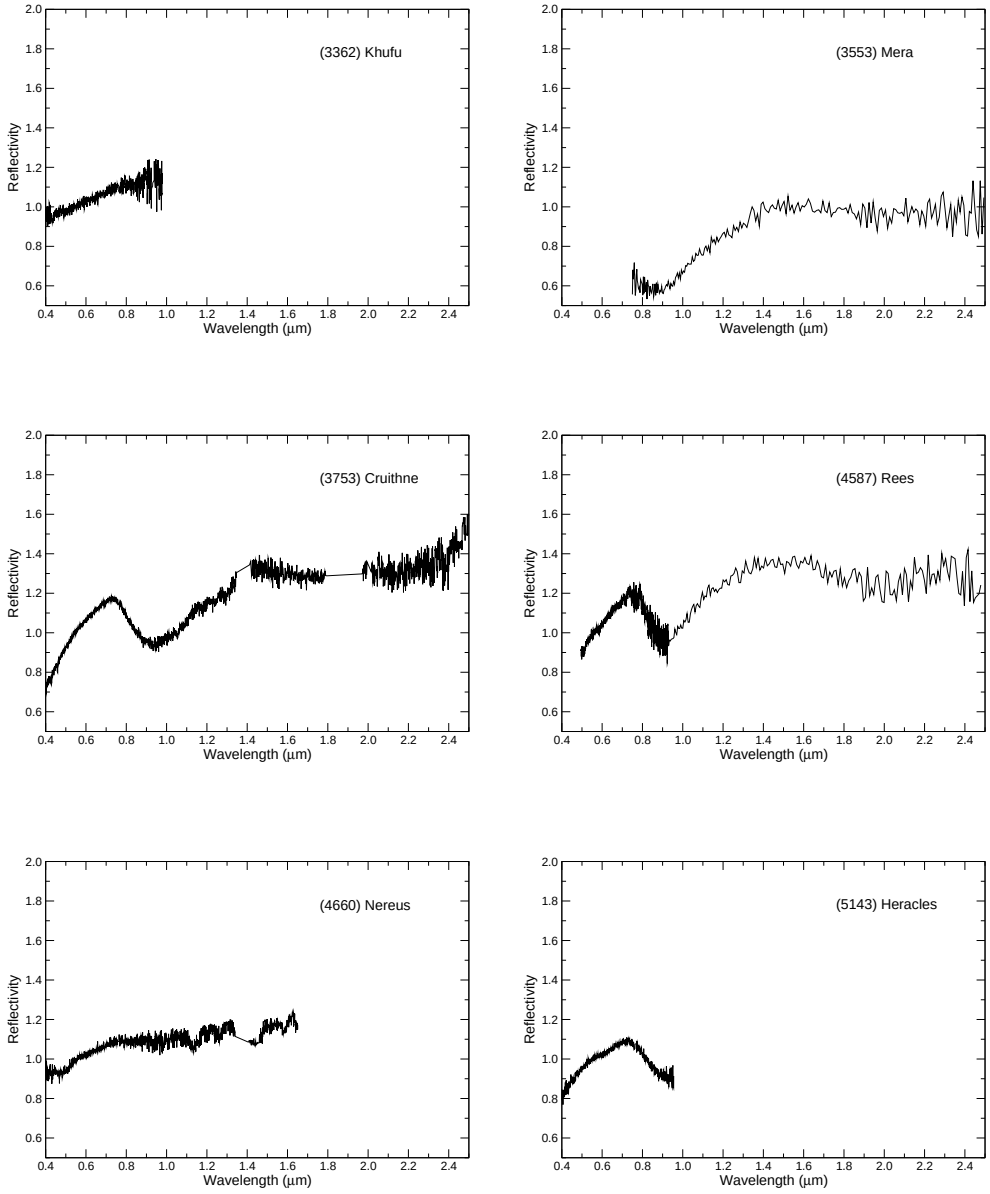

Figure 3.1: SINEO spectra (continued).

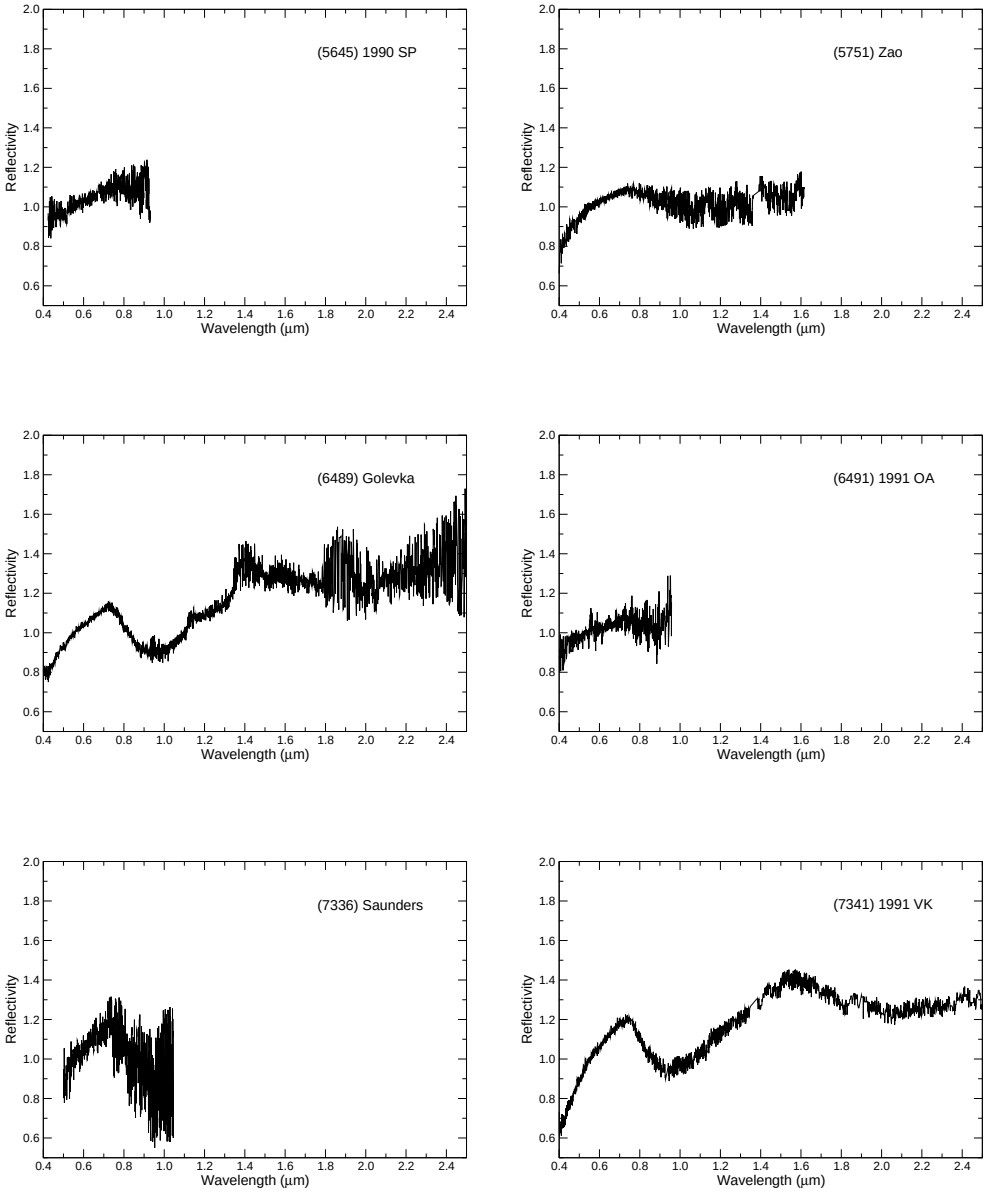

Figure 3.1: SINEO spectra (continued).

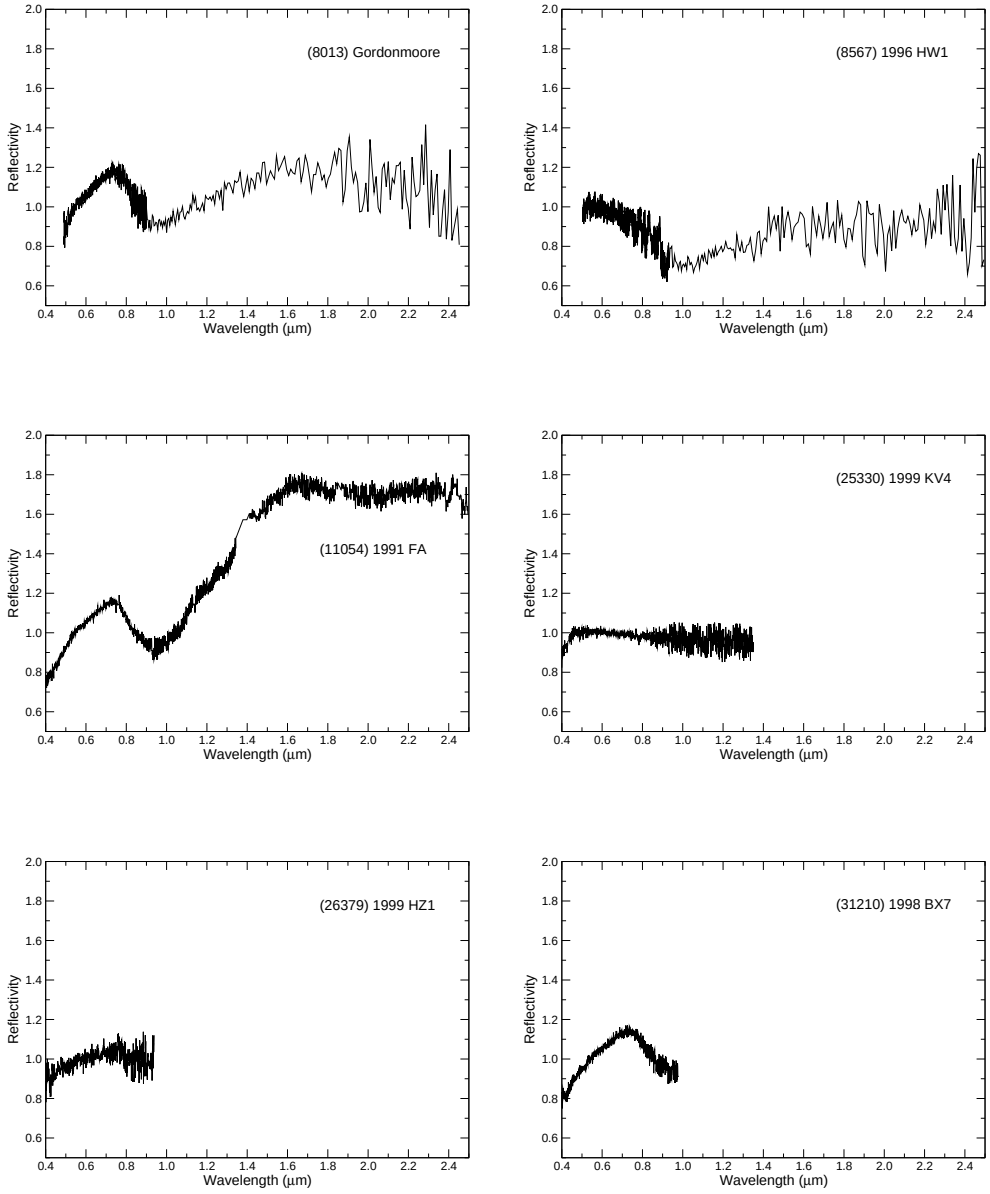

Figure 3.1: SINEO spectra (continued).

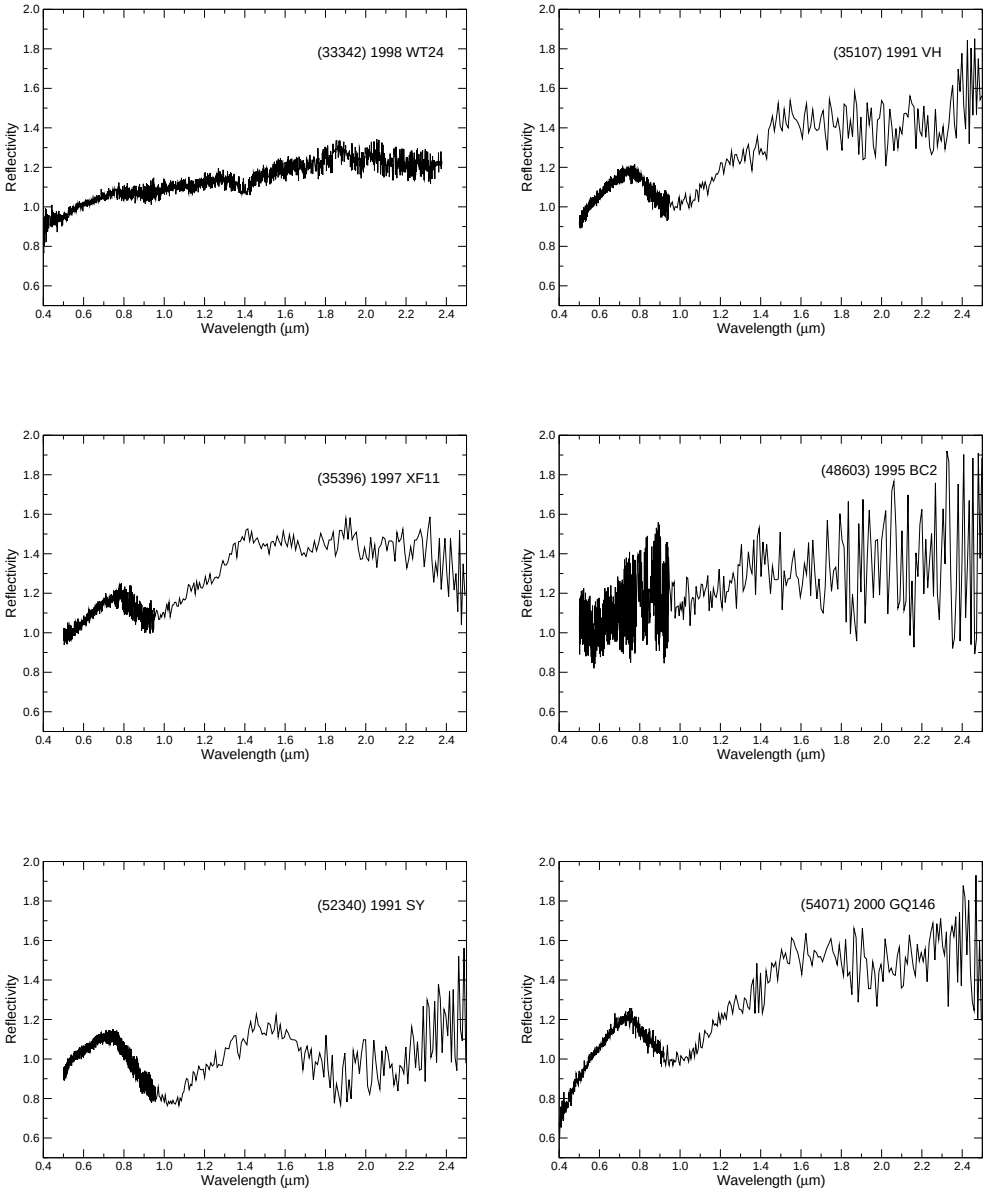

Figure 3.1: SINEO spectra (continued).

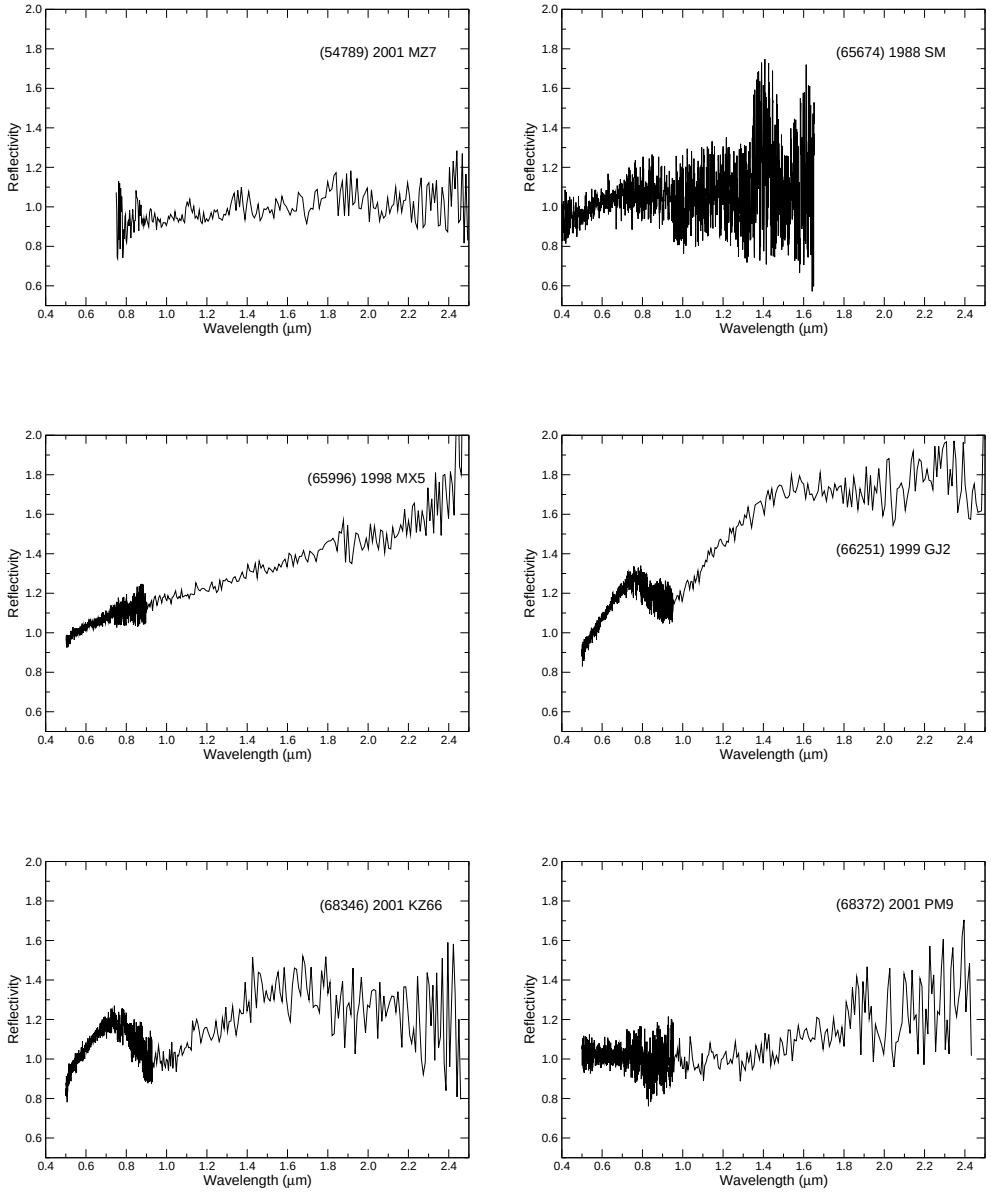

Figure 3.1: SINEO spectra (continued).

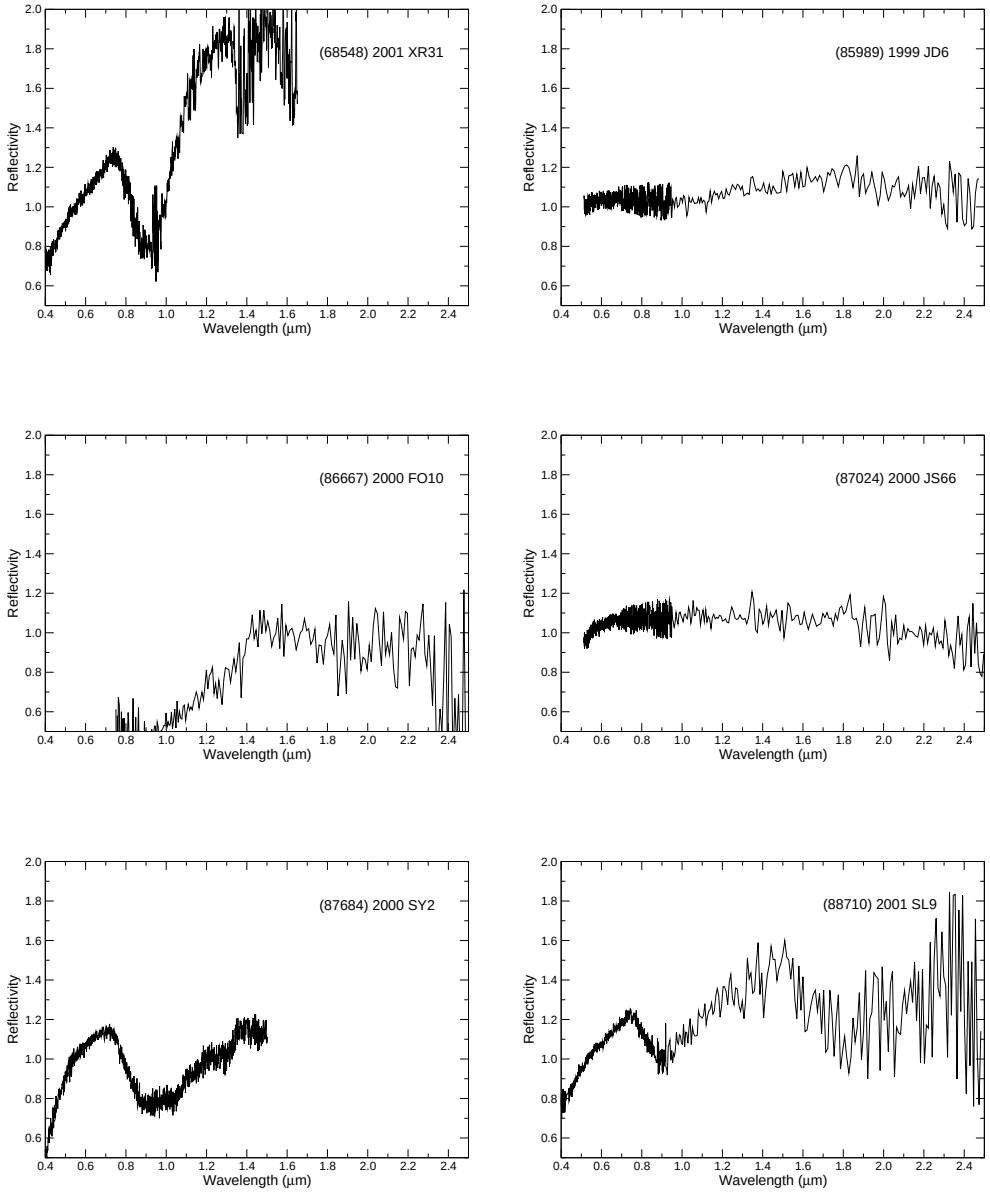

Figure 3.1: SINEO spectra (continued).

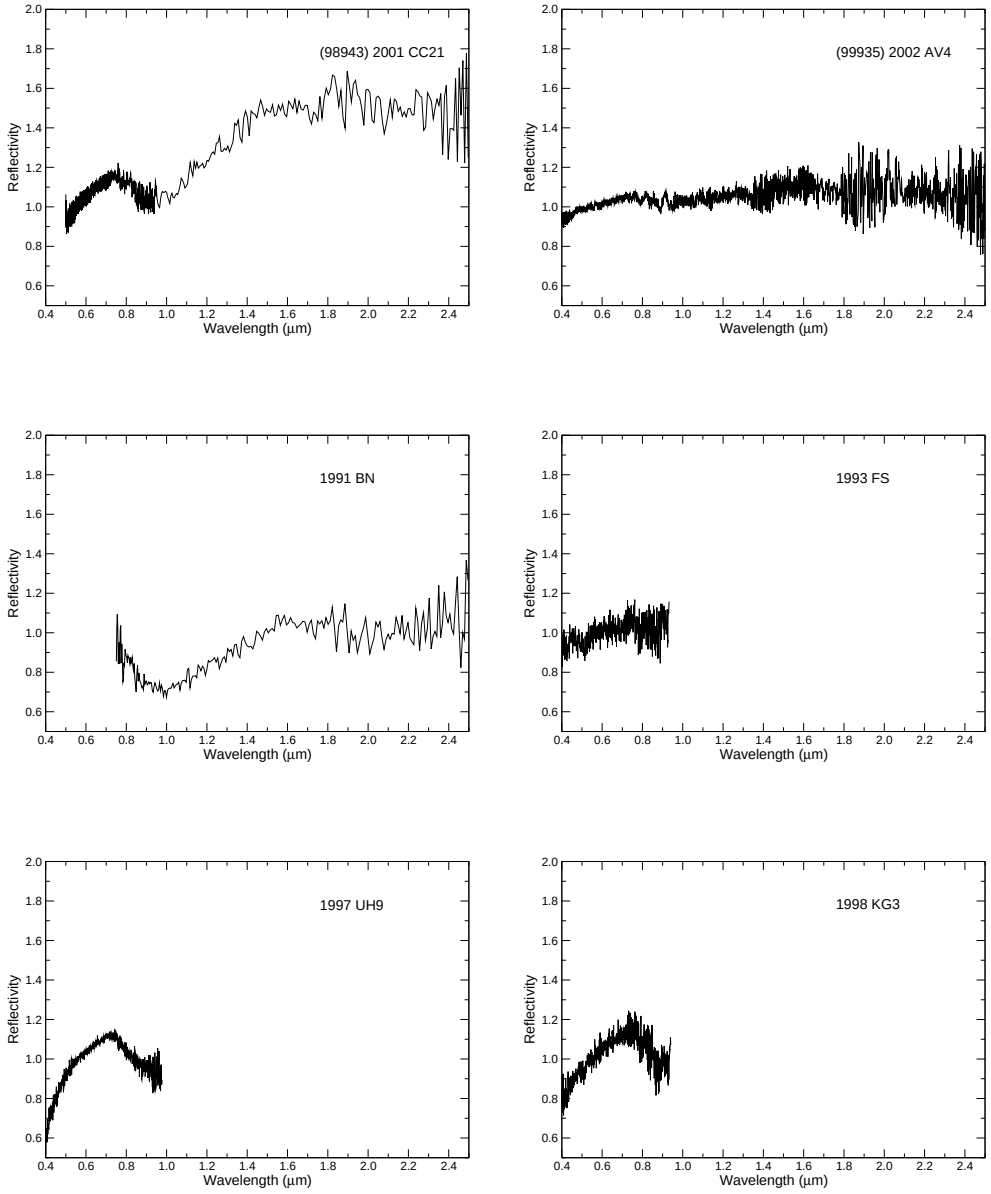

Figure 3.1: SINEO spectra (continued).

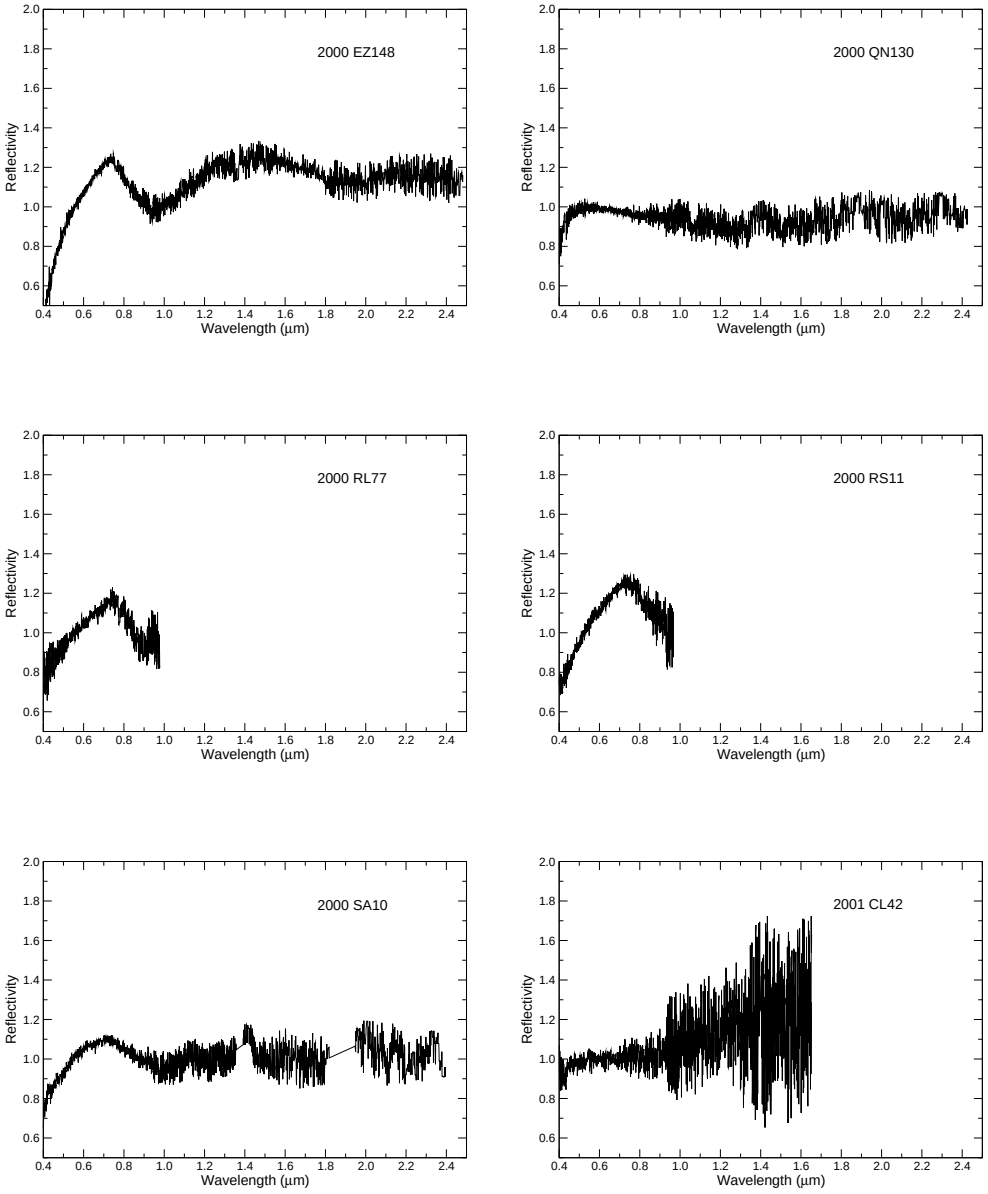

Figure 3.1: SINEO spectra (continued).

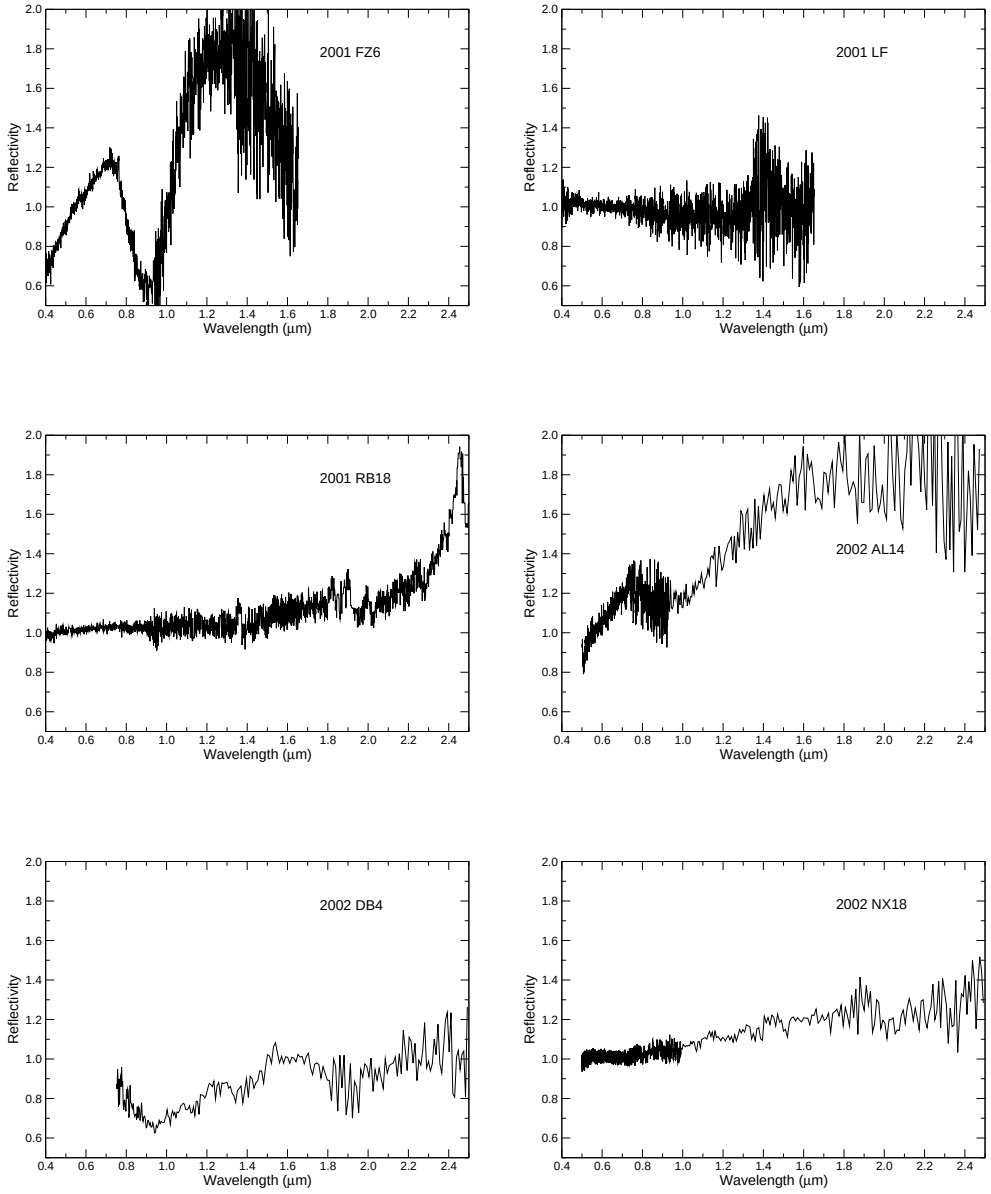

Figure 3.1: SINEO spectra (continued).

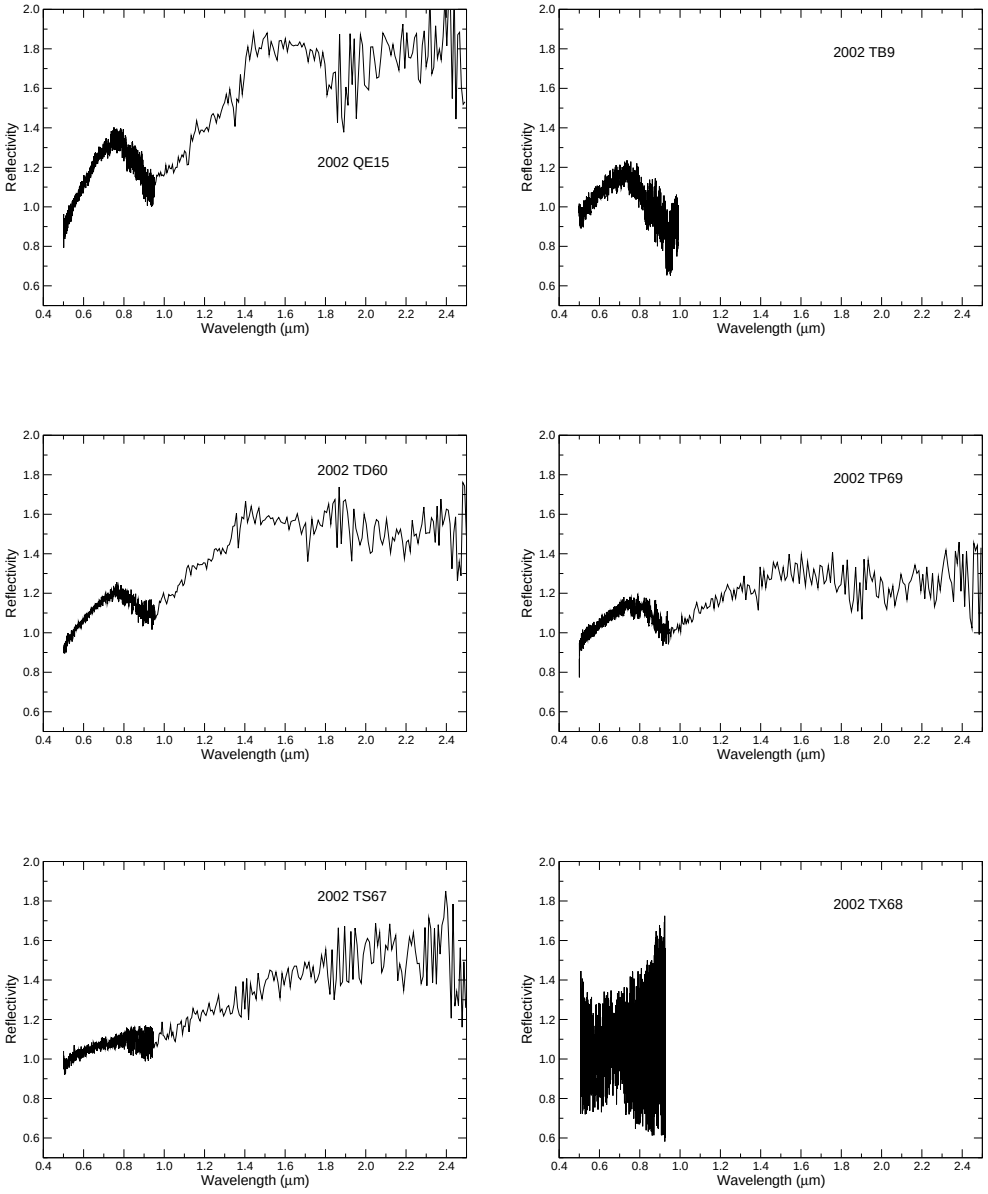

Figure 3.1: SINEO spectra (continued).

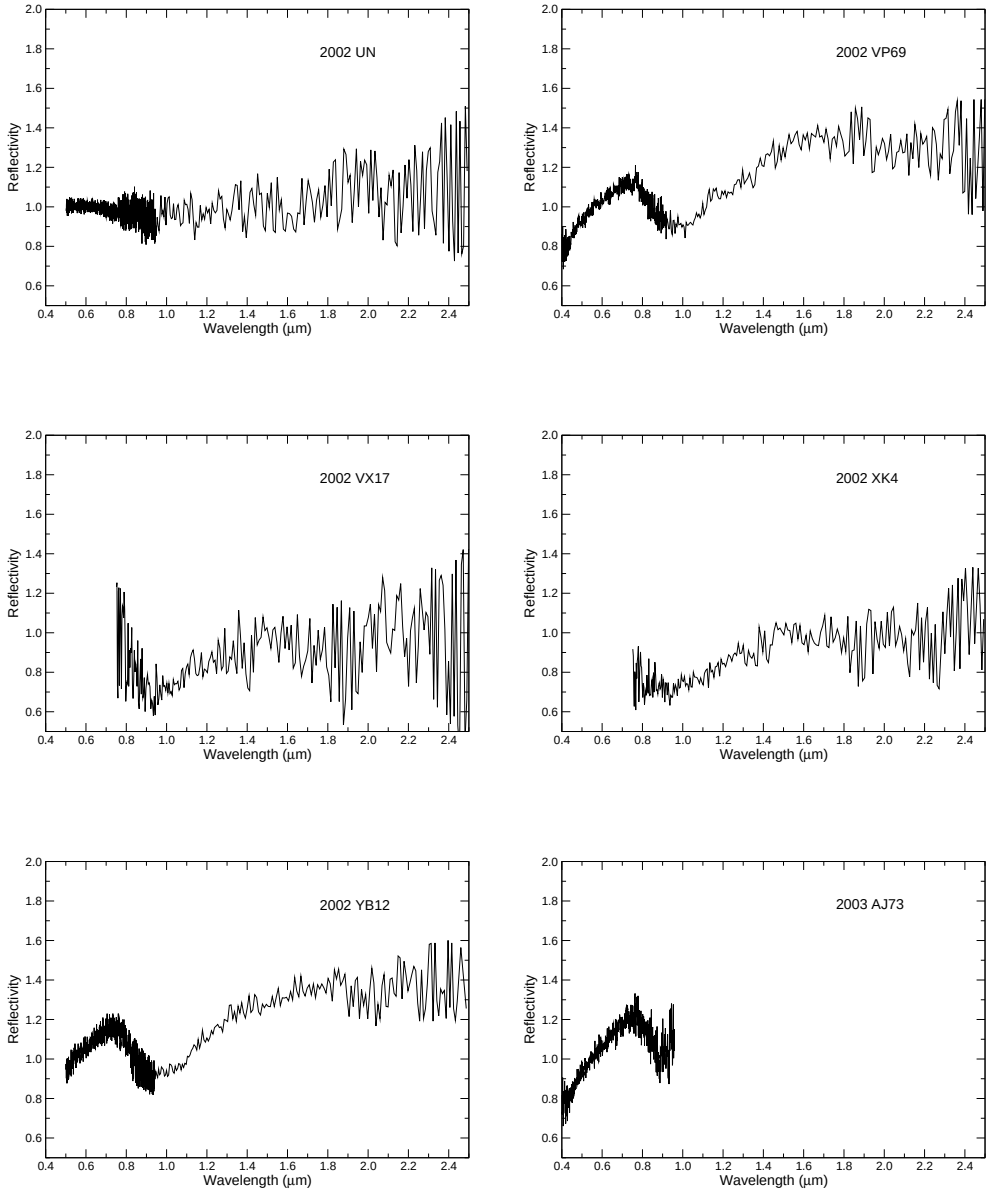

Figure 3.1: SINEO spectra (continued).

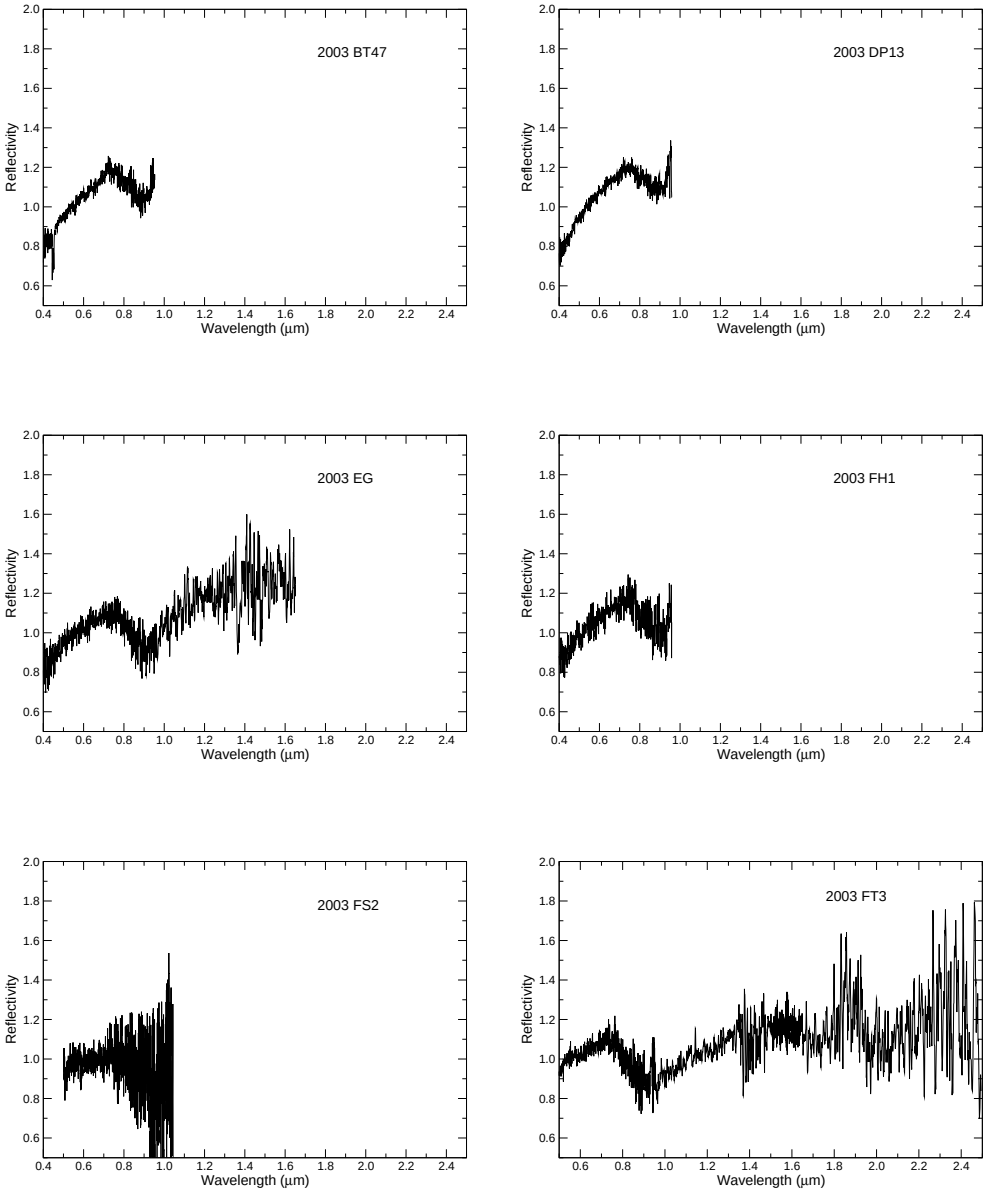

Figure 3.1: SINEO spectra (continued).

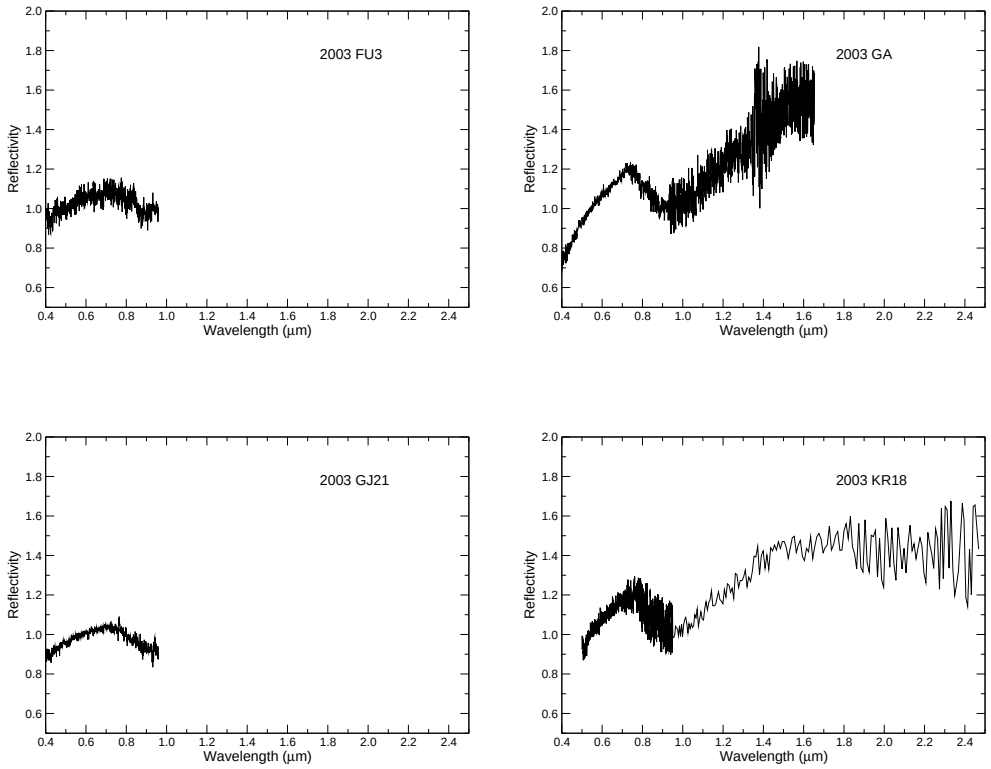

Figure 3.1: SINEO spectra (continued).

3.3 Other Surveys

3.3.1 SMASS on Near Earth Objects (SMASS NEO)

SMASS NEO consist in an internally consistent data set of visible and near-infrared spectroscopic measurements of about 310 Near Earth Objects observed from 1994 through 2002 as a complement to the Small Main-Belt Asteroid Spectroscopic Survey (SMASS, http://smass.mit.edu/). The spectra are analysed in several published SMASS results (see for example Xu et al. (1995), Bus (1999), Bus & Binzel (2002b), Binzel et al. (2001), Binzel et al. (2004), Binzel et al. (2004)).

For SMASS observations prior to 1997, visible wavelength measurements were made almost exclusively with the Mark III long-slit spectrograph coupled to the Michigan- Dartmouth-MIT Observatory (MDM) 2.4-m telescope located on the

southwest ridge of Kitt Peak, Arizona.

In 1998 the SMASS visible wavelength measurements began to be made using the Double Spectrograph on the Palomar Observatory 5-m Hale telescope. SMASS NEO visible wavelength measurements were also begun using the RCSP spectrograph on the Kitt Peak National Observatory 4-m Mayall telescope in 1999 (Binzel et al. 2001). While spectra obtained at MDM, Palomar, and Kitt Peak generally ranged only out to 0.92 μm, a program to extend measurements out to 1.6 μm was begun at the NASA Infrared Telescope Facility (IRTF) in 1997 (SMASSIR).

Some results are from a one night visible spectroscopy run on the Keck II 10-m. LRIS (low resolution imaging spectrometer) was utilised to obtain spectra over the wavelength range of 0.5- to 1.0-μm. Finally, some results are from the newly operational Magellan I 6.5-m telescope at Las Campanas, Chile, with a Boller and Chivens spectrograph, able to cover the wavelength range of 0.5- to 0.9-μm.

The MIT-UH-IRTF Joint Campaign for NEO Reconnaissance

Recent Observation (from September 2004) were obtained and by the *"The MIT-UH-IRTF Joint Campaign for NEO Reconnaissance"* (Richard P. Binzel (MIT), Andrew S. Rivkin (APL), Alan Tokunaga and Schelte J. Bus (U. Hawaii)).

The *IRTF (Infrared Telescope Facility)* on Mauna Kea, Hawaii, is operated by the University of Hawaii in cooperation with the NASA, Office of Space Science, Planetary Astronomy Program: the MIT, the University of Hawaii, and the NASA IRTF are being combined in a joint campaign to perform routine spectroscopic reconnaissance of near-Earth objects (NEOs). All spectroscopic observations obtained in this joint campaign are being made publicly available in near-real time via the website http://smass.mit.edu/minus.html.

The spectra present a 0.8-2.5 μm wavelength range measured using the instrument "SpeX" on the NASA IRTF. When available, visible wavelength spectral data are also included from the MIT SMASS observing program. Spectra presented in the website are considered to be in the public domain and may be freely used for any purpose.

Chapter 4

Data Analysis

All the spectra acquired and analysed with MIDAS are then collected in a data set and utilised for further analysis: the taxonomic classification, the *Principal Component Analysis*, the comparison with meteorite spectra, the study of slopes distribution and of the possible effects of the space weathering on asteroids.

In the following all these topics, and other works still in progress, will be described in detail.

4.1 Taxonomic Classification

The taxonomic classification of the observed NEOs has essentially been obtained by performing a best fitting between our data and the mean spectra of each spectral class proposed by Bus (1999) on SMASSII data.

Bus taxonomic definitions are restricted to visible data, so we applied this analysis only to SINEO spectra for which visible measurements were available. We looked for a best fitting between each of our spectra (the range considered was 0.52-0.92 μm) and each of the Bus' mean types restricted to the same range. We overplotted the first four solutions to the NEO spectrum to check the best solution by eye, avoiding errors due for example to the high noise on the spectrum.

In tab 4.1 we summarise the classification done till now on all SINEO spectra.

NEOs spectra for which only the NIR was available were excluded from the previous analysis. However, the "taxonomic" information contained in a NIR spectra are so important that we attempted a rough classification by visual inspection. As reported in table 4.1 we divided them only in terms of complexes (S-, C-, X-) as a more detailed classification cannot be done.

Table 4.1: NEOs observed with TNG and NTT. For each asteroid the orbit type, inferred taxonomy, absolute magnitude, spectral range and meteorite analog, where available, are reported.
[a]: AM = Amor, AP = Apollo and AT = Aten.
[b]:v=visible; n=NIR with NICS@TNG; b,r=blue and red part, respectively, of the NIR with SOFI@NTT;
[c]: OC = ordinary chondrites; EC = enstatite chondrites; CC = carbonaceous chondrites; SW = possibly space weathered objects; – = no analog found (see text for further details). Within brackets "( )" there is a proposed analog where the observed NIR spectral range is not complete.

NEO	Orbit[a]	Tax	H	Spectral range[b]	Meteorite Analog[c]
(719) Albert	AM	S	15.8	v+b+r	SW
(1916) Boreas	AM	S	14.93	v	–
(2063) Bacchus	AP	Sq	17.1	v	–
(3102) Krok	AM	S	15.6	v+b+r	SW
(3103) Eger	AP	E	15.38	v	–
(3122) Florence	AM	Sa	14.2	v	–
(3362) Khufu	AT	Xe	18.3	v	–
(3553) Mera	AM	S-	16.49	n	OC
(3753) Cruithne	AT	S	15.1	v+b+r	SW
(4587) Rees	AM	Sr	14.98	v+n	SW
(4660) Nereus	AP	E	18.2	v+b	AC
(5143) Heracles	AP	Sk	14.0	v	–
(5645) 1990 SP	AP	Xe	17.0	v	–
(5751) Zao	AM	K	14.8	v+b+r	CC
(6489) Golevka	AP	Sq	19.2	v+b+r	SW
(6491) 1991OA	AM	Xc	18.5	v	–
(7336) Saunders	AM	Sr	18.77	v	–
(7341) 1991 VK	AP	Sr	16.7	v+b+r	OC
(8013) Gordonmoore	AM	Sr	16.63	v+n	OC
(8567) 1996HW1	AM		15.3	v+n	
(11054) 1991 FA	AM	Sa	17.2	v+b+r	SW
(25330) 1999 KV4	AP	C	16.8	v+b	–
(26379) 1999 HZ1	AP	Xc	18.4	v	–
(31210) 1998 BX7	AM	Sq	16.2	v	–
(33342) 1998 WT24	AT	Xe	17.9	v+b+r	CC
(35107) 1991 VH	AP	S	16.57	v+n	SW
(35396) 1997 XF11	AP	K	16.76	v+n	SW
(48603) 1995 BC2	AM	Xe	17.42	v+n	–
(52340) 1992 SY	AM	Q	17.65	v+n	OC

continued on next page

Table 4.1 – continued from previous page

NEO	Orbit[a]	Tax	H	Spectral range[b]	Meteorite Analog[c]
(54071) 2000 GQ146	AM	S	17.28	v+n	SW
(54789) 2001 MZ7	AM	X-	14.67	n	EC
(65674) 1988 SM	AM	Xk	18.3	v+b	(CC)
(65996) 1998 MX5	AM	Xk	18.22	v+n	–
(66251) 1999 GJ2	AM	Sa	16.82	v+n	SW
(68346) 2001 KZ66	AP	S	16.48	v+n	SW
(68372) 2001 PM9	AP	B	18.71	v+n	CC
(68548) 2001 XR31	AP	R	17.0	v+b	–
(85989) 1999 JD6	AT	Cg	16.99	v+n	CC
(86667) 2000 FO10	AT	S	17.30	v	–
(87024) 2000 JS66	AP	Xc	18.64	v+n	CC
(87684) 2000 SY2	AT	Q	16.4	v+b	(OC)
(88710) 2001 SL9	AP	Q	17.43	v+n	OC
(98943) 2001 CC21	AP	Sk	18.39	v+n	SW
(99935) 2002 AV4	AP	Xc	15.72	v+b+r	CC
1991 BN	AP	S-	18.99	n	AC
1993 FS	AM	X	19.06	v	–
1997 UH9	AT	S	19.69	v	–
1998 KG3	AM	Sq	22.30	v	–
2000 EZ148	AP	Sq	14.88	v+b+r	OC
2000 QN130	AM	C	17.78	v+b+r	CC
2000 RL77	AM	Sq	16.74	v	–
2000 RS11	AP	Sa	18.86	v	–
2000 SA10	AM	K	18.07	v+b+r	OC
2001 CL42	AP	X	17.10	v+b	(iron)
2001 FZ6	AM	V	18.22	v+b	(AC)
2001 LF	AM	B	17.74	v+b	(CC)
2001 RB18	AM	C	18.41	v+b+r	
2002 AL14	AT	Sl	17.67	v+n	SW
2002 DB4	AT	S-	16.41	n	OC
2002 NX18	AM	C	17.24	v+n	CC
2002 QE15	AM	A	16.19	v+n	SW
2002 TB9	AP	Sk	16.22	v	–
2002 TD60	AM	S	19.24	v+n	SW
2002 TP69	AM	Sk	21.63	v+n	SW
2002 TS67	AM	Xe	18.71	v+n	–
2002 TX68	AM	X	17.91	v+n	–
2002 UN	AM	B	17.12	v+n	CC
2002 VP69	AP	Sq	17.79	v+n	

continued on next page

Table 4.1 – continued from previous page

NEO	Orbit[a]	Tax	H	Spectral range[b]	Meteorite Analog[c]
2002 VX17	AM	S-	21.76	n	OC
2002 XK4	AP	S-	15.53	n	OC
2002 YB12	AP	Sq	18.34	v+n	SW
2003 AJ73	AM	S	18.49	v	–
2003 BT47	AM	S	17.55	v	–
2003 DP13	AM	S	17.20	v	–
2003 EG	AP	V	16.38	v+b	(AC)
2003 FH1	AP	Sk	18.03	v	–
2003 FS2	AM	Cg	18.78	v	–
2003 FT3	AM	V	18.44	v+b+r	OC
2003 FU3	AT	V	20.90	v	–
2003 GA	AM	Sr	21.07	v+b	–
2003 GJ21	AM	V	22.84	v	–
2003 KR18	AM	S	17.76	v+n	SW

4.1.1 Principal Component Analysis

Afterwards, to have another confirmation of the taxonomic classification, we applied the Principal Component Analysis (*PCA*) technique to the data, in a modified version of that proposed by Bus (1999).

In the original technique each spectrum is simplified by interpolating it with a cubic spline in the range 0.44-0.92 μm with a step of 0.01 μm (49 channels). A large part of our data, in particular spectra obtained with TNG+LRS detector, show useful information in a spectral range shorter than that one.

We therefore decided to take a shorter spectral interval, compatible with our available visible range, to apply the *PCA* to this data set and to check the information coming from the two plots (*slope*,$PC2'$) and ($PC2', PC3'$)[1].

In Fig. 4.1 we can see the plots of the restricted definition of the PCA applied on the SMASSII data. In both plots are then reported arrows indicating the variation of the values of *slope*, $PC2'$ and $PC3'$ for the correspondent Bus' mean type (specified with a label) from the original definition of PCA to the restricted one. This shows how the two plots change: the lack of information due to a lesser number of points

[1] In this analysis we defined as *slope* of a spectrum the slope of the best fitting straight line to each spectrum in the given wavelength range.

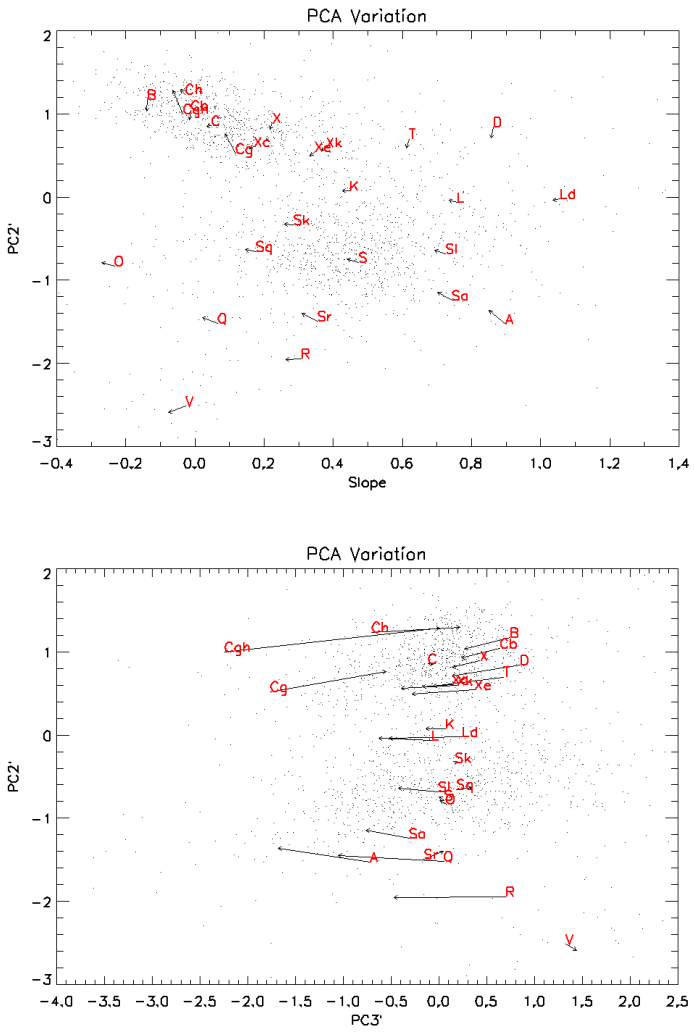

Figure 4.1: Restricted definition of PCA: $(Slope, PC2')$ and $(PC2', PC3')$ plots in the restricted range (0.52-0.92 μm). Arrows indicates the shift in the plot of the Bus' mean types from the original range (0.44-0.92 μm) to the restricted range (0.52-0.92 μm).

.

in a spectrum does not affect the statistical result of the analysis on the first two components (*slope, PC2′*). Moreover, the mean types still located in different zones on the (*slope,PC2′*) plot.

Fig. 4.2 shows histograms of the variation of the first three components from the original definition (in the 0.44-0.92 μm range) to the restricted one (in the 0.52-0.92 μm range).

In the upper panel we see a bi-modal distribution due to the the different vari-

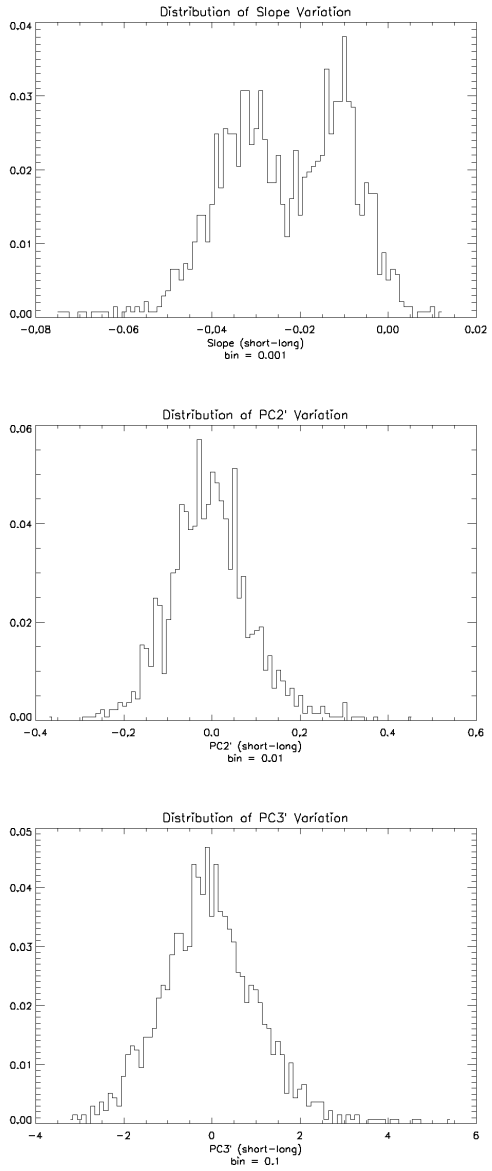

Figure 4.2: Restricted definition of PCA: histograms of the variations of *Slope* (upper panel), *PC2′* (middle panel) and *PC3′* (lower panel) between the two definitions, from the original range (0.44-0.92 μm) to the restricted range (0.52-0.92 μm). Comparison are made on the SMASSII data.

.

ation of taxonomic complexes: in the S-complex the lack of information in the 0.44-0.52 μm range subtract low reflectivity data of the blue-UV strong absorption band so that the average slope become flatter; X- and C-complexes have a generally weaker UV absorption band, so that the average slope of the spectrum is less sensi-

ble to the spectrum range shortening. This imply the two distributions of the slope variation, but not an overlapping of the different taxonomic classes and subclasses (Fig. 4.1).

Middle and lower panel of Fig. 4.2 show the distribution of variation of $PC2'$ and $PC3'$ respectively. While for $PC2'$ the variation does not imply an overlapping of the taxonomic classes and subclasses (Fig. 4.1), the $PC3'$ variation is such as to make $PC3'$ become meaningless.

Fig. 4.3 shows the plots of the first three components, in the shorter 0.52–0.92 μm range, computed on a set that includes all the SMASSII main belt data, all TNG NEOs visible spectra published in Lazzarin et al. (2005), and all the ESO-NTT NEOs visible spectra in Lazzarin et al. (2004). In the plots we also show the position of the Bus' mean types. In the upper panel it clearly results that we can still distinguish between the C-X-complexes and the S-complex. Moreover all S subclasses are still well separated.

As a final result, we found an excellent compatibility between the taxonomic classification obtained by the best fitting with the mean types and the location of the NEOs in the ($Slope$,$PC2'$) plane, as predicted by the PCA.

4.2 Taxonomy of peculiar objects

One characteristic of the observational strategy of the SINEO survey is to give taxonomic information of some near earth asteroids previously unclassified. Among them some objects present peculiar characteristics. We describe them here in detail.

4.2.1 An R-type asteroid within near-Earth objects?

We present now the visible and near-infrared spectroscopy of 2001 XR31, a previously unclassified small NEO. Although its spectrum resembles that of a basaltic body (V-like), it is somewhat peculiar and we discuss whether it can be a R-type instead of a V-type. If confirmed, this object would be the only R-type detected among NEOs so far. This would be very important because the R-class is very rare among minor bodies: only other 4 bodies (all main belt asteroids (MBAs)) have been classified as R-types.

Its spectrum presents the overall behaviour of igneous, V-like, objects. However its visible spectrum also presents many common aspects with another group of igneous bodies, those belonging to the R-class. Tholen (1989) introduced the dis-

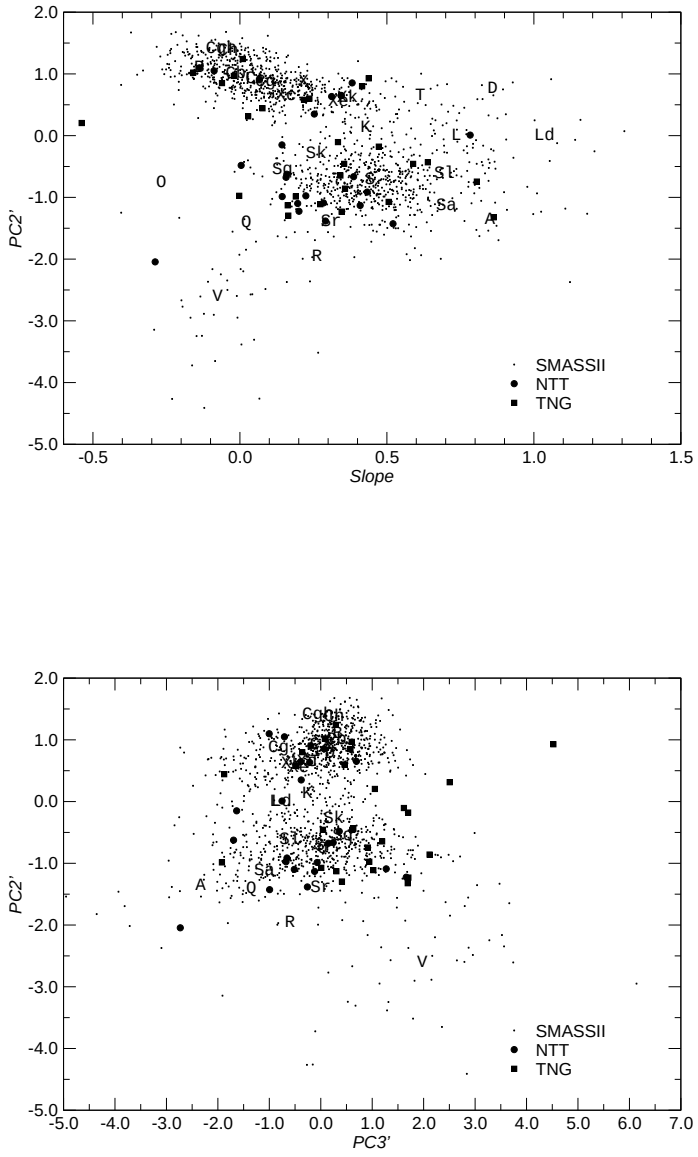

Figure 4.3: PCA computed in the range (0.52-0.92 μm) of the SMASSII data and SINEO data.

tinction between V- and R-class on the basis of the spectra of two peculiar MBAs, (4) Vesta and (349) Dembowska, respectively (for further details, see Gaffey et al. (1993). Bus taxonomy (Bus 1999) still kept this distinction, although he provided new spectra in both classes increasing the spread between each class. In particular

he found 3 more objects similar to (349) Dembowska, and hence classified as R-types. However, a detailed inspection of all the visible spectra of V- and R-types show that this division is somewhat weaker than that introduced by Tholen. This is because many asteroids classified as V-type have spectra similar to those of the R-types. Following the classification of Bus, the spectra are discriminated between V and R by a complex analysis which involves the value of the reflectivity at 0.75 μm and 0.92 μm, and in particular the latter has to be less than 0.82, for the V-type.

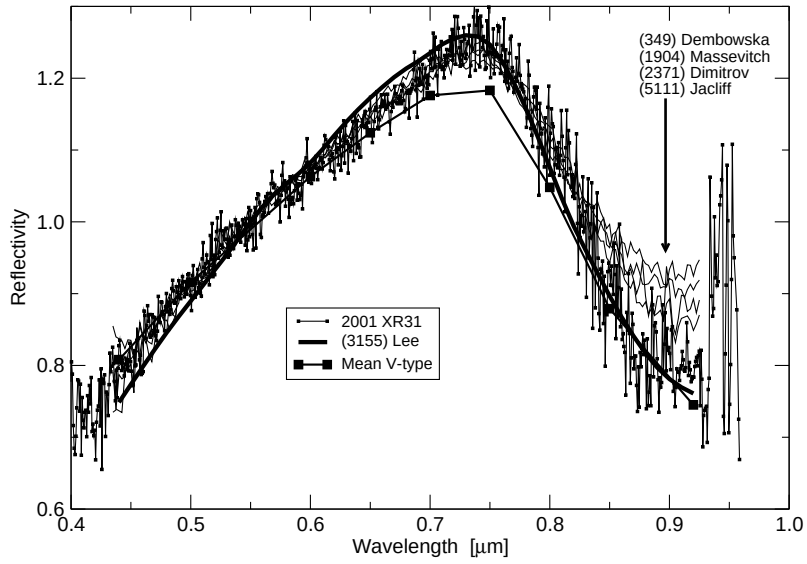

Figure 4.4: Comparison of 2001 XR31 with R-type MBAs (taken from Bus (1999)) in the visible region. The mean V-type and (3155) Lee are also shown (both from Bus (1999)).

According to this classification, 2001 XR31 would be at the border between V- and R-class (see fig. 4.4). However, we underline also that the spectrum of 2001 XR31 surprisingly overplots exactly the R-types in the range 0.4-0.85 μm. Moreover, we point out another similarity between the R-types and our NEO, namely on the basis of their behaviour within the range 0.86-0.95 μm. In fact, the reflectivity of all the R-type objects in this interval is noticeably constant (see fig. 4.4) while for the V-types it is generally slightly decreasing. In other words, the bottom of the 1 μm band is almost flat. Now, it is difficult to understand the origin of this behaviour, but it is believed to be significant for compositional differences. We point out that

it could be due to mixture of compounds which have the peak of the 1 μm band at slightly different wavelengths, for example by a mixture of olivine and pyroxene or a mixture of pyroxenes with different contents of Fe (e.g. see Gaffey 1997). To better show the differences between V-types and R-types, in fig. 4.4 we also report the object (3155) Lee which, among the V-types, is the one which closer resembles 2001 XR31. Figure 4.4 clearly shows that although the overall behaviour of these two objects is quite similar, there are differences in slope and the shape of the 1 μm band, reasons for which the spectrum of 2001 XR31 is best fitted by the R-types, instead of V-types.

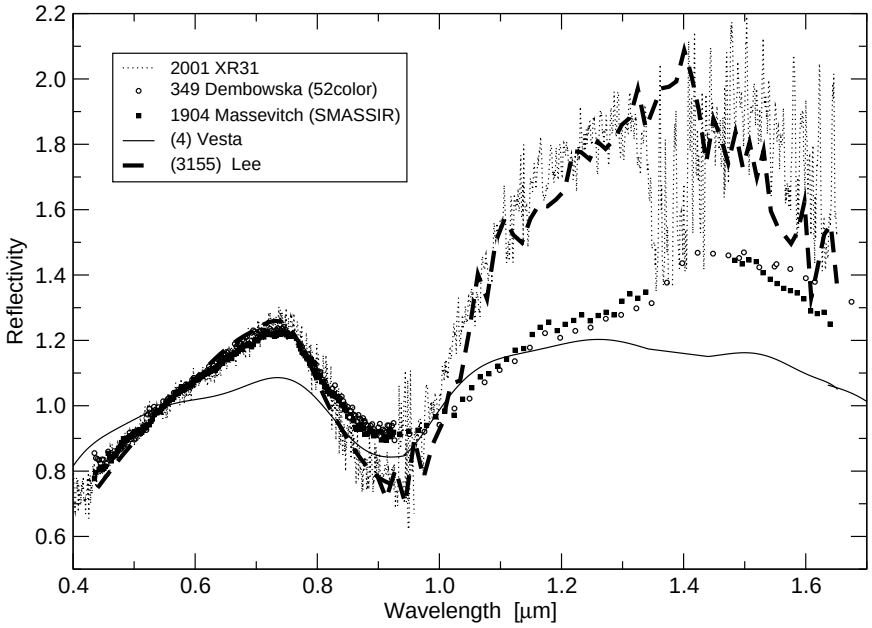

Figure 4.5: Comparison of 2001 XR31 with R-type asteroids in the visible and near infrared region. On the same plot, (4) Vesta and (3155) Lee are also shown. The NIR of (1904) Massevitch and (3155) Lee are from SMASSIR (Burbine & Binzel 2002), while the NIR of (349) Dembowska is from 52-Color survey (Bell et al. 1988).

However, the NIR (see Fig. 4.5) of 2001 XR31 does not resemble those of the only two available R-types. Anyway, the 2001 XR31 high values of reflectivity in the range 1.3-1.5 μm with respect to (349) Dembowska is likely the same kind of

discrepancy shown by the V-types and Vesta. For the latter a possible explanation has been found in grain size effects (Burbine et al. 2001): smaller particle sizes produce higher values of reflectivity. Other possible reasons able to increase the reflectivity could be compositional differences or space weathering. As shown by Hiroi & Sasake (2001), the spectrum of (349) Dembowska is well fitted by a mixture of space-weathered olivine (55%), space-weathered orthopyroxene (44%), and fresh olivine (1%). If 2001 XR31 is a fragment of (349) Dembowska, their differences could be affected by different degree of space weathering. Finally, the steep right-hand limb of the 2 μm band of 2001 XR31 would indicate a greater concentration of pyroxene on 2001 XR31 with respect to (349) Dembowska.

Concerning the intriguing possibility that 2001 XR31 (having an estimated diameter of about 1.3 km) is related to R-type instead of V-type, notice that the only possible known parent body is (349) Dembowska. This is because it has a diameter of about 140 km, while the other main belt R-types have diameter in the range 6-12 km, unless they are remnants of a larger R-type body which suffered a collision, but there is no evidence for that at the moment. Nevertheless other sources cannot be excluded.

The surface of (349) Dembowska is still poorly known. The only information about its shape comes from the analysis of the light curves (e.g. see Zappala et al. (1979)). As pointed out by Abell & Gaffey (2000), the light curves and spectral variations seem to indicate the presence of an albedo spot near the equator. Possibly it could be a trace of a cratering event, as also noted by Abell and Gaffey. If so, the differences observed in the NEOs spectra with respect to the R-types can results from NEOs being fragments of deepen layers which should have different composition considering the spot albedo variation.

However, (349) Dembowska is placed far from the strong ν_6 and 3:1 resonances, which are thought to be the main sources for near-Earth objects, and the delivery of its fragments into near-Earth space would have followed other routes. It has a proper semimajor axis of 2.925 AU which falls inside the 5:2 and 7:3 mean motion resonances. These resonances are probably not too efficient to produce NEOs, because they tend to push objects into high eccentricity orbits and eventually, when they reach a critical eccentricity for becoming Jupiter crosser, the objects are subsequently removed from the inner Solar System by close encounters with Jupiter (Moons & Morbidelli 1995; Gladman et al. 1997; Morbidelli & Gladman 1998). However this possibility cannot be ruled out, because for eccentricity lower than the critical value, some objects can have close encounter with Mars and the Earth

(Moons & Morbidelli 1995; Morbidelli & Gladman 1998), and eventually, they can be trapped in near-Earth space, as maybe indirectly prove by the presence of many C-types among NEOs. Concerning the inclinations, hypothetical (349) Dembowska fragments would have values within few tenths of that of (349) Dembowska itself (i.e. about 8 deg). For a comparison the present inclination of 2001 XR31 is 22.7 deg. Notice that, the dynamical behaviour of such fragments would be quite similar to that of Eos-like objects which have been investigated recently by Tsiganis et al. (2003). They found a mean resident-time in the 7:3 of 12.4 Myr, and that such Eos-like objects can reach inclination of about 16 deg, before being ejected from the resonance by close encounter with Jupiter. The variation of the inclination due to the evolution driven by the resonances alone can be of a few degree at most (see Fig. 3b in Tsiganis et al. (2003); Yoshikawa (1989)). A similar increase in inclination can probably also be achieved by close encounters with Earth and/or Venus, as shown for the Alinda class by Milani et al. (1989). Moreover, notice that at the present time, the orbit of 2001 XR31 is such that it can have ”strong” close encounter with the Earth and with Mars, and for this reason it is difficult to get constraints of its origin (see http://newton.dm.unipi.it/cgi-bin/neodys/neoibo).

Concerning the possibility that (349) Dembowska fragments can reach any resonance, we show in fig. 4.6 the distribution of fragments generated by (349) Dembowska after both a catastrophic collision and a cratering event. The fragments have been considered to be ejected isotropically (suitable for a catastrophic collision) or in a cone of semi aperture of 40 deg (suitable for a cratering event), with uniform distribution of velocity modules between 0 and 0.15 km s-1, which is roughly the escape velocity of (349) Dembowska (for more details of the model used see Marchi et al. (2001), Marchi et al. (2002)). The figure shows that fragments can easily reach the 7:3 resonance, for which a velocity of about 0.1 km s-1 is sufficient; while higher velocity ($\sim$ 0.5 km s-1) are needed to reach the 5:2 resonance. Also taking into account possible semimajor axis mobility, i.e. the Yarkovsky effect (Farinella & Vokrouhlicky 1999), it seems unlikely that the 5:2 has played a role in delivering fragments from (349) Dembowska.

4.2.2 New V-type asteroids in near-Earth space

Here we present visible and near-infrared spectroscopic observations of 4 previously unclassified small NEOs. In the visible range, they exhibit a good spectral match with Vesta: among the observed V-type NEOs and MB asteroids they are the

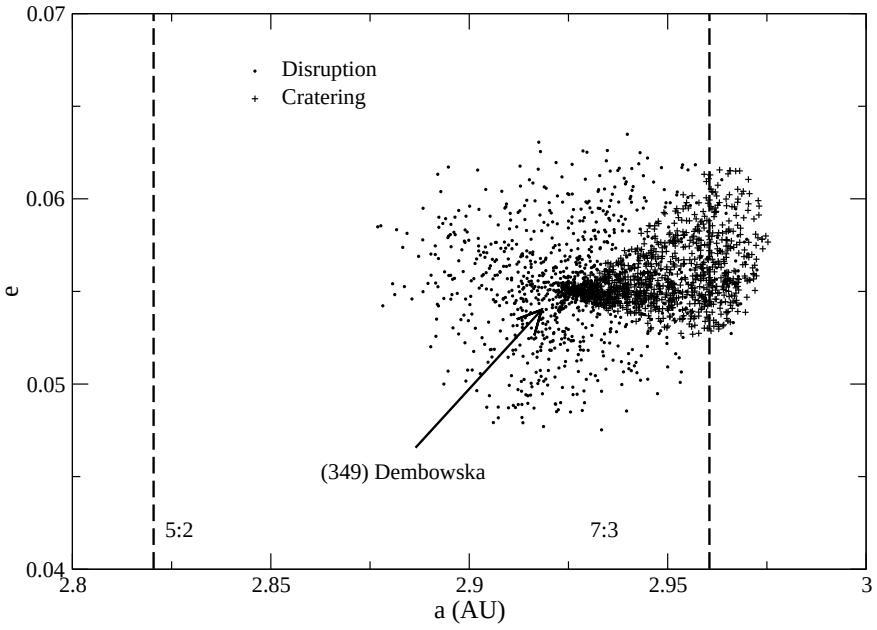

Figure 4.6: Distribution of ejecta from (349) Dembowska in the (a,e) plane, for catastrophic disruption and cratering event. In the latter case, the ejection cone is oriented along the direction of motion of (349) Dembowska. In both cases, the fragments are generated with a uniform distribution of velocity modules between 0 and 0.15 km $s^{-}1$, and for (349) Dembowska's true anomaly of 90 deg (see text).

most similar to Vesta. On the contrary, the near-infrared (NIR) spectra, obtained for two of them, show some discrepancies from Vesta. However, the quality of NIR data is too poor for a detailed compositional analysis.We discuss also, from a dynamical point of view, their possible delivery path from the MB.

In fig. 4.7 the visible spectra of the four observed NEOs are shown. For each body, the spectrum of the Asteroid (4) Vesta has been overplotted for a direct comparison.

They exhibit an excellent spectral match with Vesta, and no kind of systematic spectroscopic difference, as those, for instance, differentiating MB and NEO S-type asteroids (Binzel et al. 2002) is present. We also report the range of variation concerning the previously defined V-type asteroids on the basis of 39 V-type objects

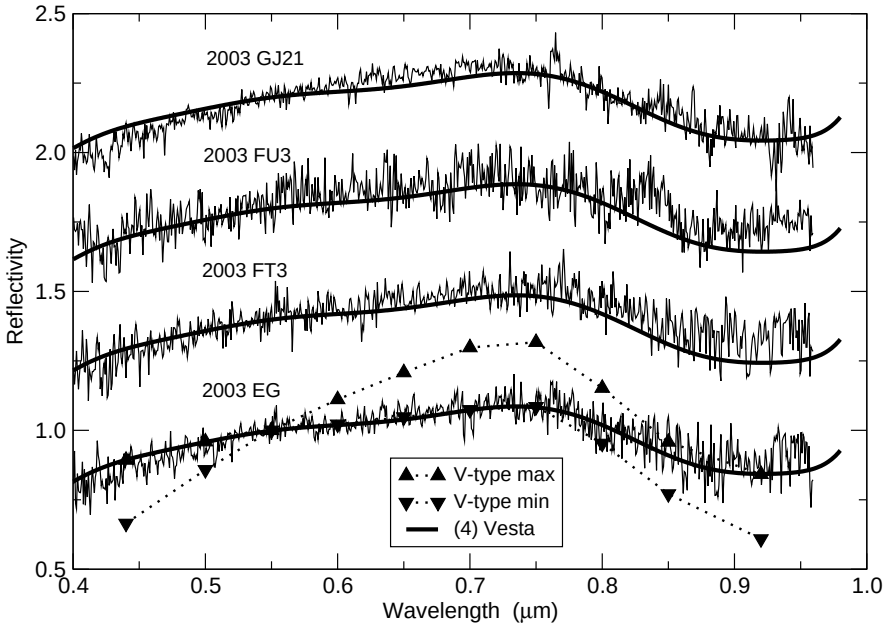

Figure 4.7: Comparison between the observed NEOs (namely, 2003 EG, 2003 FT3, 2003 FU3, and 2003 GJ21) and (4) Vesta in the visible region. The spectrum of (4) Vesta has been recorded (2001, November) with the same facilities. The spectra are shifted vertically for clarity. The reflectivity values are valid for 2003 EG. For 2003 EG the maximum and minimum spreading among V-types (Bus 1999) is also shown. In some parts of the plot the maximum or minimum curves are coincident with Vesta and thus masked.

found within SMASSII (Bus 1999; Bus & Binzel 2002b; Bus & Binzel 2002a). The presented NEAs are significantly more similar to (4) Vesta than the previously known V-type MB asteroids. The same may be true within the sample of V-type NEAs (a total of 15 bodies, see Binzel et al. (2002)), but the available information is not enough complete. The main differences between (4) Vesta and the other V-types are the slopes in the range 0.40-0.72 μm (from moderately to much redder than Vesta) and the depth of the 1 μm band (deeper than Vesta's: see Florczak et al. (2002); Burbine et al. (2001); Binzel & Xu (1993)). We are aware that neither differences in slope does necessarily indicate differences in composition, as shown by Kelley et al. (2003), nor the similar spectral behaviour between two objects necessarily establishes a genetic link. However, the similarity between (4) Vesta

and the NEOs, whose observations are presented here, stands as a striking feature. For this reason, in the following we shall compare our data not only to V-types in general, but also often to Vesta.

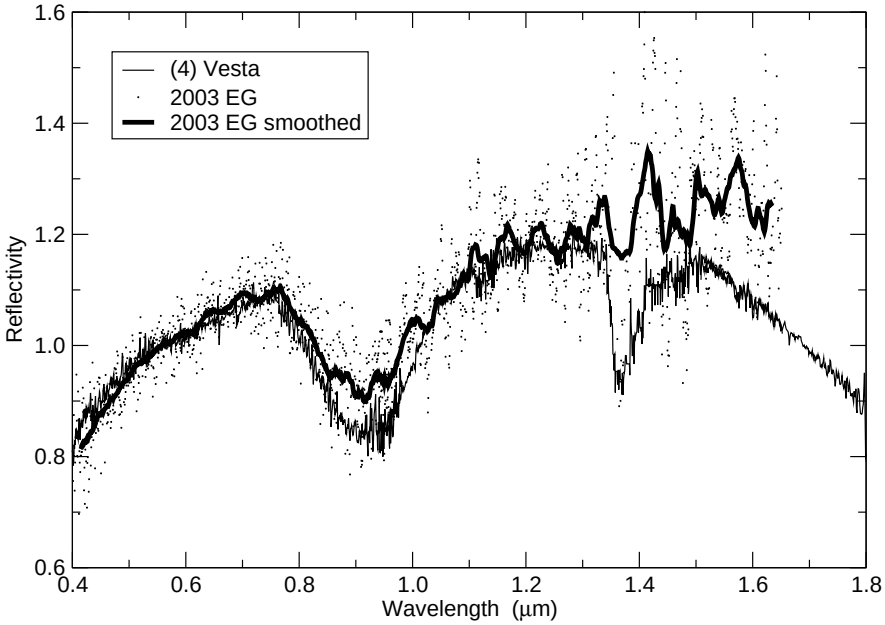

Figure 4.8: Comparison of the visible and near-infrared spectra of 2003 EG and (4) Vesta. The smoothed spectrum of 2003 EG is also shown, for a easier comparison.

For two NEAs in our sample, namely 2003 FT3 and 2003 EG, we performed also NIR observations; unfortunately these spectra are too noisy for a quantitative analysis of bands position and depth, which would be necessary for a detailed compositional analysis. The composite visible-NIR spectrum of 2003 EG (fig. 4.8) resemble that of (4) Vesta throughout all the observed range, and in particular the shape of the 1 μm band is similar. However, the depth of the 1 μm band is not the same, being deeper on Vesta than on 2003 EG, perhaps indicating a different content of pyroxene and/or olivine. Unfortunately, the 2 μm band is out of the measured range, thus preventing any detailed compositional analysis. Anyway, the high reflectivity level of 2003 EG at 1.6 μm suggests a lower content of pyroxene with respect to Vesta.

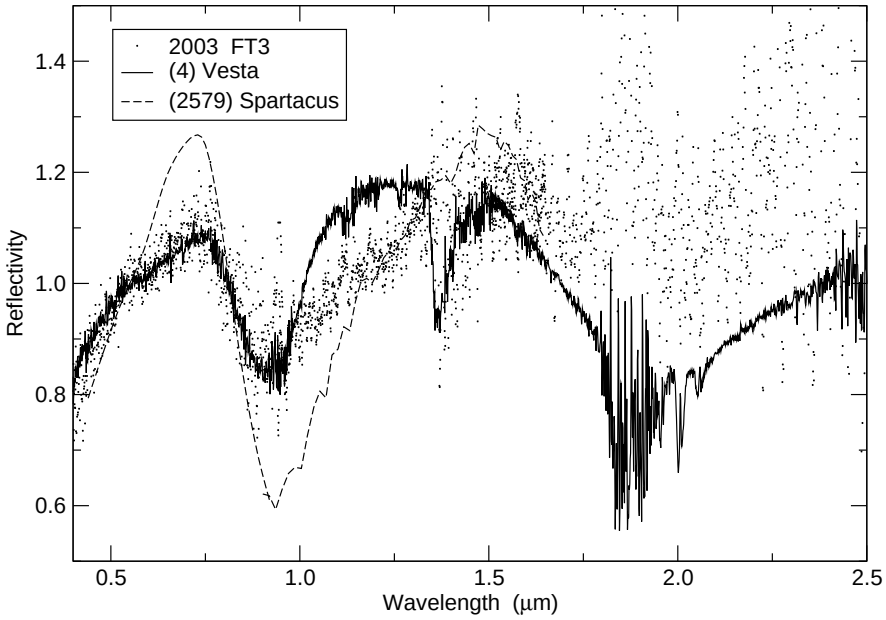

Figure 4.9: Comparison of the visible and near-infrared spectra of 2003 FT3 and (4) Vesta. The Main-Belt Asteroid (2579) Spartacus is also overplotted (Burbine & Binzel 2002).

The overall NIR spectrum of 2003 FT3 (fig. 4.9) is consistent with the V-type, but the right-hand limb of the 1 μm band is very peculiar and much different from other V-types (and from Vesta as well). Moreover the 2 μm band is less deep than that of Vesta. Similar features, for the first time detected among NEOs, have been observed at least in another MB V-type object, namely, (2579) Spartacus (Burbine et al. 2001). We stress that the spectra of Vesta, Spartacus and 2003 FT3 are rather different each other. However, the broad 1 μm bands of Spartacus and 2003 FT3 may suggest a compositional similarity (note also that no similar features have been detected among HED meteorites). The peculiar spectral features can be seen (here as for (2579) Spartacus, see Burbine et al. (2001)) as diagnostic of an excess of olivine and/or plagioclase, compared to typical V-types. Indeed, olivine has a broad profile at the right side of the 1 μm band and has no 2 μm band (e.g., see Hiroi & Sasaki (2001)) while plagioclase has a wide band that extends from 1 to 1.5 μm, and has no 2 μm band.

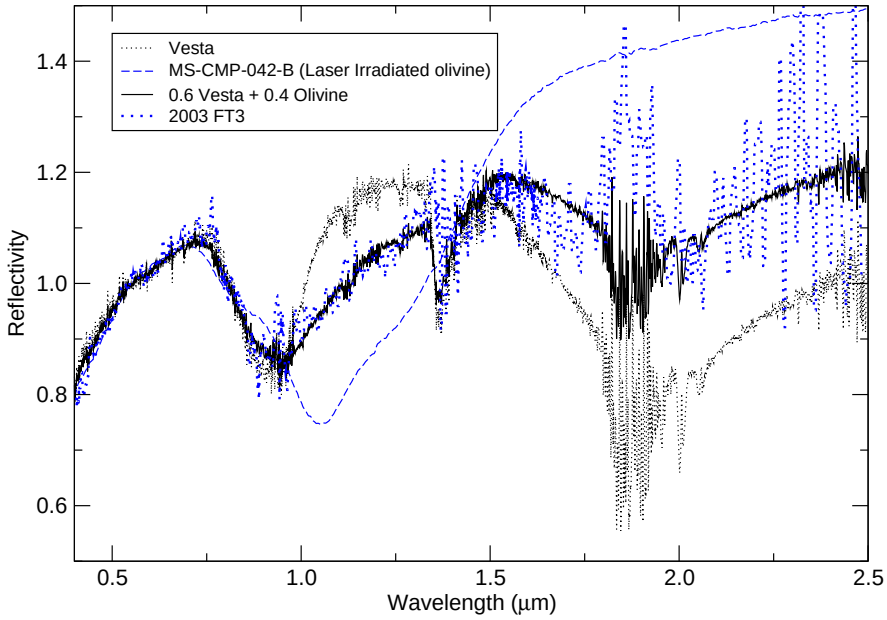

Figure 4.10: Linear combination of Vesta's spectrum with laser irradiated olivine (MS-CMP-042-B). The percentages which give the best fit are 60% Vesta and 40% olivine (see text for further details).

In order to investigate such hypothesis, we computed a linear combination (e.g., see Hiroi et al. (1993)) of Vesta spectrum with the spectrum of olivine (taken from RELAB, http://www.planetary.brown.edu/relab/). The result is shown in fig. 4.10. Although the linear combination could represent a oversimplification of the actual 2003 FT3 surface (it holds only if the diverse species have separate locations on the surface), an excellent match has been achieved. We recall that a spot of olivine has been identified (Gaffey 1997; Binzel et al. 2002; Cochran & Vilas 1998) on the surface of Vesta: 2003 FT3 might originate from a surface layer of Vesta, close to the spot. However this hypothesis has to be considered only as a bare speculation, given also the low S/N ratio of the NIR observations.

Whether the V-type asteroids are really originated from Vesta is a time-honoured question. The discovery of the Vesta dynamical family (comprising many V-types, Zappala et al. (1990)) and the discovery of a 460 km crater on Vesta (Thomas et al. 1997) strongly supports this scenario. Recently, Kelley et al. (2003) have provided

the first firm genetic link between a MB V-type (1929 Kollaa) and (4) Vesta.

On the other hand, the discovery of a basaltic body in the outer MB (Lazzaro et al. 2000) showing a definitely different composition from (4) Vesta (Hardersen et al. 2004), along with some mineralogical differences among V-types (see, e.g., Cochran et al. (2004)), entails the existence of at least two basaltic parent bodies.

The discovery of these new V-types among NEOs is significant. Their basaltic composition and sizes (inferred diameters range from $\sim$ 60 m to $\sim$ 1.1 km, see Table 1) are consistent with being fragments of the surface layer of Vesta.

In principle both the resonances (3:1 and ν_6), usually considered as the most relevant gateways for the production of NEAs, may have been active to transfer Vesta's fragments into near-Earth space. Moreover, if we wish to exclude a very large original ejection velocity (also on the basis of recent general ideas on collisional processes; see Michel et al. (2003)), the delivery of Vesta's ejecta to the resonances requires the contribution of Yarkovsky effect (Farinella & Vokrouhlicky 1999). Many theoretical and numerical works have analysed the delivery of Vesta fragments (Gladman et al. 1997; Migliorini et al. 1997). We point out that all the NEAs here presented may have been transferred both through the 3:1 and/or the ν_6 resonance. However, by analysing the proper elements of 2003 FT3 and 2003 GJ21 (see near-Earth Objects Dynamic Site: http://newton.dm.unipi.it/cgi-bin/neodys/neoibo) further considerations are possible. First of all, their orbits are quite stable having short variation of eccentricity (up to a few percent) and inclination (up to a few degrees).

Moreover, they may undergo close encounters with Mars, but none with Earth nor Venus, and hence also their semimajor axes are somehow stable, thus the present orbit might be correlated to the original one (the current elements for 2003 FT3 are $a = 2.67AU$, $e = 0.57$, $i = 4.3^\circ$, while those for 2003 GJ21 are $a = 1.81AU$, $e = 0.4$, $i = 7.1^\circ$). If so, 2003 FT3 likely originates from the 3:1 resonance, and 2003 GJ21 from ν_6 (see also Figs. 4 and 7 of Migliorini et al. (1997)). It is likely that these NEOs have reached the resonances under the influence of the Yarkovsky effect. Our conjecture might be confirmed finding, in future observations, a prograde spin for 2003 FT3 and a retrograde spin for 2003 GJ21 (La Spina et al. 2004).

Both 2003 EG and 2003 FU3 experienced multiple close encounters with the Earth and Venus, thus their origin cannot be constrained by the present dynamical properties.

4.2.3 Comet-like objects

(65996) 1998 MX5 and 2002 UN have comet-like orbits. They, in fact, have Tisserand invariants with Jupiter (T_J) of 2.95 and 2.81, respectively. We remind that objects with $T_J < 3$ are usually considered comet-like asteroids. Moreover they have a high probability to origin from the Jupiter family comet channel (see Tab. 4.2).

Table 4.2: Probability for 2002 UN and (65996) 1998 MX5 to origin from different channels of the Solar System (total= 1.00). *IMC*: Inner Mars Crossers; *JFC*: Jupiter Family Comet; *OB*: Outer Belt; *HUN*: Hungarias; *PHO*: Phocaeas; *3:1* and ν_6: a mean motion and a secular resonance, respectively.

	Tax	T_J	3:1	IMC	JFC	ν_6	OB	HUN	PHO
2002 UN	B	2.81	0.02	0.01	0.91	0.00	0.05	0.00	0.01
(65996) 1998 MX5	X	2.95	0.00	0.01	0.61	0.00	0.37	0.00	0.00

This dynamical condition has been strengthened by our observations: these objects are indeed B- X-types respectively. The reddish and featureless spectra of 1998 MX5 and 2002 UN are typical of primitive objects, cometary nuclei and most asteroids in cometary orbits studied in the 0.5-2.4 μm range. Unfortunately the very few cometary nuclei spectroscopically observed in this wavelength range did not show any kind of peculiar absorption feature (Lazzarin et al. 1996; De Sanctis et al. 2000; Licandro et al. 2002; Licandro et al. 2002; Licandro et al. 2003). Licandro et al. (in preparation), also observed 17 asteroids in cometary orbits, and found that 15 of them present featureless, slightly red spectra, and failed to find any feature that could distinguish between them and main belt primitive asteroids.

4.3 Comparison with meteorites

In this section we deal with the problem of finding possible meteorite analogues to the asteroids. This topic has been widely discussed in literature (Burbine et al. 002a).

For this task, we developed a code which is able to automatically perform a fit between our NEOs spectra and the vast meteorite's spectra database available on RELAB: http://www.planetary.brown.edu/relab/. We used all the public spectra catalogued as 'XT' (namely extraterrestrial), for a total of 847 spectra. Some of them correspond to the same meteorite, but obtained in different conditions (different grain size, different laser irradiation dose, different portion, etc...).

For each NEO of which we had NIR measurements we found the best fit solution with each meteorite spectrum. We selected the first 20 solutions, in order of fit quality. We did not use any automatic cut-off for the quality of the fit because this can be sometimes misleading, as it strongly depends on S/N ratio of the asteroid spectrum. We automatically traced out five graphs each one containing the asteroid spectrum and four solution out of the 20 selected. This was done in order to compare by eye each meteorite, to avoid possible mistakes, especially in the case of too noisy NEOs spectra, and to check if there were a real acceptable solution or not. In fact in some cases we did not find a good meteorite analog in the database.

NEOs with only the visible part of the spectrum have not been considered as the fit in this interval does not tell much of their relationships with meteorites (Lazzarin et al. 2004).

NEO	Sample ID	Name	Class§	Type	Texture	Size (μm)	Comments
2002 AV4	MB-CMP-018	B-7904,108	CC	CM	Chip Powder	0-125	
2000 QN130	MB-CMP-020	Y-86720,77	CC	CM	Chip	-	
2000 SA10	MH-CMP-013	Lubbock	OC	L5	Powder	0-250	
1999 JD6	RS-CMP-040	Allende	CC	CV3	Powder	0-45	
2002 UN	RS-CMP-046	Boriskino	CC	C2	Powder	0-45	
1992 SY	RS-CMP-064	Pervomaisky	OC	L6	Slab	-	
Mera	RS-CMP-065-T	Tsarev 15384,3-2	OC	L5	Thin Section	-	
2002 VX17	MH-FPF-053-B	Nuevo Mercurio	OC	H5	Powder	0-150	Olivine-Bronzite
2000 EZ148	MH-FPF-054	La Criolla 50	OC	L6	Powder	0-50	
Gordonmoore	MP-FPF-027-A	Bjurbole top	OC	L4	Powder	0-1000	
1991 BN	LM-LAM-009-B	ALHA77005,112	AC			-	Shergottite Martian
2001 MZ7	MR-MJG-038	Pillistfer	EC	E6		-	
2000 JS66	MR-MJG-116-C	Warrenton	CC	CO3	Slab	-	Whole rock
1998 WT24	MB-TXH-064	Murchison	CC	CM2	Powder	0-125	
1991 VK	MB-TXH-084-B	Y-74191	OC	L3	Powder	25-45	
2002 DB4	MB-TXH-085-B	Y-74646	OC	LL6	Powder	25-45	Dry-sieved
2002 XK4	MB-TXH-085-B	Y-74646	OC	LL6	Powder	25-45	Dry-sieved
2001 PM9	MP-TXH-011	Y-74662,101	CC	CM2	Powder	0-125	
2002 NX18	MP-TXH-047	MAC88176,16	CC	C2	Powder	0-125	

Table 4.3: Examples of meteorites best fitting. For each meteorite we report the RELAB Sample Identity; the meteorite name, class and petrological type; the sample texture and the grain size range in case of powder texture. §: OC = ordinary chondrites; EC = enstatite chondrites; CC = carbonaceous chondrites; AC = achondrites (see text for further details).

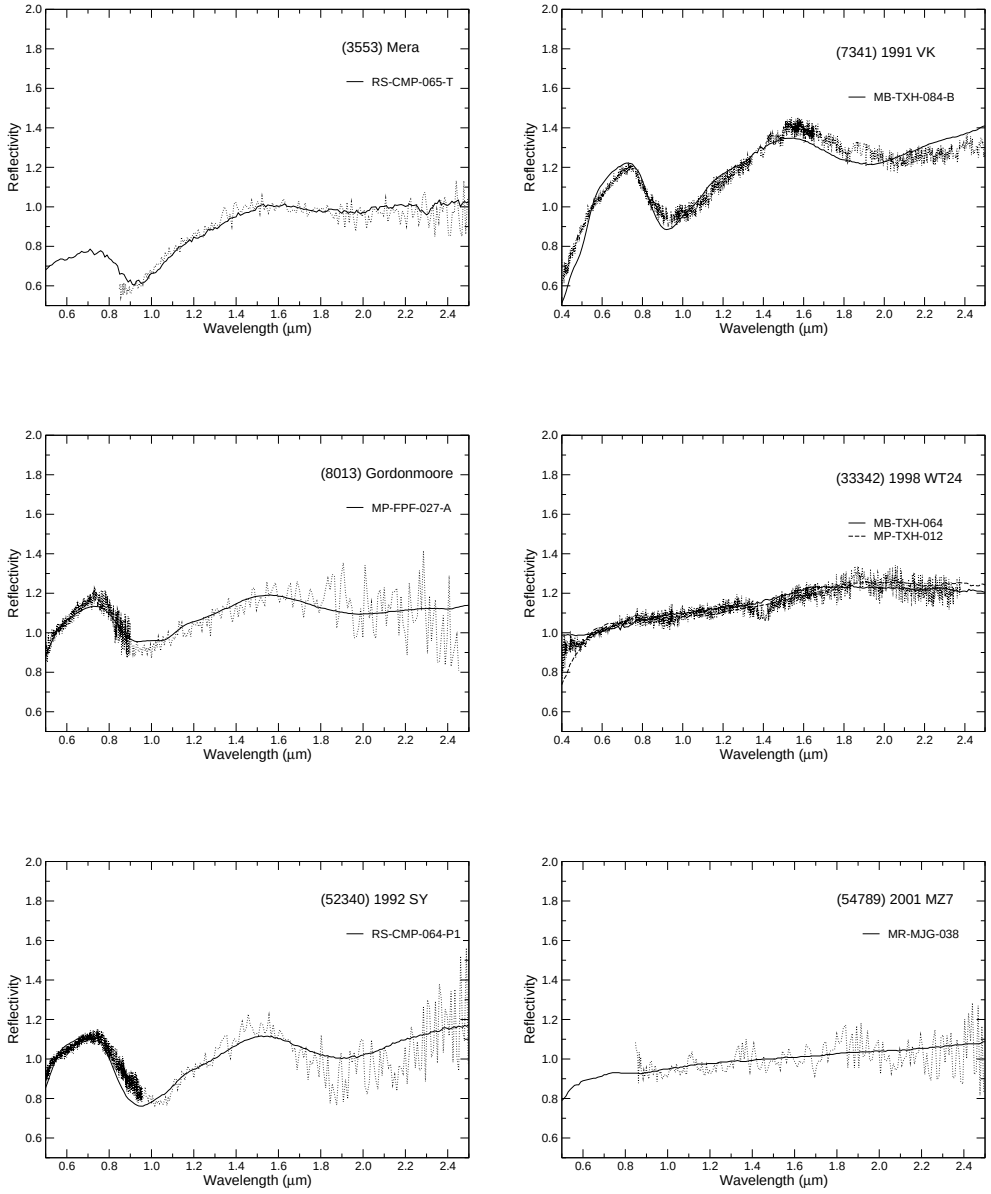

Figure 4.11: Meteorite analogs to SINEO spectra.

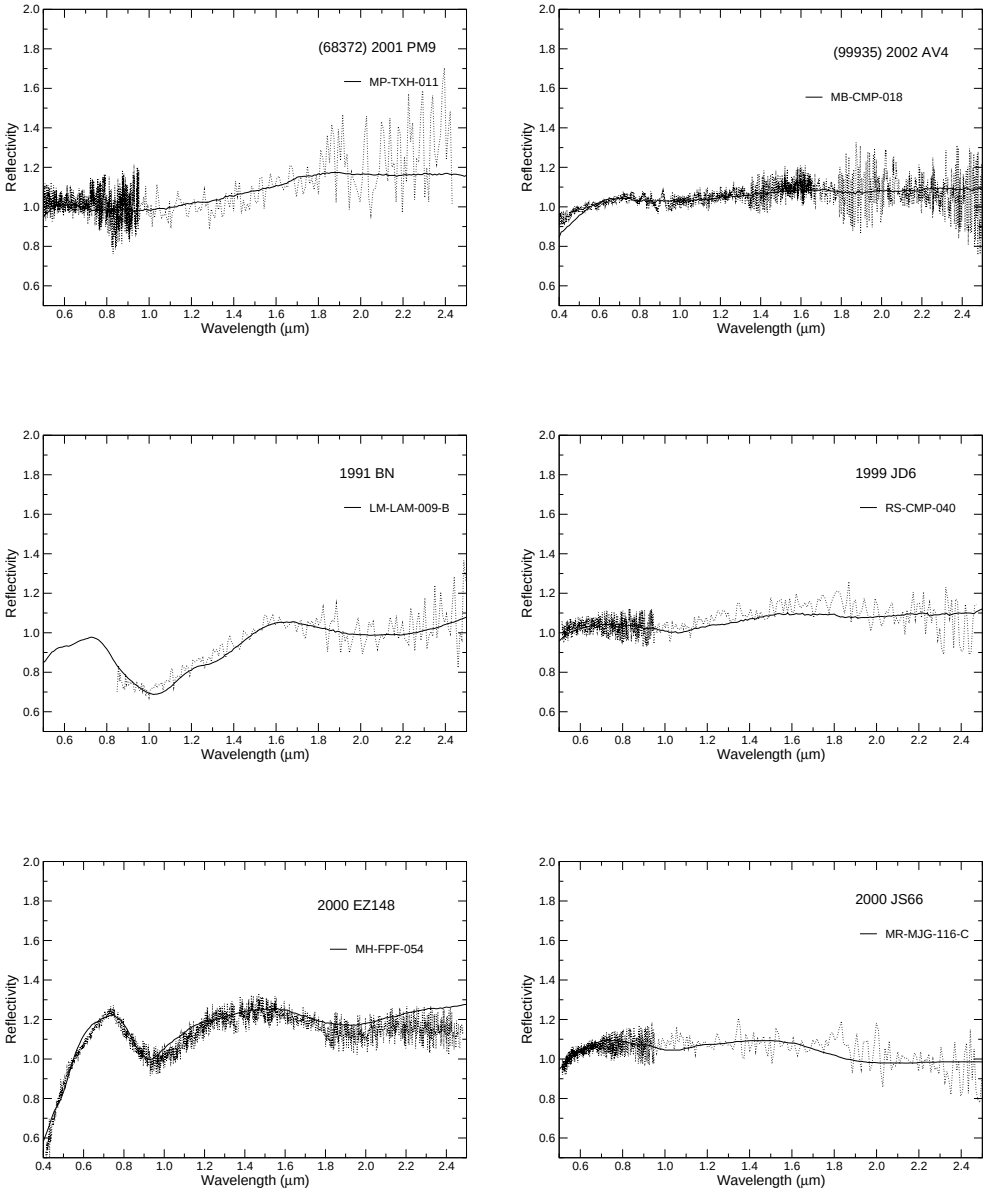

Figure 4.11: Meteorite analogs to SINEO spectra (continued).

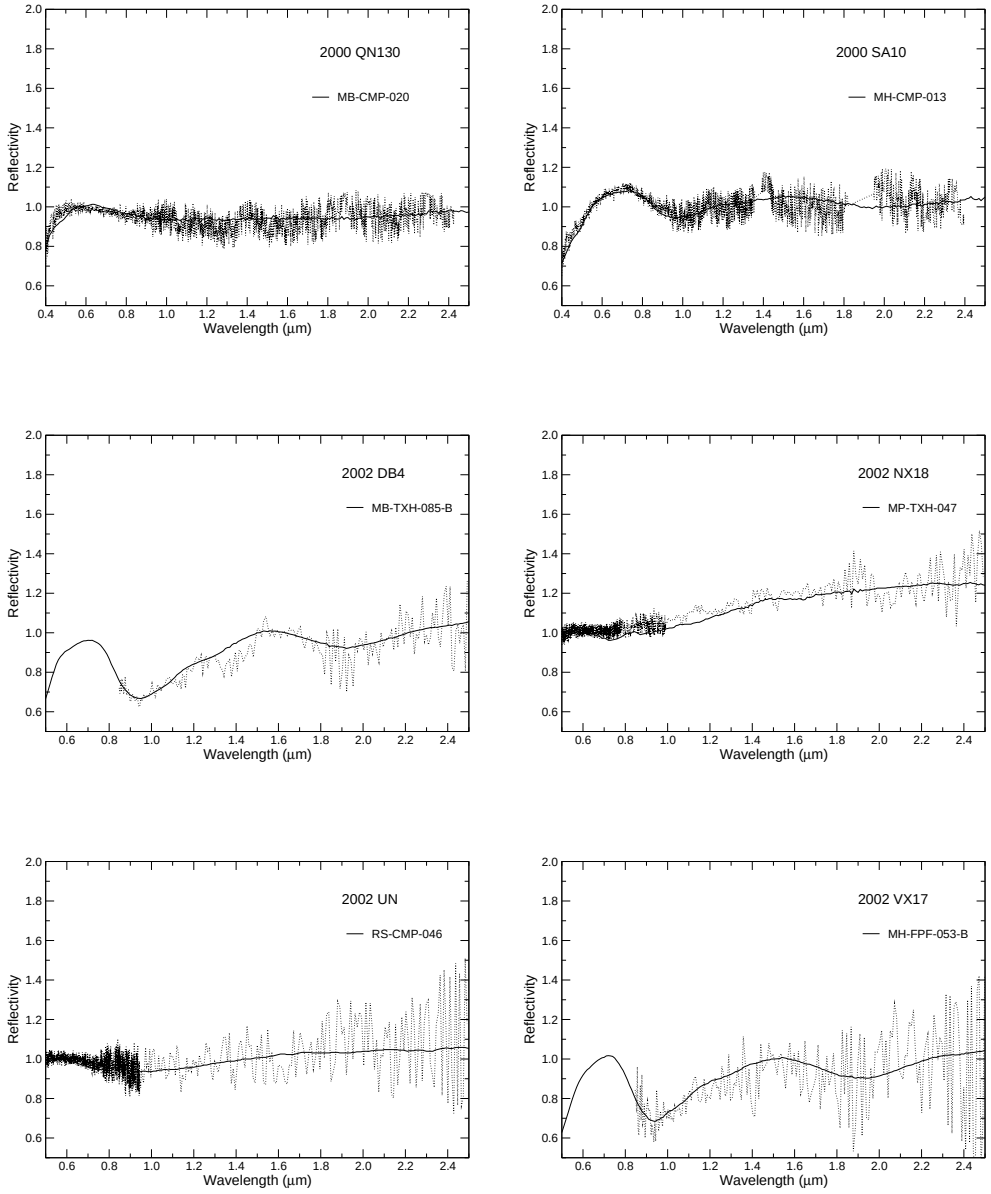

Figure 4.11: Meteorite analogs to SINEO spectra (continued).

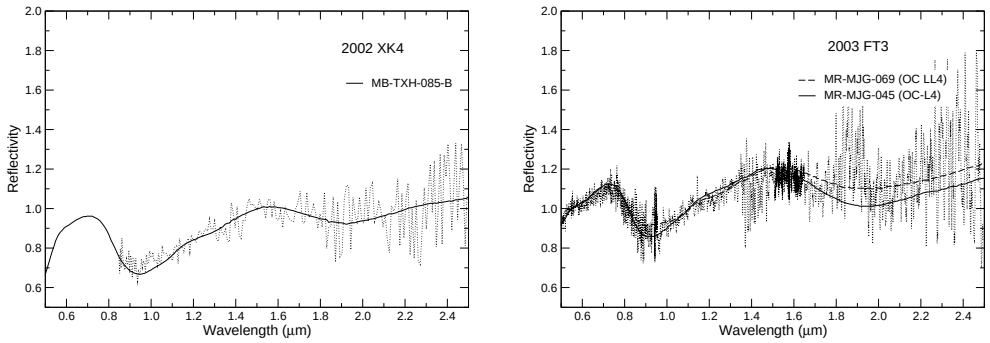

Figure 4.11: Meteorite analogs to SINEO spectra (continued).

In fig. 4.11 we report some NEOs for which a good fitting has been achieved (notice that we looked for a best fitting meteorite only for asteroids with at least the 1.0-2.4 μm spectral range observed). We found possible "analogues" for 9 ordinary chondrite meteorites (OCs). OCs represent about 80% of all falls on Earth. Despite of this, the detection of OC-like asteroids for long time has been problematic (Gaffey et al. 1993). Only recently, it has been shown that OC-like asteroids indeed exist among small size asteroids (Burbine et al. 002a). Among our OC-like NEOs we found: 2 LL6, 1 L3, 1 L4, 2 L5, 2 L6, 1 H5. We point out that, among these NEOs, we found quite big compositional variations (also observed among OCs) as clearly appears from the depth and shape of the 1 and 2 μm bands due to olivine and pyroxene. So, for instance, 1992 SY has an high content of pyroxene (deep 2 μm band) while 2000 GQ146 has virtually no pyroxene (it does not exhibit the 2 μm band). We stress that even if this is a result of particular interest, the fit for those objects for which we have only the NIR should be taken with caution. While there is no doubt about their OC-like composition, possible influences of space weathering (see in the following) could have been masked by the normalisation at 1.5 μm.

Moreover, one NEO (2001 MZ7) has a good fitting with an enstatite chondrite (EC) of type E6. Although this was the best fitting achieved, we stress that owing to the flat, featureless spectral behaviour of 2001 MZ7, it is difficult to clearly establish if it is really an EC, an aubrite or an iron meteorite which also present flat, featureless spectra.

Notice that a NEOs (namely 1991 BN), observed only in the NIR, has been best fitted by a shergottite martian achondrite. However, the NIR of this objects is also not too different from some OC meteorites. Indeed it is not easy to distinguish

between these two groups of meteorites, but important indications could come from visible measurements, since shergottite is considerably different from OCs in this interval.

Finally, we also found good match with 8 carbonaceous chondrites (CCs), and within them 2 CM, 1 CV3, 2 C2, 1 C03, 2 CM2 (see tab. 4.3). Some of them (e.g. 1999 JD6, see fig. 4.11) show shallow absorption bands centred at around 1 μm, probably due to olivine. CCs are only $\sim$5% of all falls. The reason is that they are generally linked with C-complex type asteroids which are mainly in the outer MB. Therefore, the existence of CC-like NEOs is an important link between CC and their source region.

For other 7 NEOs observed in the whole 0.50-2.40 μm spectral range the fit, even if not completely bad, was not satisfactory. Typically, the shape and/or the band positions are slightly different. Several processes could be invoked to explain the differences observed, like slight compositional variations, grain size effects and/or the space weathering.

4.4 Space Weathering

For many S-type objects the fit with a OC meteorite was really bad, indicating that for these objects we are dealing either with big compositional differences having no analogues among meteorites, or we are in presence of big alteration processes. We think the latter is more likely, because if such big composition difference were so common among S-types we would expect to find some similar meteorite samples.

While their overall composition should not greatly differ from that of OCs (all basically made of olivine and pyroxene as witnessed by the presence of typical olivine/pyroxene bands), the spectra of these NEOs are moderate to much redder than typical OCs. As pointed out by several works (Pieters et al. 2000; Ueda et al. 2002b; Ueda et al. 2002a) such red slopes can be achieved by increasing the content of metal (Fe-Ni) with respect to that of silicates.

The origin of this metal is not easily determined by remote analysis, and it could be both primordial or due to some alteration process, like the so-called *Space Weathering*. In fact, as described in Pieters et al. (2000), silicate grains under the flux of micrometeorites and solar wind sputtering develop nanophase iron rims, which alter the optical properties of silicates.

In order to quantify this mismatch we determined the spectral slopes of all S-type NEOs and a large sample (about 300) of OCs as the slope of the best fitting

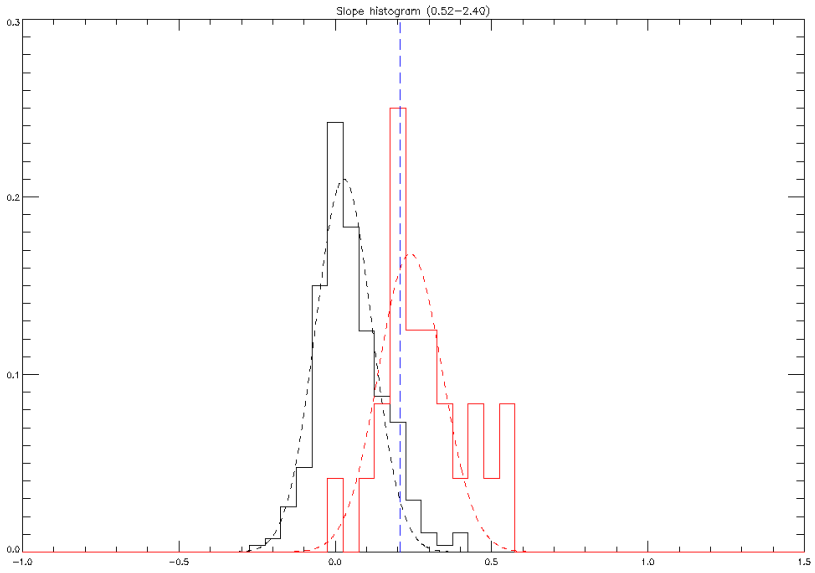

Figure 4.12: In this plot we report the distributions of OCs slopes (left distribution) and S-type NEOs slopes (right distribution) in the 0.52-2.40 μm spectral range. The vertical dashed line represents the limit of 95% between non-weathered and weathered objects, as determined from the OCs slope distribution. The corresponding slope value is 0.208 μm^{-1}. Both distributions have been normalised to unity area (see text for further details).

straight line to the spectrum in the 0.52-2.40 μm range. The results are reported in fig. 4.12. As expected, the vast majority of OCs have small slopes, although some OCs exhibit a red spectrum. The 95% of OCs are below a slope of $S_w = 0.208\ \mu m^{-1}$. So, in this analysis we assumed this value as indicator for the space weathering process. The striking feature is that in comparison with OCs, many NEOs are redder than S_w. On the basis of these considerations, NEOs having a slope greater than S_w have been considered to be space weathered, as reported in tab. 4.1. This result is of particular interest because it clearly shows that space weathering may alter also the surface spectral properties of small size asteroids, usually considered little weathered.

However it is not yet possible to say whether we are in presence of space weathering or not and a final discernment between these two different origins can only be obtained with the help of more data of NEOs, and also with asteroid albedos. Unfortunately, for none of the observed NEOs albedo measurements are available yet, and further researches are needed.

4.4.1 Comparison with ion irradiation experiments

For this reason we started a collaboration with the Catania Observatory with new dedicated experiments (prof. Strazzulla and coll., see Marchi et al., A&A, in press). We report here the results of a comparison between ion irradiation experiments on silicates and a large spectral data set of silicate-rich (S-type) asteroids, and ordinary chondrite meteorites (OCs).

By analysing the spectra of OCs, MBAs, and NEOs we find a similar mineralogy between most asteroids and meteorites, but different distributions of spectral slopes. We interpret this as due to space weathering induced by solar wind ion irradiation. We also observe a higher weathering efficiency for olivine-rich asteroids than pyroxene-rich ones, that is confirmed by our experiments.

Observational data

The observational data used in this work consist of a large set of visible and near-infrared spectra of silicate-rich asteroids. We added to SINEO data all the spectra available of main belt S-type objects and all the useful meteorite spectra from RELAB (http://www.planetary.brown.edu/relab/). We considered only objects for which the whole 0.4-2.4 μm range is available. This is because we are interested in a detailed analysis of the diagnostic 1 μm and 2 μm absorption bands (in the following reported as BI and BII bands respectively) due to olivine and pyroxene.

In the following we report a detailed description of the data used.

Main Belt data The NIR spectra of MBAs have been retrieved from the 52 color survey (Bell et al. 1985) and SMASSIR (Burbine 2000). As they cover the range 0.9-2.4 μm we extended them in the visible by using the data from SMASSI (Xu 1994), SMASSII (Bus 1999). Spectra have been joined by minimising the RMS of the differences in the overlapping region. Notice that, for some asteroids the range 0.9-1.6 μm was present in both the 52 color and SMASSIR. In this case we privileged the spectral data instead of the photometric ones. A detailed description of the data used is provided in tab. 4.4.

Table 4.4: List of Main Belt asteroid considered. Column 2 indicates the origin of data used to obtain spectra in the entire range until 2.4 μm. s1: SMASSI data; s2: SMASSII data; sIR: SMASSIR data; 52c: 52 COLOR data. The slope considered is the slope of the tangent line over BI; λ_{BI} is the wavelength in microns of the centre of the BI band; BII/BI: is the area ratio of the BII over BI band.

Number	**Reference**	**Spectral range**	**Slope**	λ_{BI}	BII/BI
3	s2+sIR+52c	0.44-2.46	0.164	0.940	0.512
5	s2+sIR+52c	0.44-2.46	0.256	0.910	0.568
6	s2+sIR+52c	0.44-2.51	0.248	0.930	0.475
7	s2+sIR+52c	0.44-2.56	0.332	0.940	0.268
11	s2+sIR+52c	0.44-2.56	0.262	0.980	0.385
12	s2+sIR+52c	0.44-2.46	0.274	1.140	0.196
15	s2+sIR+52c	0.44-2.41	0.227	1.000	0.137
18	s2+sIR+52c	0.44-2.56	0.309	0.900	0.340
20	s2+sIR+52c	0.44-2.51	0.164	0.920	0.967
25	s2+sIR+52c	0.44-2.56	0.513	0.952	0.294
26	s2+sIR+52c	0.44-2.46	0.209	0.974	0.226
27	s2+52c	0.44-2.51	0.237	0.960	0.473
29	s2+sIR+52c	0.44-2.56	0.216	0.980	0.623
32	s2+sIR+52c	0.44-2.41	0.206	0.910	0.263
33	s2+sIR+52c	0.44-2.56	0.164	0.910	0.674
37	s2+sIR+52c	0.44-2.51	0.400	0.910	0.947
39	s2+sIR+52c	0.44-2.46	0.147	1.050	0.345
40	s2+sIR+52c	0.44-2.56	0.148	0.930	0.401
42	s2+sIR+52c	0.44-2.56	0.241	1.060	0.009
43	s2+sIR+52c	0.44-2.56	0.324	0.980	0.291
57	s2+sIR+52c	0.44-2.51	0.342	0.920	0.892
63	s2+sIR+52c	0.44-2.51	0.539	0.930	0.376
67	s2+52c	0.44-2.46	0.176	0.930	0.574
68	s1+sIR+52c	0.47-2.56	0.263	1.040	0.209
80	s2+sIR+52c	0.44-2.51	0.410	0.940	0.231
82	s2+sIR+52c	0.44-2.46	0.027	0.910	1.108
89	s2+52c	0.44-2.46	0.274	1.030	0.364
101	s2+52c	0.44-2.51	0.181	0.930	0.748
103	s2+52c	0.44-2.51	0.167	0.930	0.433
113	s2+sIR+52c	0.44-2.46	0.256	1.020	0.026
115	s2+52c	0.44-2.56	0.254	0.950	0.393
116	s2+52c	0.44-2.56	0.185	0.890	0.657
138	s1+52c	0.49-2.51	0.209	1.010	0.090

Table 4.4 – continued on the next page

Table 4.4 – continued from the previous page

Number	Reference	Spectral range	Slope	λ_{BI}	BII/BI
152	s2+52c	0.44-2.51	0.279	0.920	0.934
218	s1+52c	0.47-2.56	0.249	0.980	0.908
246	s2+sIR+52c	0.44-2.56	0.555	1.100	0.247
258	s2+52c	0.44-2.46	0.165	0.910	0.709
264	s2+52c	0.44-2.51	0.181	0.930	0.374
289	s2+sIR+52c	0.44-2.46	0.882	1.100	0.007
346	s2+sIR+52c	0.44-2.56	0.346	0.950	0.327
349	s2+sIR+52c	0.44-2.51	0.472	0.940	0.696
354	s2+sIR+52c	0.44-2.46	0.594	1.080	0.033
376	s2+52c	0.44-2.46	0.349	0.960	0.468
387	s2+52c	0.44-2.51	0.179	1.050	3.992
389	s2+sIR+52c	0.44-2.41	0.219	0.900	0.619
446	s2+sIR+52c	0.44-2.41	0.826	1.090	0.055
532	s2+52c	0.44-2.41	0.265	0.960	0.158
584	s2+sIR+52c	0.44-2.51	0.571	0.970	0.433
653	s2+sIR+52c	0.44-2.46	-0.082	1.060	0.825
674	s2+52c	0.44-2.41	0.177	0.910	0.830
863	s2+sIR+52c	0.44-2.41	1.118	1.090	0.060
980	s2+sIR+52c	0.44-2.51	0.109	1.000	0.389

Near-Earth objects Most part of these data come from our SINEO survey, as it is the only existing NEO survey up to 2.5 μm available so far. It consists of more than 100 spectra, 30 of which belonging to the S-complex and having the full 0.4-2.5 μm coverage. Only few spectra come from Binzel et al. (2004) and from Rivkin et al. (2004). Other 3 spectra were obtained joining data from Binzel et al. (2004) and the 52 color survey. A list containing all NEOs considered in this paragraph can be found in tab. 4.5

Table 4.5: List of Near Earth asteroids considered. Column 2 indicates the source of data. sineo: SINEO project; sm6, sm8 and sm9: NEOs within SMASS survey (respectively: Binzel et al. (2004), Binzel et al. (2004); Rivkin et al. (2004)); 52c: 52 COLOR data. The slope considered is the slope of the tangent line over BI; λ_{BI} is the wavelength in microns of the centre of the BI band; BII/BI: is the area ratio of the BII over BI band.

Number	**Name**	**Reference**	**Spectral range**	**Slope**	λ_{BI}	BII/BI
719	Albert	sineo	0.40-2.45	0.320	0.951	0.276
3102	Krok	sineo	0.40-2.45	0.213	0.961	0.152
3753	Cruithne	sineo	0.40-2.54	0.219	0.950	0.264
4587	Rees	sineo	0.50-2.48	0.213	0.909	0.455
6489	Golevka	sineo	0.40-2.54	0.252	0.956	0.403
7341	1991 VK	sineo	0.40-2.51	0.268	0.969	0.428
8013	Gordonmoore	sineo	0.49-2.45	0.013	0.975	0.073
11054	1991 FA	sineo	0.40-2.50	0.667	0.961	0.079
35107	1991 VH	sineo	0.50-2.50	0.361	0.985	0.698
35396	1997 XF11	sineo	0.50-2.49	0.418	0.958	0.048
52340	1992 SY	sineo	0.50-2.50	0.072	1.021	1.020
54071	2000 GQ146	sineo	0.40-2.50	0.390	0.999	0.264
66251	1999 GJ2	sineo	0.50-2.49	0.603	0.949	0.364
68346	2001 KZ66	sineo	0.50-2.46	0.245	0.974	0.100
88710	2001 SL9	sineo	0.40-2.48	0.317	0.918	1.786
98943	2001 CC21	sineo	0.50-2.50	0.445	0.956	0.089
	2000 EZ148	sineo	0.40-2.48	0.026	0.963	0.340
	2002 AL14	sineo	0.50-2.47	0.705	0.971	0.504
	2002 QE15	sineo	0.50-2.49	0.601	0.968	0.336
	2002 TD60	sineo	0.50-2.50	0.527	0.937	0.235
	2002 TP69	sineo	0.50-2.49	0.235	0.950	1.252
	2002 VP69	sineo	0.40-2.50	0.267	0.991	0.252
	2002 YB12	sineo	0.50-2.49	0.187	0.938	0.097
	2003 KR18	sineo	0.50-2.47	0.306	0.969	0.214
433	Eros	sm9	0.44-2.49	0.333	0.970	0.318
1036	Ganymed	sm8+52c	0.44-2.51	0.344	0.920	0.737
1627	Ivar	sm8+52c	0.44-2.56	0.254	0.950	0.174
1685	Toro	sm6	0.44-2.43	0.202	0.970	0.441
1866	Sisyphus	sm8+52c	0.44-2.46	0.197	0.950	0.243
1943	Anteros	sm6	0.36-2.43	0.561	0.960	0.457
19356	1997 GH3	sm9	0.44-2.41	0.100	0.960	0.541

Meteorites We retrieved from RELAB a large number of meteorites spectra. Details of the materials used are provided in tab. 4.6. All the meteorites selected belong to the ordinary chondrite (OC) group. This is because OCs have been suggested to represent the best analogues of S-type asteroids by several authors (see for example Gaffey et al. (1993). As in this study we deal with space weathering, we considered only those meteorites for which no trace of alteration was reported. For this reason all the spectra reporting indications of some natural alteration process (in the headers or in the description files) were discarded. Also those altered in laboratory (e.g. laser irradiated, washed etc...) were not considered.

Table 4.6: This research utilises spectra acquired by different investigators with the NASA RELAB facility at Brown University. This table lists the number of RELAB OC meteorites used from different Principal Investigators.

PI code	**PI full name**	**spectra used**
CMP	Carlé M. Pieters	85
DTB	Dan Britt	12
FPF	Fraser P. Fanale	25
JFB	Jeffery F. Bell	4
LAM	Lucy Ann McFadden	5
MJG	Michael J. Gaffey	39
TXH	Takahiro Hiroi	14
Total		184

Objects characterisation procedures Asteroid surface material characterisation is based upon the interpretation of observable diagnostic properties to determine presence, abundance and/or composition of one or more mineral or chemical species on the surface of that object.

So, all the spectra have been analysed in terms of the spectral parametrisation developed by Gaffey et al. (1993). Spectral slope was determined as a straight line tangent to the spectrum over the 1 μm feature[2]. Band centres were derived

[2]Note that this definition is slightly different from the definitions of slope used in previous sections.

from polynomial fits to the spectral curve in the region of the band minimum after dividing the continuum. BI band areas were computed as areas between the linear continuum over BI and the polynomial fit to BI. To compute BII band areas we computed areas between the linear continuum over BII (tangent over 2 μm feature) and the polynomial fit to BII.

We underline that by this analysis the ratio BII/BI area and the BI peak position are representative of the composition, and that the slope is highly representative of space weathering alteration (see Strazzulla et al. (2005), Hiroi & Sasaki (2001)). However, we should keep in mind that this analysis is not able to constrain the presence of featureless compounds, like metals and glasses. Nevertheless it remains a good way to describe the silicate-rich bodies which are thought to be mostly made of olivine and pyroxene.

Experimental data

Ion irradiation experiments have been performed in the Laboratory of Experimental Astrophysics in Catania, thanks to prof. Strazzulla and dr. Brunetto, using different ions at 200 keV, monitored by reflectance spectroscopy (0.3-2.5 μm). Space weathering by solar wind ions has been simulated by ion irradiation experiments of pure end-member silicates, i.e. pressed powder of olivine (forsterite) and pyroxene (enstatite), and irradiation of bulk silicate-rich rocks (Eifel silicate, from Germany). End-member silicate pellets are obtained by pressing powder of pure forsterite (from San Carlos, Arizona, USA) and enstatite (from Bamble, Norway), having a grain size of about 100-200 μm. For a better comparison with asteroid spectra we also considered irradiation of Epinal meteorite and of other bulk silicate-rich rocks (Jackson silicate), that are described in Strazzulla et al. (2005), Brunetto & Strazzulla (2005).

The experimental set-up consists of a stainless steel vacuum chamber ($P < 10^{-7}$ mbar), where the samples are in contact with a finger (at room temperature), held up in place by a metal corona ring. The vacuum chamber is interfaced to an ion implanter (Danfysik 1080-200) from which ions with energy from 30 keV up to 200 keV (400 keV for double ionisation) can be obtained. Hemispherical reflectance spectra have been acquired using a UV-VIS-NIR spectrometer (Perkin Elmer, Lamba 19). A $BaSO_4$ substrate is used as reference material in the 0.3-2.5 μm spectral range. Further experimental details can be found in Brunetto & Strazzulla (2005).

The ion mean penetration depth (R_p), the stopping power (energy deposited per unit path length), and the amount of elastic versus inelastic energy loss, are functions of the ion energy, ion mass, and of the properties of the target. When ion irradiation experiments are performed to simulate solar wind and cosmic ion irradiation, the corresponding type of ion can be easily obtained in laboratory, though it is more difficult to reproduce the energy distribution of these ions. Therefore, the laboratory results can be used for astrophysical application only when we find out which is the physical mechanism that is causing the observed effects, i.e. when we can extrapolate the laboratory data to a wider range of ion masses and energies.

Brunetto & Strazzulla (2005) have found that the physical mechanism that is responsible for the weathering effects is the energy lost by elastic collisions between ions and target nuclei, and the parameter d (number of displacements/cm^2) can be used to compare the effects of different ions and energies. This means that ion irradiation experiments can be considered a direct reproduction of solar wind irradiation effects, and we can apply our simulations to space weathering of MBAs and NEOs. We have consequently calculated the damage parameters (number of displacements per ion, stopping power, and mean penetration depth) for our experiments, by using the SRIM simulation code (at http://www.SRIM.org/, Ziegler et al. (1985)).

Results

Bulk Eifel silicate rocks are rich in olivine, and have minor content of pyroxene, as can be seen in fig. 4.13 (upper panel). Indeed, the spectrum of unirradiated Eifel sample exhibits a very strong and broad band at about 1 μm (BI), which is due to the presence of ferrous iron Fe^{2+} in olivine crystals but is also present in pyroxene. It is also evident a less intense broad 2 μm band (BII), characteristic of pyroxene but not olivine. We have irradiated Eifel sample with 3.7×10^{16} N^+/cm^2 (energy of 200 keV, d = 830 displ./ion, and Rp = 360 $\pm$ 100 nm). The spectrum of irradiated Eifel (upper panel of fig. 4.13) shows strong darkening and reddening; weathering effects are strong in the whole observed spectral range. The area of BI is reduced as the slope of the continuum across BI increases, and a similar effect is observed for BII.

The reflectance spectra of end-member silicates are plotted in Fig. 4.13 (middle and lower panel), showing bands (BI and BII) characteristic of low iron content olivine (forsterite), and of low iron and low calcium pyroxene (enstatite). End-

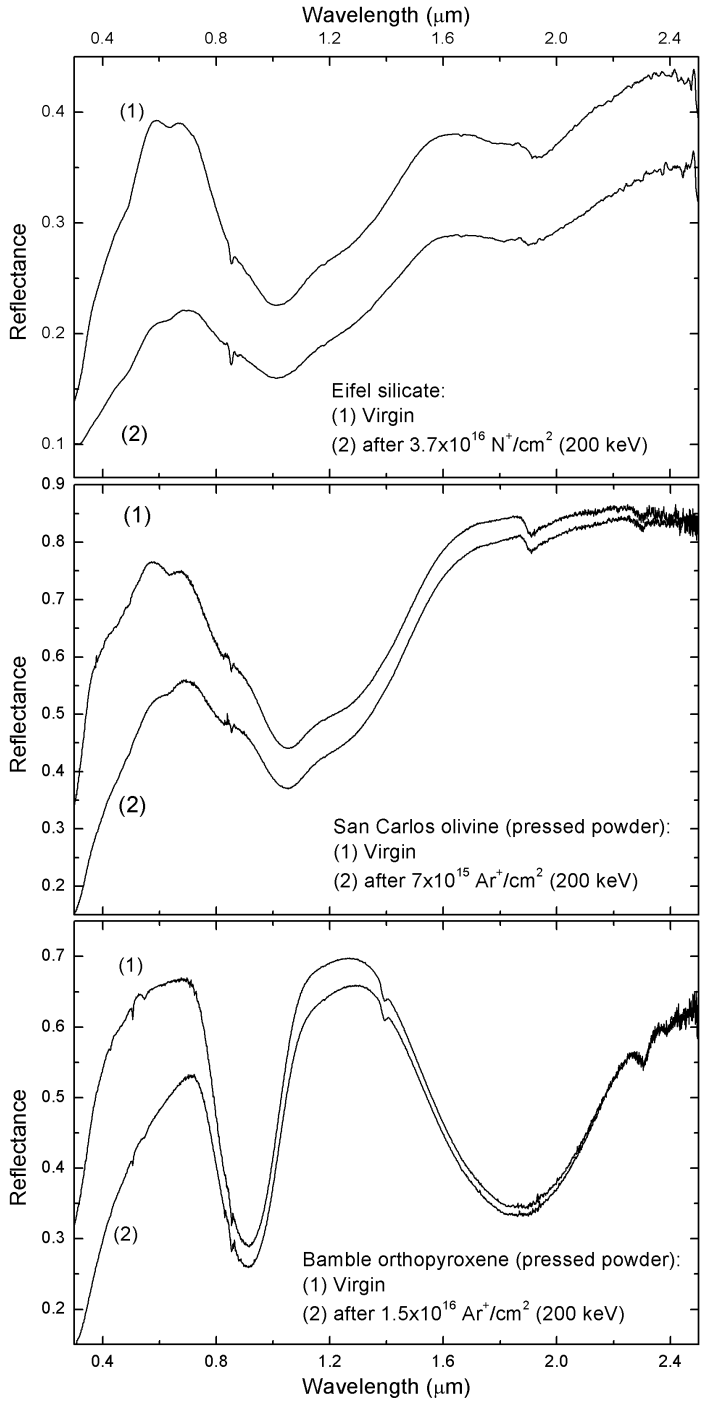

Figure 4.13: Reflectance spectra of virgin and irradiated Eifel (upper panel), forsterite (middle panel), and enstatite (lower panel).

member forsterite and enstatite have been irradiated with 7×10^{15} Ar^{+}/cm^{2} and 1.5×10^{16} Ar^{+}/cm^{2} (energy of 200 keV, d = 2000 displ./ion, and Rp = 160 $\pm$ 60 nm) respectively (see fig. 4.13). Also in these cases, darkening and reddening of reflectance spectra are apparent.

This spectral reddening agrees with the results of previous experiments of ion irradiation of OC Epinal meteorite (Strazzulla et al. 2005) and of Jackson silicates (Brunetto & Strazzulla 2005). Furthermore, we remark that weathering process is active both on bulk samples and pressed powder samples.

Notice that the thickness of the damaged region at these energies is lower than 1 μm, i.e. the reddening and darkening process of reflectance spectra is due to displacements in the very upper layers of the target. A similar effect of upper layer alteration should be present in asteroids, and this would cause the mismatch between the slope of asteroids and that of OCs.

In this respect, one result we would like to point out concerns the well-known lack of OCs analogues (which represent the largest number of falls on Earth) among minor bodies. The situation is shown in Fig. 4.14. It clearly shows that the slope distributions of OCs, NEOs and MBAs are very different. Some authors (Lazzarin et al. 1997; Binzel et al. 1996) reported the occurrence of OC-like bodies among small asteroids (and in particular among NEOs). Indeed the blue tail of MBAs and NEOs distributions overlap the OCs distribution. However, in terms of numbers, these findings still represent only some exception.

Nevertheless, OCs distribution (representative of pristine materials) peaks at slope = 0, and is by far bluer than the NEOs and MBAs distributions. On the contrary, the two latter distributions are basically indistinguishable. The striking feature is that, if we consider the limiting slope ($S_w = 0.138$) below which 95% of the OCs lays, we find that 83% of the NEOs and 94% of the MBAs are redder than S_w. Thus only the 17% of NEOs and 6% of MBAs are compatible with OCs spectra. Although these percentages can be affected by low numbers statistic, NEO population seems to contain a higher percentage of OC-like objects. We also underline that, in spite of the wide size range involved, NEOs and MBAs span over a similar interval of slopes, and that the asteroid slope distributions have a broader FWHM with respect to that of OCs.

Fig. 4.14 also reports the results for two ion irradiation experiments, namely Epinal and Jackson. The first one shows the trend for a typical OC, while Jackson is representative for the maximum reddening attained in laboratory experiments, which overcome the asteroid slopes. Therefore the shift between OCs and asteroids

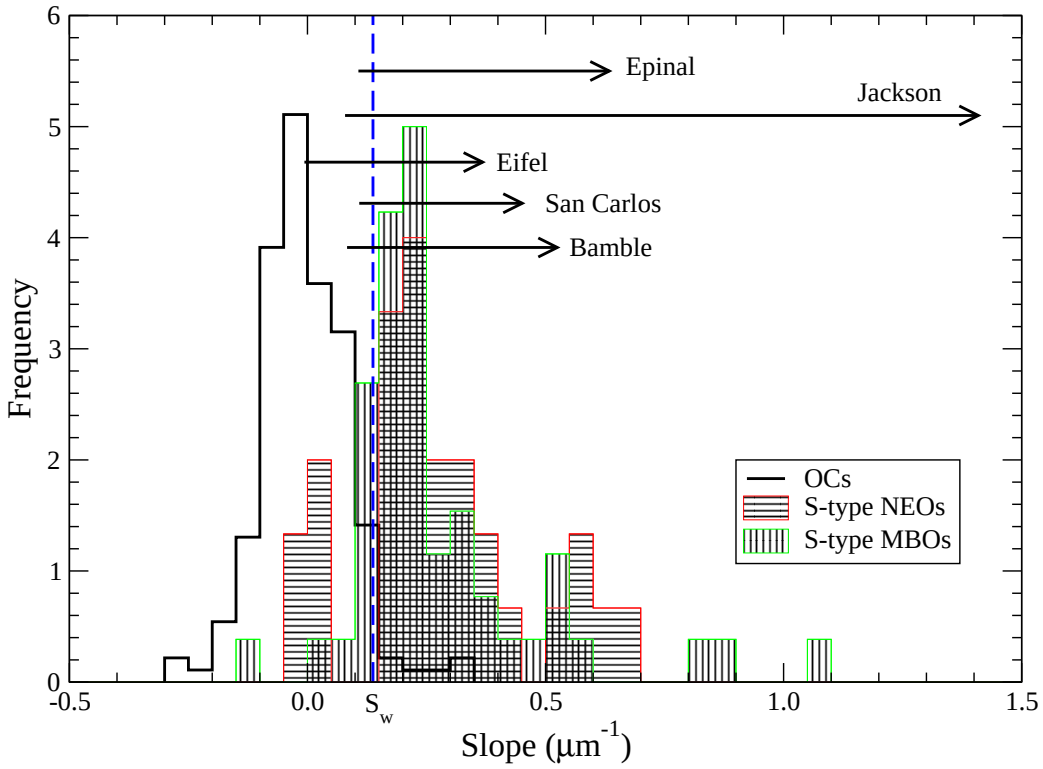

Figure 4.14: Spectral slope distributions of OCs, NEOs, and MBAs. The vertical dashed line marks the 95% OCs limit (corresponding to a slope of $S_w = 0.138$), while horizontal arrows mark the reddening measured for irradiated Epinal and Jackson.

distributions can be explained by ion irradiation experiments. A possible explanation for the different FWHM between the asteroid and OC slope distributions could be that asteroids spend different exposure time in weathering environment, suffering also resurfacing processes.

Fig. 4.15 shows the BI peak position as a function of the area ratio BII/BI. From this plot one can get information about the mineralogy of the analysed bodies. Gaffey et al. (1993) had used a similar plot to separate the S-type asteroids into seven classes (from SI to SVII), where the SIV class had been defined from the corresponding mineralogy of OCs. We have enlarged the statistic of both asteroids and

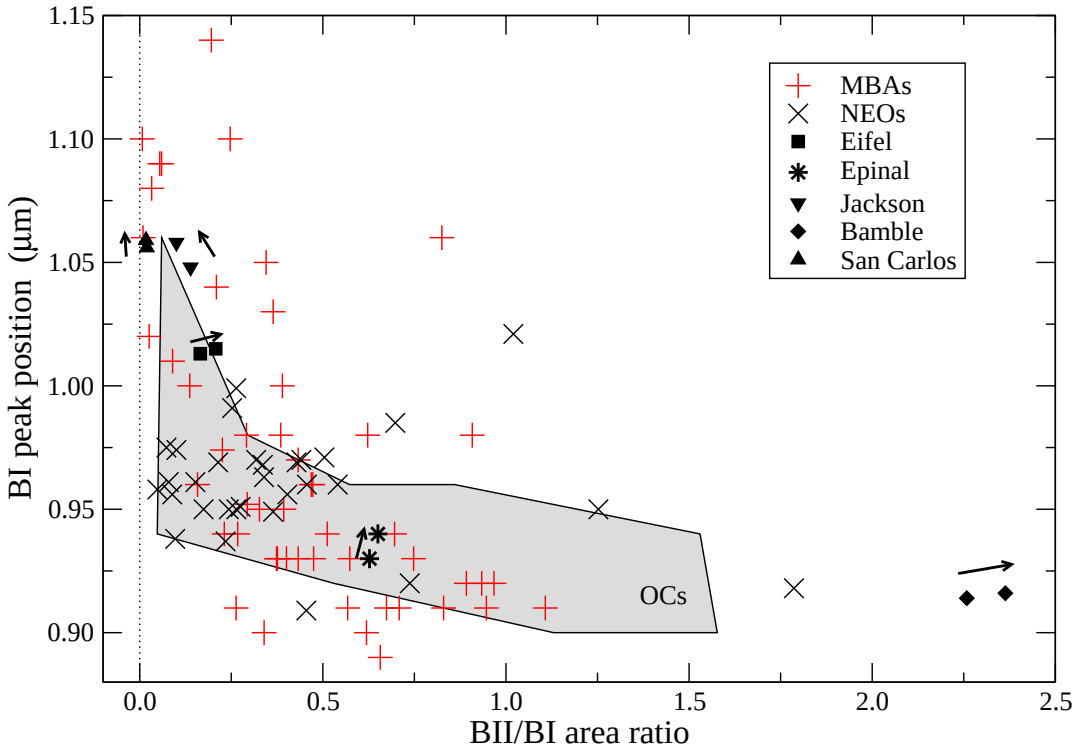

Figure 4.15: Band I peak position vs. BII/BI area ratio for MBAs and NEOs. Positions for virgin and irradiated silicate are also shown. The shaded area corresponds to the region occupied by OCs.

OCs, so that from Fig. 4.15 we can deduce that the SIV class (shaded area) is much wider than that defined by Gaffey et al. (1993). A second point that arises from Fig. 4.15 is that irradiation experiments do not change significantly the mineralogy of the irradiated silicates (see arrows over the symbols of the five silicates). This is not surprising since, as stated above, sputtering process is not relevant at these ion fluences.

A further important result concerns the suitability of the use of the slope parameter to study the effects of space weathering. In Fig. 4.16, we show the spectral slope as a function of the ratio BII/BI, for MBAs, NEOs and OCs, and for laboratory experiments. It results that space weathering acts mainly on the slope, and only

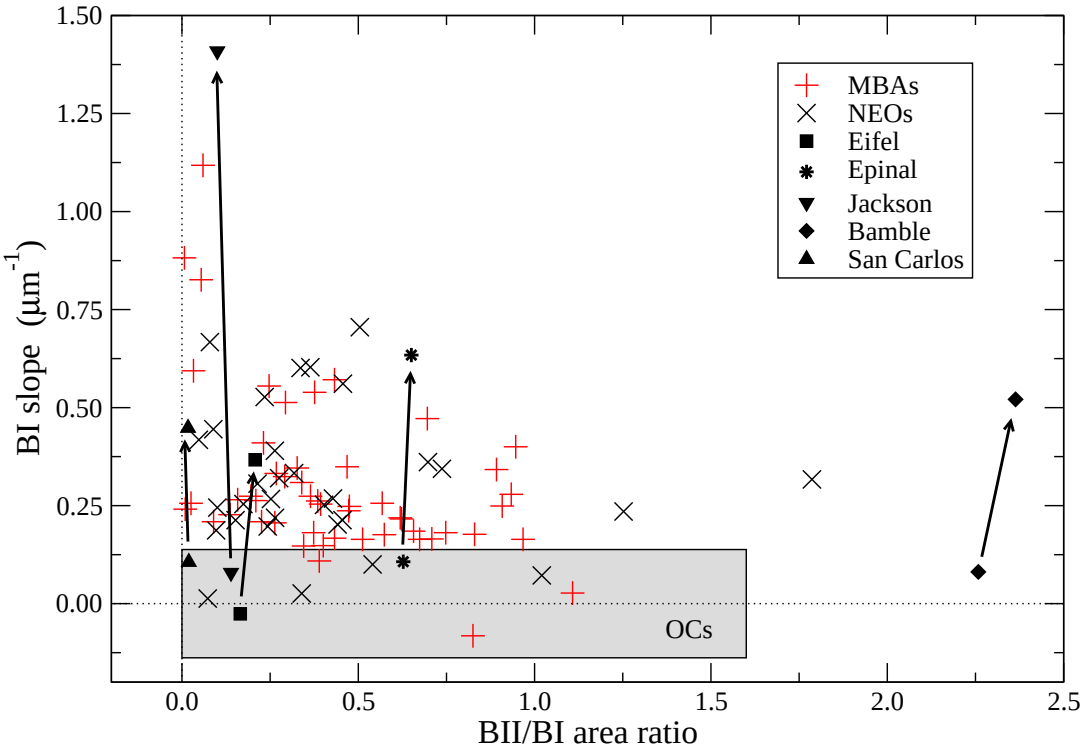

Figure 4.16: Spectral slope vs. BII/BI area ratio for MBAs and NEOs. Vertical arrows show the trend from virgin to irradiated silicates. The shaded box contains 95% of OCs as described in fig. 4.14. The dashed oblique line indicates the different rate of weathering between olivine-rich and pyroxene-rich asteroids (see text for details).

marginally on the ratio BII/BI, for both pressed powder (forsterite and enstatite), and bulk samples (Jackson, Eifel, Epinal). On the other hand, the ratio BII/BI is representative of the composition. Thus, the discrepancy between meteorites and asteroids has mainly to be ascribed to the spectral slope, and this process is well reproduced by our ion irradiation experiments.

Another interesting issue related to fig. 4.16 is that MBAs (and NEOs) have a triangle-shaped distribution: the highest slopes being achieved for low values of BII/BI, namely for high olivine contents. This is in agreement with experimental

data: forsterite reddens more efficiently than enstatite. Indeed, both forsterite and enstatite reach a similar spectral slope of about 0.5 μm^{-1}, but their damage values are about 1.4x10^{19} displ./cm^2 and 3x10^{19} displ./cm^2 respectively.

From the spectra of irradiated Epinal, Strazzulla et al. (2005) had estimated a reddening time-scale of about 10^5 years at 1 AU (Astronomical Unit) from the Sun. The results reported here indicate that most of the spectral slopes of asteroids can be reproduced by damage values in the range 1-3x10^{19} displ./cm^2 (see fig. 4.16), in agreement with what calculated for Epinal (Brunetto and Strazzulla, 2005). We therefore confirm that ion irradiation is a very efficient weathering process. Nevertheless, this is only one of the processes that can affect asteroid surfaces; in particular, the time-scale of ion-induced reddening is not expected to strictly correspond to the lifetime of the asteroid surfaces, as several rejuvenating mechanism can be present, whose efficiency could be able to partially compensate the reddening induced by solar wind ions.

Summary

We have compared a wide set of asteroid and meteorite spectra with ion irradiation experiments (200 keV). From the results of this comparison, some points can be established:

- OCs and S-type asteroids exhibit a similar mineralogical composition, as deduced from band parameters, more than that previously assumed. Nevertheless, a significant mismatch is observed in the VIS-NIR spectra, which is due to very different distributions of spectral slope.

- The slope above BI is a good parameter to quantify the degree of space weathering. Thus, we define a 95% OC slope limit beyond which an asteroid can be considered as 'weathered': we find that about 83% and 94% of observed NEOs and MBAs respectively have slope higher than this limit. The asteroid slope distributions have a broader FWHM with respect to that of OCs.

- Ion irradiation can explain the shift of the OC distribution toward asteroid distributions. Spectra of unaltered and irradiated silicates have slopes that span over a wider range than that observed in NEOs and MBAs.

- MBA and NEO slope distributions do not differ significantly from each other. However, if compared with OCs, they exhibit an asymmetrical slope distribution, possibly due to a different rate of weathering between olivine-rich

asteroids and pyroxene-rich ones, a behaviour that is also confirmed by our laboratory experiments.

4.5 Links between weathering and dynamics

We present here a general and significant relation between the spectral slope of silicate–rich asteroids (both Main Belt bodies and near–Earth asteroids) and the *exposure* to space weathering, computed taking into account the age and the distance from the Sun. We find strong evidences on the existence of a slope–distance relation, which may identify the dominant space weathering processes as Sun–related.

In turn, the age estimates depend on various parameters and in particular on the effectivity of the Yarkovsky–driven orbital mobility. We show that values of the parameters of Yarkovsky effect consistent with the recent experimental measurements can lead to a unique slope–age relation for Main Belt and near–Earth asteroids.

Space environment acts on optical properties of silicate–rich asteroid surfaces (Hapke 2001; Pieters et al. 2000; Chapman 2004): older asteroids are expected to be generally redder and darker than their younger siblings. Recently, an analysis limited to Main Belt asteroid families (Jedicke et al. 2004; Nesvorný et al. 2005b) has evidenced a colour–age relation. Also the size–spectral slope relation suggested to hold for near–Earth asteroids (NEAs) (Binzel et al. 2004) can be qualitatively included in the same scenario (larger asteroids are –in mean– older). These results show the relevance of space weathering (SW hereinafter) processes. The intensity and the properties of SW depend mainly on the age of the body, but also on the relative importance of the various involved physical processes (as, for instance, micro–meteorite impacts and ion bombardment), some of them related to the distance from the Sun.

Silicate–rich asteroids (namely those belonging to the S–complex (Bus 1999)) are of particular interest for SW studies, being a representative and rather homogeneous sample of objects. Moreover, laboratory experiments have simulated SW processes on silicate samples (Moroz et al. 1996; Yamada et al. 1999; Strazzulla et al. 2005). According to both experimental and observational investigations, it is now widely accepted that SW may be quantitatively estimated in terms of the spectral slope (e.g. Pieters et al. (2000)). In the present work, slopes have been derived from high quality visible (0.52-0.92 μm) SMASSII spectroscopic survey (Bus 1999) which represents the baseline for the definition of S-complex (and, more in general, for a feature–based taxonomy). From SMASSII we selected 559 Main Belt aster-

oids (MBAs) belonging to the S-complex. 170 NEAs spectra have been taken from SMASS-NEO (Binzel et al. 2004), while other 44 come from the SINEO survey (Lazzarin et al. 2004; Lazzarin et al. 2005).

In the following sections we describe our approach to the complex problem of SW, by a novel method which takes into account for the ages of individual asteroids and their distances to the Sun.

4.5.1 A general approach to SW

A complete analysis of SW would require the knowledge of all the relevant parameters. The most important one is the age of the body, owing to the "progressive" nature of SW. Other parameters follow from the properties of the physical processes (micrometeorites impact, ion bombardment, sputtering etc). Some of these processes depend on the distance from the Sun, which may be an important parameter of SW whenever the related processes are important.

Age estimate

The age of Main Belt asteroids can be constrained by the age of the Belt and by collisional times. It depends on the assumed physical modelling of collisions between asteroids and on the overall evolution of the Belt population with time. We adopted an estimate of the collisional lifetime, as a function of the size, derived from Bottke et al. (2005), which seems to be consistent with the most commonly accepted ideas on the subject. The adopted lifetime–size relation is also represented in Figure 4.17.

In general, the probability that a body created at a time t (the time is counted backwards, so that $t = 0$ means the present epoch) survived catastrophic collisions until now is: $e^{-t/\tau_{coll}}$. The present population can be obtained integrating this probability, multiplied by the past collisional creation rate, both functions of t. The mean age T_{MB} can be obtained by multiplying the same integrand per t and dividing by the population integral.

According to Bottke et al. (2005) the asteroid population did not undergo a dramatic evolution during the last 4 Gy (after the end of the Late Heavy Bombardment, LHB); consequently, we can approximately factorise out the number of bodies created per unit time, both in the population and in the age integrals. After that, the population integrand is essentially $e^{-t/\tau_{coll}}$. The integral is smaller than unity, since the maximum past time is finite (we used 4 Gy), and is equal to $1 - e^{-t_{LHB}/\tau_{coll}}$. We have to add the contribution of primordial MBAs, i.e. those which have survived the

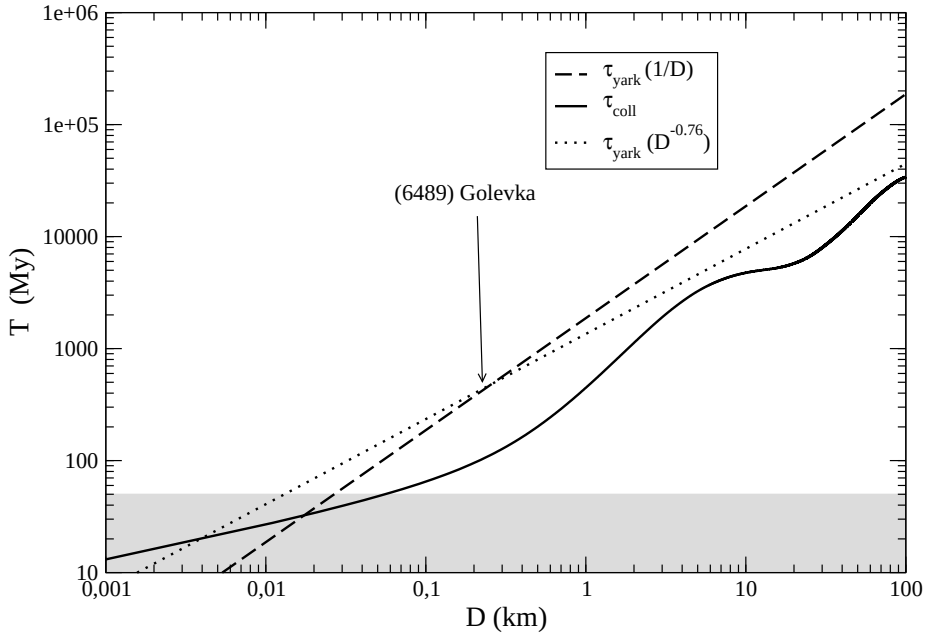

Figure 4.17: We represent the collisional lifetimes (according to Bottke et al. (2005), solid curve) and the Yarkovsky times (two cases, both fitting the observations; see text), as functions of size. The shadowed region in the bottom of the figure represents a rough upper estimate of the lifetimes of NEAs after their injection into the "channels". Thus the age estimates concerning the size ranges, for which the collisional and Yarkovsky times are within this region, might be unreliable. However, this happens for objects smaller than a few tens of meters, which are not present in our spectroscopic database.

long period of time between the end of LHB and the present epoch. They affect both the population integral and the mean age estimates. Since an estimate of this fraction, consistent with the same physical hypotheses which we adopted to compute the collisional lifetime, is presently not available from the literature, we adopted a simplified estimate, adding a fraction $e^{-t_{LHB}/\tau_{coll}}$ of bodies of age $t_{LHB} \simeq 4\ Gy$. This estimate seems qualitatively consistent with the analysis presented by Bottke et al. (2005), according to which bodies larger than about 100 km are mostly primordial: our formula gives very similar results.

Finally, the mean age for MBAs can be estimated with the equation:

$$T_{MB} \simeq \tau_{coll}\left[1-\left(1+\frac{t_{LHB}}{\tau_{coll}}\right)e^{-\frac{t_{LHB}}{\tau_{coll}}}\right]+t_{LHB}e^{-\frac{-t_{LHB}}{\tau_{coll}}} \tag{4.1}$$

The age estimate of NEAs is by far more difficult, owing to their rapid, often chaotic, orbital evolution. We assumed that none of them is primordial, and that their lifetime in the Main Belt has been limited by the "Yarkovsky time" τ_{yark}, defined as the time that an asteroid requires to change its semimajor axis by 0.5 AU, instead of t_{LHB} as for MBAs. This last value estimates the mean distance between a random original orbit in the Belt and the closest resonant or dynamically unstable region. A more refined analysis might correct this rough estimate, but, in our opinion, by a factor not too different from unity. In Figure 4.17 we reported the behaviour of the Yarkovsky time as a function of the size, in two cases. We assume that it is consistent with the only existing observational value (Chesley et al. 2003) and that it depends on the size D, either proportionally to $1/D$ (consistently with simple theoretical arguments, e.g. see Farinella & Vokrouhlicky (1999)), or according to the smoother size–dependence discussed by Penco et al. (2004) as a consequence of the numerical data presented by Spitale & Greenberg (2001). In our computations we used both assumptions, and performed additional tests. However we obtained our best results (in terms of the uniqueness of the relations for NEAs and MBAs) in the former case, which has been adopted in the final plots (see in the following).

In general τ_{yark} is larger –but not far larger– than τ_{coll}, but is usually far smaller than t_{LHB}; it is enough to cut the ages of NEAs, which result systematically younger than the MBAs of the same size. We assumed that no original body has been delivered into the present NEAs region; for this to happen, a very fine tuning of its semimajor axis mobility should be required. According to all these considerations, the mean NEAs age can be estimated as:

$$T_{NEA} \simeq \tau_{coll}\frac{1-\left(1+\frac{\tau_{yark}}{\tau_{coll}}\right)e^{-\frac{\tau_{yark}}{\tau_{coll}}}}{1-e^{-\frac{\tau_{yark}}{\tau_{coll}}}} \tag{4.2}$$

Exposure estimate

In order to estimate the amount of radiation from the Sun that a body receives along its orbit (i.e. what we call *exposure*), the following integral has to be evaluated:

$$\text{Exposure} = \alpha \int \frac{1}{r(t)^2} dt$$

where $r(t)$ is the Sun–asteroid distance, as function of time t, and α is a constant. Since the angular momentum is conserved, the above integral can be simply written as:

$$\text{Exposure} = \alpha \frac{f(t)}{l}$$

where l and f are the angular momentum per unit mass and the true anomaly. According to the above equation the exposure grows linearly with t, with an additional periodic term depending on the eccentricity. Averaging on a period P, and thus eliminating the periodic term, the exposure per unit time is:

$$\text{Exposure} = < \text{Exposure} > \cdot t = \alpha \frac{\oint f(t)/l}{P} \cdot t$$

Finally, in terms of a new constant α_1, we obtain:

$$\text{Exposure} = \alpha_1 [\Phi(a,e) \cdot \text{age}]$$

where:

$$\Phi(a,e) = \frac{1}{a^2\sqrt{1-e^2}}$$

where a is the semi–major axis and e is the eccentricity. Φ is essentially proportional to the mean energy flux received from the Sun, during a orbit, per unit time, and thus accounts for the Sun–asteroid distance effect. Notice that the equation above does not take into account the orbital evolution of asteroids with time.

4.5.2 Results for S-complex asteroids

The slope–age plot is shown in Fig 4.18. Asteroids show a wide spread in slope, as likely due to compositional variations within the S–complex (Bus 1999). However, the mean slope increases with the age, and a unique slope–age correlation holds for NEAs and MB bodies younger than 2.7 Gyr. The correlation is statistically significant: for NEAs the 2-tailed probability (P) for the linear correlation is 2%, while for NEAs + MBAs younger than 2.7 Gy it is less then 0.1%. We remind that a linear correlation is considered significant whenever $P < 5\%$.

For estimated ages larger than about 2.7 Gyr the slope becomes almost constant. This result may be due to a sort of age–saturation, consistent with recent outcomes from laboratory experiments (e.g. see Brunetto & Strazzulla (2005)); however the SW depends also on other parameters; therefore it is not easy to draw firm conclusions on this point (see also the following discussion).

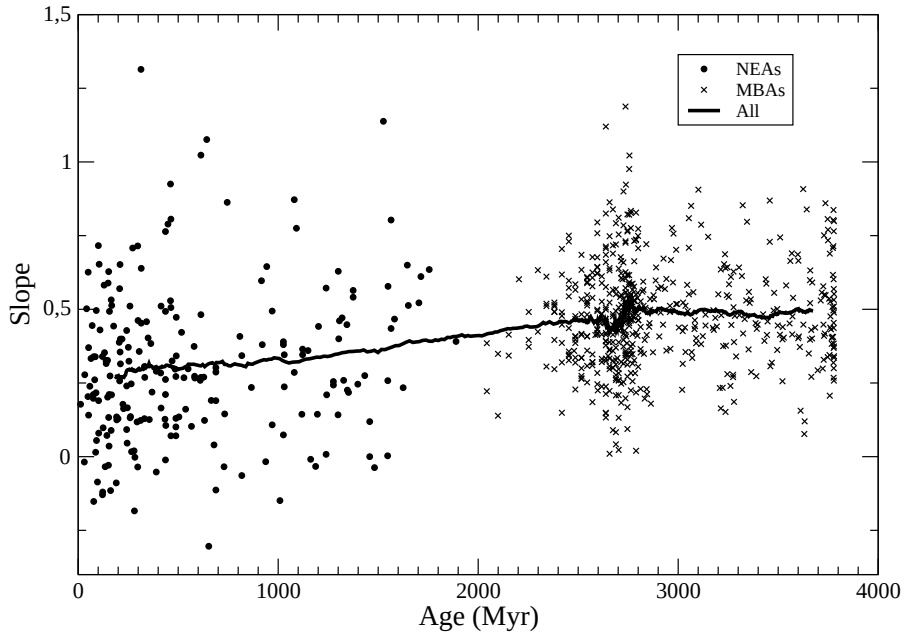

Figure 4.18: A slope–age relationship for NEAs and MBAs. Solid curve corresponds to a running box average (100 points) of the data. The figure shows a clear, statistically significant, increasing trend for NEAs. NEAs rate is $(8.3 \pm 3.5) \cdot 10^{-5}$ Myr^{-1}. This rate is slightly reduced for young MBAs (i.e. age < 2.7 Gyr), and after a "knee" at 2.7 Gyr MBAs slope becomes almost flat.

Notice that the possibility of joining together NEAs and MBAs with a unique relation is critically dependent on the assumed lifetimes, and in particular on the adopted values of τ_{yark}. For instance, with larger values of τ_{yark} (i.e.with a less effective semi–major axis mobility) the NEAs slope–age curve should have been systematically moved down. Since we expect no systematical difference between NEAs and MBAs –apart, maybe, a small selection effect due to the origin of NEAs, more frequently in the inner Belt– the parameters of Yarkovsky effect are constrained within a given range in order to ensure a reasonable continuity from NEAs to MB bodies. The present fit has been achieved assuming a scaling of Yarkovsky effect with the size $\sim (1/D)$, and a mobility of 40 km/yr (for 1 meter bodies), in fair agreement with experimental values (Chesley et al. 2003).

Notice also that our slope–age relation is consistent with the NEAs slope–size

relation found by Binzel et al. (2004). However, the correlation we find is statistically more significant (P for the slope–size relation is only of 7%).

Among the several processes leading to SW, two have been suggested to dominate: ion bombardment (Strazzulla et al. 2005; Brunetto & Strazzulla 2005) and micrometeorite impacts (Moroz et al. 1996; Yamada et al. 1999). Ion bombardment (as also other less relevant processes) are due to the Sun, and thus depending on the Sun–body distance. Other processes (such as micrometeorite impacts) don't. Recent experimental work seems to entail for a predominant role of the ion contribution (Strazzulla et al. 2005), at least at the Sun–Earth distance. The dependence of the slope on the Sun–distance may allow to evaluate the relative importance of these effects at different distances.

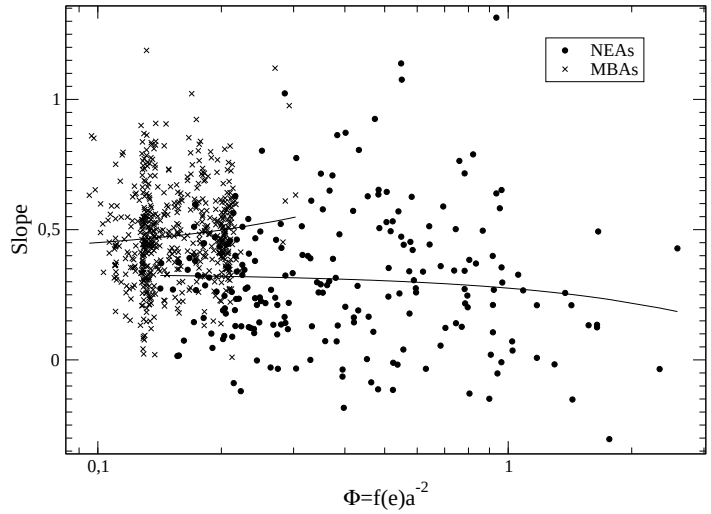

Figure 4.19: The slope–Φ relationship for MBAs and NEAs. Solid curves represent the linear regressions of the data (notice the logarithmic scale). Slopes of MBAs show a significant positive correlation with Φ (P is about 2%). The same correlation does not hold for NEAs, which indeed show a smooth negative trend (see text).

Accordingly to the discussion above, the estimate of the mean distance of a MB asteroid from the Sun can be easily performed in terms of the parameter $\Phi(a,e)$. The same analysis can be extended to NEAs, using their present orbits. The results are summarised by Figure 4.19, and show a slope–distance anti–correlation for MBAs, while NEAs behave in the opposite way. However, we have to recall

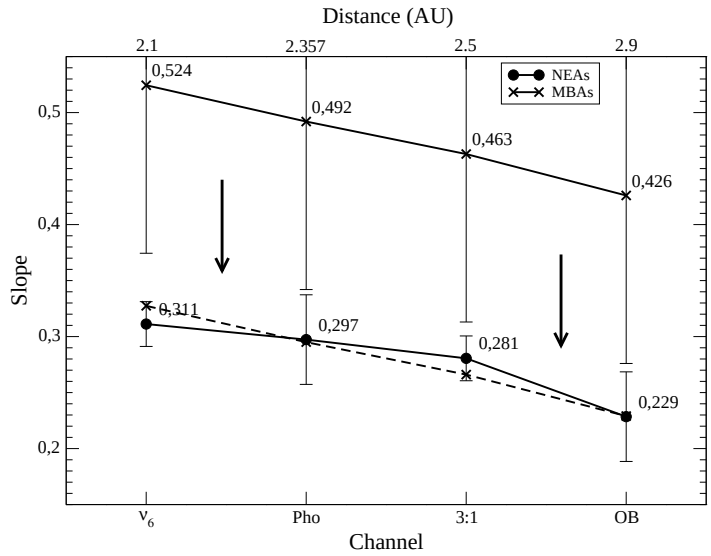

Figure 4.20: Mean slope distribution of NEAs as a function of the four "narrow" channels of origin, compared to the behaviour of MBAs, at the same distances. The channels are the resonances ν_6 and 3:1, the Phocaea region (Pho) and the Outer Belt (OB). Notice that the effective NEAs channel distances should be corrected taking into account possible selection effects; for example most of the bodies passed through ν_6 should come from a larger original distance (La Spina et al. 2004). Maybe this correction will improve the fit between MBAs and NEAs.

that the present orbital status of a NEA has a typical lifetime of a few million years (Morbidelli et al. 2002), and the previous transition stage (within resonances, or due to close encounters with Mars) has been even shorter (Gladman et al. 1997). Thus the reddening of a NEA should be mainly due to its past life within the Main Belt, and, in particular, to its mean distance from the Sun as a MBA. We have no direct information, but we can estimate the probability –for each NEA– to have been injected passing through one of the 7 main channels (Morbidelli et al. 2002). Some of them are "narrow", i.e. allow to identify the region of the Belt from which the asteroid has been extracted: the secular resonance ν_6 (~ 2.1 AU), the Phocaea region (~ 2.375 AU), the mean–motion resonance 3:1 (~ 2.5 AU) and the Outer–Belt (~ 2.9 AU). Thus we can define a "mean channel original distance" by weighting the distances of the narrow channels with the related probabilities (and taking into account only these channels). The results are shown in Fig. 4.20. NEAs slopes are anti–correlated with the channel distance, with a best–fit slope–distance relation

which is almost parallel to the corresponding one obtained for MBAs (the slope offset is obviously due to the different mean ages). The presence of a slope–distance correlation entails that SW is mainly due to Sun–related effects (presumably to the ion bombardment).

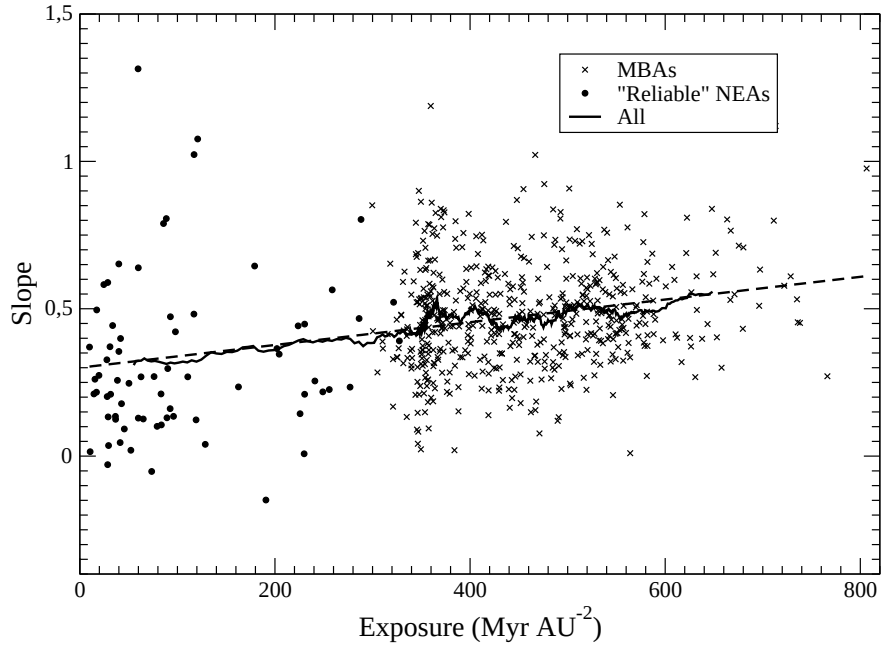

Figure 4.21: A general slope–exposure relationship for “reliable” NEAs and MBAs. Only NEAs having a total probability of origin from ν_6, Pho, 3:1 and OB exceeding 75% have been considered as “reliably” distance–assessed (only in this case the estimate of Φ can be considered as enough accurate). The solid curve corresponds to a running box average (50 points) of the data, putting together NEAs and MBAs. The curve can be approximately fitted with a line (dashed line). *P* of the linear fit is less then 0.1%, supporting a full statistical significance.

Finally, we can put together age and distance estimates in order to obtain a slope–exposure plot (Figure 4.21), where the exposure is defined by the product of Φ and the age, as described before. A unique (holding for NEAs and MBAs), approximately linear fit comes out, with an angular coefficient of $3.8543 \cdot 10^{-4}$ MyrAU^{-2}. The *P* of the linear fit is less then 0.1%, supporting a full statistical significance.

Notice that the slope–exposure plot does not exhibit the knee shown by the

slope–age relationship at 2.7 Gyr. This supports the idea that it was indeed not physically significant. Consequently, the introduction of the exposure represents an important improvement in our understanding of reddening process.

4.5.3 Conclusions

In spite of a few simplified assumptions and of their intrinsic uncertainties we have found a significant relation between the asteroid spectral slopes and their past evolution (and thus their cumulated SW), providing a unique and general slope–exposure plot, valid for the whole S–complex. Most noticeably, the use of both NEAs and MBAs, has allowed us to obtain a general description of the SW in the range 10 Myr–3.7 Gyr. Moreover, by using NEAs we were able to link their reddening with their past evolution into the Main Belt.

Doing so, we find important constraints on several physical processes, like the efficiency of the NEAs Yarkovsky delivery and the dominance of Sun–related effects among SW processes. Indirectly, our results support also the existing reconstructions of the past dynamical evolution of NEAs.

Chapter 5

Works in Progress and Future Analysis

5.1 Extension the Principal Component Analysis

Since the near infrared part of the spectrum contains lot of information it is a natural to think to extend the taxonomic classification and the principal component analysis to this part of the spectrum.

This means essentially that we have to find some diagnostic properties, some decisive feature or useful characteristics able to define new “mean types” for every taxonomic class.

This can be done only with a high number of spectra for each class and/or subclass. Again we have to merge all the data set available (SINEO, SMASS, S3OS2...). At the present day a statistically useful data set can be obtained only considering a 0.52-1.60 μm spectral range.

In this contest we produced a preliminary plot of the principal component analysis reported in fig. 5.1.

Further analysis have to be done on that topic to better understand the statistic significance of the PCA in that specific spectral range.

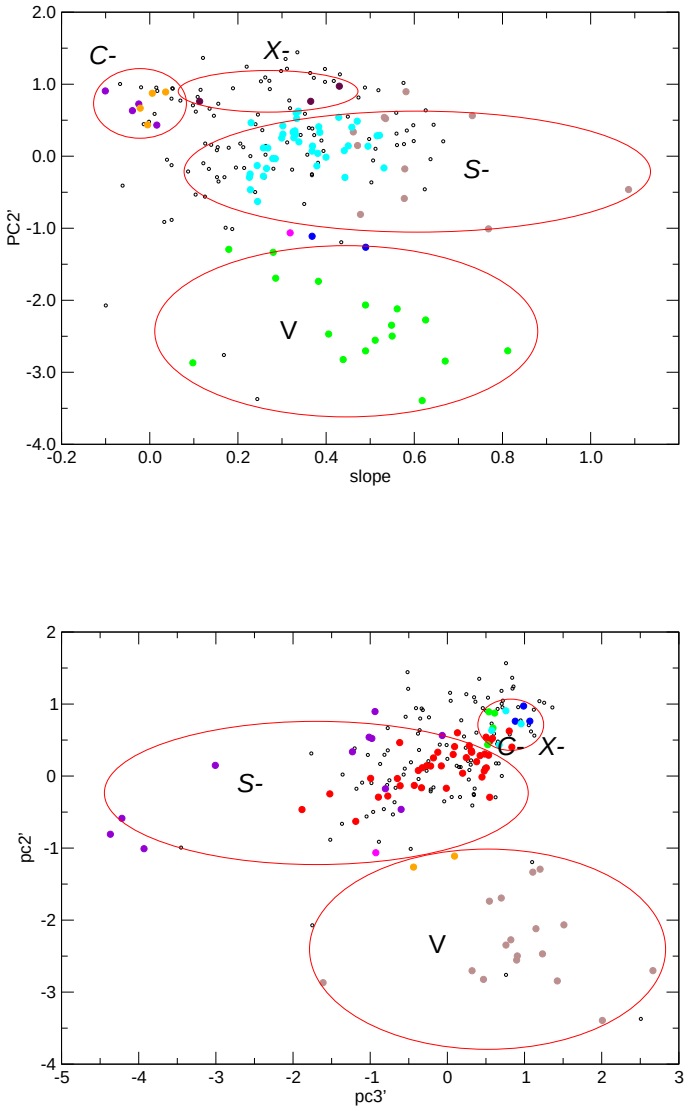

Figure 5.1: PCA example in the 0.44-1.60 μm spectral range. In both plots objects reported refer to SMASSII spectra available in that range. Taxonomic classes reported refer to the the position of taxonomically known asteroids.

5.2 Deepen the study of the Space Weathering effect

5.2.1 A spectral slope vs. perihelion distance correlation for planet–crossing asteroids

Here we present a recently started work in collaboration with David Nesvorný (SouthWest Research Institute, Boulder, CO, USA) and Paolo Paolicchi (Physics

Department, Pisa University, Italy).

The observational and laboratory measurements of the space weathering (SW) rate (Jedicke et al. 2004; Brunetto & Strazzulla 2005) suggest that space weathering processes operate on a timescales of the order of 10 My to modify a typical OC spectrum (i.e. Q–type) into a S–type spectrum. Therefore, the observed Q–type NEOs should have surface ages $\lesssim$10 My, or, in other terms, should have been originated by collisional breakups of large bodies within the past $\lesssim$10 My.

This is clearly in contrast with the estimated average age of NEOs (of the order of some hundreds of Myr; see for instance Bottke et al. (2005)). This value comes from the usually accepted collisional and dynamical models of the NEOs' origin, which predict long lifetimes, allowing slow processes like the Yarkovsky effect and small resonances to insert collisional fragments into the planet–crossing space (Migliorini et al. 1998; Bottke et al. 2002). This evolutionary scenario has also been indirectly strengthened by the slope vs. original distance trend found to hold for NEOs (Marchi et al. 2005). Moreover several red surfaces of small NEOs have been observed (Marchi et al. 2005; Marchi et al. 2006).

Thus, the buildup of a self consistent scenario requires to take into account some additional effect. Recently, Nesvorný et al. (2005b) speculated about the possibility that close encounters with terrestrial planets can remove by tidal stripping the upper part of asteroidal surfaces. If so, fresher layers would rise up to the surface, creating the overall features of a younger surface.

So far this intriguing suggestion has not been supported by observational evidences. We are thus studying a new observational property, namely the existence of a spectral slope vs. perihelion distance correlation, which may represent the first evidence for the occurrence of the tidal stripping as a rejuvenating process.

There is probably a statistically significant relation between the perihelion distance and the spectral properties of NEOs and MCs. This trend seems to be real and not affected by the history of individual bodies, and its significance is also indirectly confirmed by the distribution of the relative number of Q–types with respect to S–types (see fig. 5.2).

The obtained relation seems to entail a sort of "surface reset" due to close encounters with the inner planets. This process, if confirmed, could be regarded as a sort of "dynamical" reverse space weathering. A more detailed dynamical analysis of this effect is urged, and a more quantitative assessment of the (tidal) effect of a close encounter to remove the space–weathered surface layers of a typical km–sized asteroid is also required.

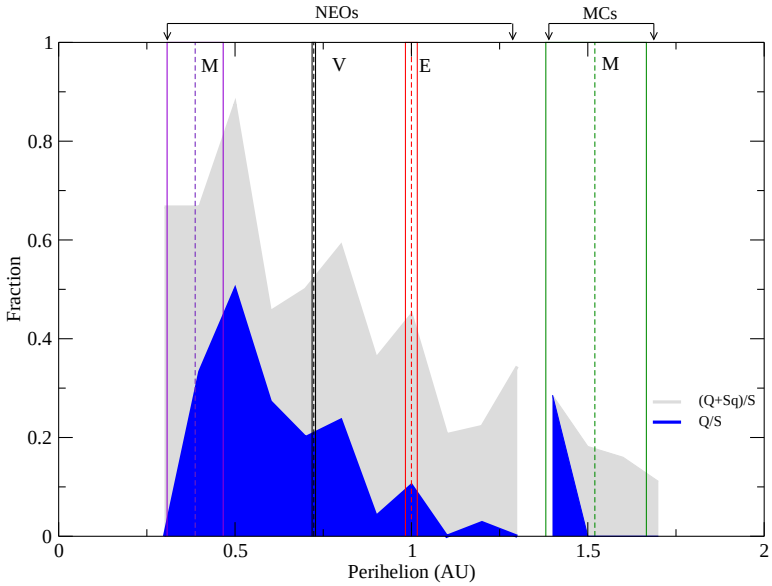

Figure 5.2: Histogram of the fraction of Q-type and (Q+Sq)-type NEO and MC bodies as functions of perihelion distance. Vertical lines indicate the perihelion, semimajor axis and aphelion distances for terrestrial planets, i.e. the region where close encounters can happen. Notice that the gap of asteroids for $1.3 < q < 1.4$ AU is not real, but rather due to a lack of observed bodies within this range.

Nevertheless, our findings establish a new step toward a global model of asteroid spectral alteration.

5.2.2 Space Weathering on C-complex?

Here we describe an analysis in progress we are doing with Liuba Moroz (Institute of Planetology, University of Muenster, Germany; German Aerospace Center (DLR) Institute of Planetary Research, Berlin, Germany).

Since all asteroids orbit in the same space environments, whether they are S-type, or C-type or whatever, they can be affected by ageing effects. These effects ave evident on S-complex bodies because they somewhat change silicates optical properties by making them darker and redder. Are there some optical effects also in other taxonomic complexes?

The situation with C-complex asteroids may be quite complicated.

C-complex asteroids are mineralogically diverse and may show slope variation due to variation in mineralogy as well as degree (and possibly ”type”) of space weathering. Their material usually is not well represented in meteorite collections: carbonaceous chondrites (CCs) are rare among meteorite falls and finds, and they usually are mineralogically diverse and probably show different trends when subject to space weathering (may show reddening or flattening or no change in slope).

Very few space weathering simulation experiments are available in literature.

Content of organics (compared to silicates) as well as properties of organics seem to be important.

Anhydrous CV3-CO3 Carbonaceous Chondrites. Sho Sasaki uses nanosecond pulsed laser which is, in terms of pulse duration, more suitable to simulate bombardment of asteroid surfaces by micrometeorites observing some reddening. Moroz et al. (1996) irradiated CV3 Allende powder with with a 0.5-1 microsecond pulsed laser and found some NIR reddening after irradiation, simulating heating by larger impactors.

CV and CO CCs are anhydrous and have very low contents of organics which are significantly carbonised, almost graphitic. This extremely low organic content can be the reason for their ”silicate-type” response to space weathering. Also, the ”reddening” effect is diminished compared to pure silicates or ordinary chondrites, probably because of fine opaques - sulfides and carbon in the matrix material.

Primitive Carbonaceous Chondrites. All available primitive CCs are hydrated and also contain much more organics than anhydrous ones. They also vary in organic content and even organic composition. Both organic content (compared to silicates) and composition of organics can influence the way how they would ”react” to space weathering. Space weathering simulations have so far been tested only on two primitive CCs - CM2 Mighei (Moroz et al. 2004) and Tagish Lake (Hiroi et al. 2003).

Mighei showed some mild reddening. The small effect on slope can be because of ”competition” between ”silicate-type” and ”organic-type” of space weathering, with some dominance of ”silicate-type” of space weathering. They performed irradiation only on this single CM2 chondrite, while these meteorites may also have lower organic contents than the meteorite tested.

Tagish Lake has not extremely high content of organic material (about 2.5%) but composition of organic material has highly aromatic nature which makes it more ab-

sorbing and thus more optically dominant in the UV-NIR range. The laser-irradiated sample shows a flatter spectrum.

As we know space weathering is not only micrometeoritic bombardment but also irradiation by solar wind that can be simulated by laboratory ion bombardment. Such experiments were made on ices, pure silicates (darkening and reddening was observed), organics (flattening), but no experiments exist on CCs or silicate-organic mixtures. The effects could be comparable to those produced by laser irradiation but we do not know at what silicate/organic ratio "silicate-type" of space weathering would start to be dominant.

Experimental Data

In this contest we planned some laboratory experiments with the help of Rosario Brunetto and Giovanni Strazzulla (Catania Observatory) and Luigi Folco (Museo Nazionale dell'Antartide, Siena University).

From Folco et al. (2002) and from the catalogue available on-line

http://www.mna.unisi.it/english/Collections/collezioni_set.htm

we selected and requested to "Museo Nazionale dell'Antartide" a list of samples belonging to Carbocaneous Chondrites (CC), Enstatite Chondrites (EC), Achondrites (AC) and Iron meteorite types.

This material is now in Catania laboratory ready for first experiments of ion bombardment and first analysis. The whole procedure has been already done on Ordinary Chondrites samples by our groups and fully described in chapter 4, so we think that some preliminary results will be available in the next future.

Other data come from Near Earth and Main Belt asteroids from our SINEO database, added with SMASS and S3OS2 spectra.

5.3 Modified Gaussian Model

The Modified Gaussian Model (MGM), originally developed by Sunshine et al. (1990), is a method for decompose spectra into their physical components: continuum and absorption bands. The modelled absorption bands can then be used to infer compositions and amounts of co-existing phases. Derived absorption bands are determined directly from measured spectra and are not connected on pre-determined assumptions about the spectral constituents.

Modified Gaussian distributions are more related to the physical processes involved in electronic transition absorptions and so they are the first accurate mathematical description for the shape of isolated absorption bands (Sunshine et al. 1990; Sunshine & Pieters 1993). Under the MGM spectra are modelled as sums of absorption bands, each represented by a modified Gaussian distribution, superimposed onto baseline curves, or continua. Each absorption is described by three model parameters; a band centre, width and strength. Similarly, continua, which are typically modelled as straight lines in energy, are characterised by two additional model parameters, a slope and an offset.

The MGM accurately resolve individual absorption bands in laboratory spectra and has been used to quantify variations in absorption bands as a function of composition in the spectra of pyroxene mixtures (Sunshine & Pieters 1993; Sunshine et al. 1993) and olivines (Sunshine & Pieters 1998). In addition, the MGM has made it possible to compare spectra of HED meteorites with those of Vesta-like asteroids (Hiroi et al. 1995), and to quantify and help interpret minor absorptions in spectra of S-asteroids (Hiroi et al. 1996).

We are doing many progress in applying the Modified Gaussian Model (in the following MGM). First of all we started with some known pure silicates downloaded from RELAB catalogue (olivines and pyroxenes, see Fig. 5.3 and Tab. 5.1), then we tried with some silicate mixtures and with some known meteorites to check our ability in decompose spectra. Now we are trying to apply this method to our asteroid spectra, starting with not weathered S-type spectra showing better signal to noise ratio.

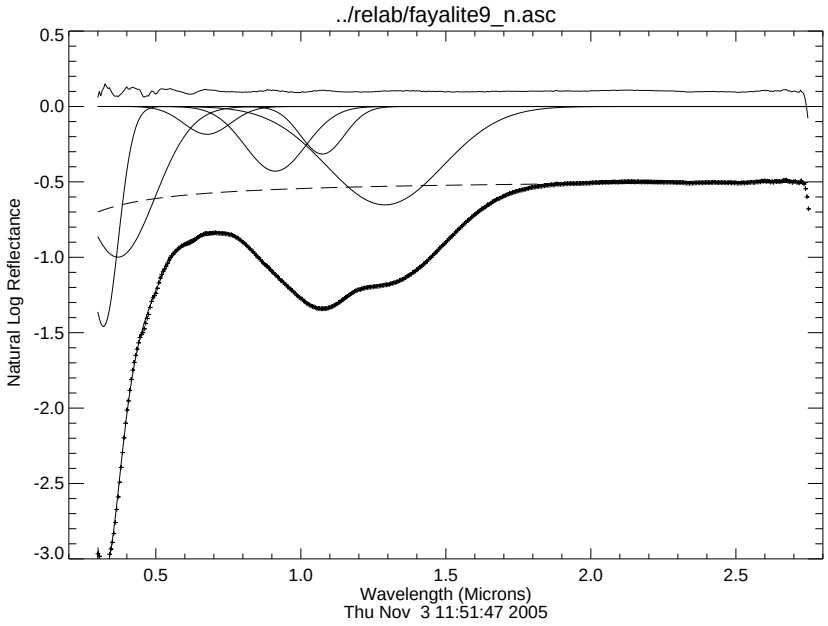

Figure 5.3: Application of MGM on a Fayalite sample. Wavelengths in abscissas are in microns and ordinates are expressed as logarithm of the reflectivity. The dashed line is the extracted continuum, while bands are reported as gaussian profiles. "+" in the lower line indicate the spectrum and upper line shows MGM fit residuals.

Band	**Centre**	**FWHM**	**Strength**
1	319	121	-1.46
2	369	300	-1.00
3	677	190	-0.18
4	913	246	-0.43
5	1075	178	-0.32
6	1290	471	-0.65

Table 5.1: Application of MGM on a Fayalite sample. Here position, width and strength of each band are reported. Band centre and FWHM are in microns, while strength are expressed as logarithm of the reflectivity (adimensional).

Conclusions

In this thesis I described the SINEO (*Spectroscopic Investigation of Near Earth Objects*) project and I discussed all results obtained till now, ongoing works and future analysis.

The project started in Padova in 2000. It consists in spectroscopic observations in the visible and near infrared spectral range (about 0.40-2.50 μm) of minor bodies that approach or intersect the Earth's orbit (NEOs).

In these five years time was allocated both at ESO-NTT (*New Technology Telescope*, La Silla, Chile) and at TNG (*Telescopio Nazionale Galileo*, Canary Islands) during eight observing runs. We have obtained until now a total of 117 asteroid spectra of which 63 have both visible and NIR range (Lazzarin et al. 2004; Lazzarin et al. 2005).

We performed a first taxonomic classification for most of them, principally by means of a best fit with mean taxonomic types defined by Bus (1999) on SMASSII spectra and through the *Principal Component Analysis* (PCA), obtaining all the classes defined by main belt asteroids. Both these methods refer to the visible part of the spectra. Where available near infrared data have revealed essential to discriminate between subclasses with similar visible features.

In particular we classified some peculiar objects. We observed four V-type and an R-type, rare in the Main Belt and even more rare in the NEO space, and we gave some preliminary hypothesis on their possible genetic link with Vesta and Dembowska, respectively (Marchi et al. 2004; Marchi et al. 2005). We also observed two bodies whose orbits suggest a cometary origin. Their spectra showed a primitive composition also consistent with that origin (Lazzarin et al. 2005). These are cases where spectroscopy can give important hints on dynamics.

To better understand asteroids mineralogy we compared them with meteorites. So we selected a set of more than 800 meteorite spectra from the RELAB catalogue and we performed a best fit for every SINEO object observed finding in many cases good agreements. However in some cases, in particular on reddish S-type asteroids,

we could not find any meteorite analogue. This can be in part explained considering the *space weathering* effect.

We therefore started a deep study of this effect principally by analysing the spectral slope of meteorites, NEOs and Main Belt Objects. We started a collaboration with Prof. Strazzulla and Dr. Brunetto (Observatory of Catania) who made laboratory experiments of ion bombardment on Ordinary Chondrites, able to simulate the effect of space weathering due to solar wind. Through the comparison of our S-type NEOs' spectra with laboratory ones we obtained important hints on space weathering time scale on different compounds (Marchi et al. 2005).

With Prof. Paolicchi (Pisa University) and Prof. Morbidelli (Nice Observatory) we also started to examine possible implication on asteroid history, mainly by comparing age deduced from space weathering with age deduced by dynamics (computed from asteroid collisional lifetime) and finding a unique general relationship valid both for NEOs and MBOs (Marchi et al. 2006).

All results obtained till now led us to deepen some other aspects of the topics studied. In particular we are now collaborating with Dr. Nesvorný (SwRI, Boulder, Colorado), with Dr. Moroz (DLR, Berlin), with Dr. Folco (Siena University) and again with Observatory of Catania.

With Dr. Nesvorný we are concentrating on the distribution of weathered and non weathered S-type NEOs and Mars Crossers as a function of their perihelion distance. First results showed that the fraction of Q-type (fresh surface) above the whole S-complex increases as perihelion become shorter: the NEO population looks younger, in average, as the number of intersection with inner planets orbit increases. This led us to study the efficiency of a possible resurfacing effect due to close and/or very close encounters of asteroids with one or more inner planet. A more quantitative assessment of the (tidal) effect of a close encounter to remove the space weathered surface layers of a typical km-sized asteroid is required.

Dr. Folco helped us to select from the "Museo Nazionale dell'Antartide" a list of meteorite samples comprising some Carbocaneous Chondrites (CC), Enstatite Chondrites (EC), Achondrites (AC) and Iron meteorite. Dr. Brunetto is now applying laboratory experiments of ion bombardment on these samples.

With Dr. Moroz, we are working on the analysis of possible optical effect of space weathering on primitive compounds, on C-complex and on X-complex Near Earth and Main Belt asteroids.

Our group is also acquiring abilities in analysing meteorite and asteroid spectra

through the Modified Gaussian Model (MGM). The method is in principle able to decompose spectra in continuum part plus absorption bands so that it can help us to better understand mineralogy, surface composition and space weathering degree of minor bodies observed.

References

Abell, P. A. & M. J. Gaffey (2000, March). Probable Geologic Composition, Thermal History, and Meteorite Affinities for Mainbelt Asteroid 349 Dembowska. In *Lunar and Planetary Institute Conference Abstracts*, pp. 1291–+.

Adams, J. B. (1974, November). Visible and near-infrared diffuse reflectance spectra of pyroxenes as applied to remote sensing of solid objects in the solar system. *J. Geophys. Res. 79*(18), 4829–4836.

Angeli, C. A. & D. Lazzaro (2002, August). Spectral properties of Mars-crossers and near-Earth objects. Results of the S^3OS^2 survey. *A&A 391*, 757–765.

Barbieri, C. (2003). *Lezioni di Astronomia* (Second ed.). Zanichelli.

Barucci, M. A., M. T. Capria, A. Coradini, & M. Fulchignoni (1987, November). Classification of asteroids using G-mode analysis. *Icarus 72*, 304–324.

Bell, J. F., D. R. Davis, W. K. Hartmann, & M. J. Gaffey (1989). Asteroids - The big picture. In *Asteroids II*, pp. 921–945.

Bell, J. F., B. R. Hawke, P. D. Owensby, & M. J. Gaffey (1985, June). The 52-Color Asteroid Survey: Results and Interpretation. *BAAS 17*, 729–+.

Bell, J. F., P. D. Owensby, B. R. Hawke, & M. J. Gaffey (1988). The 52-Color Asteroid Survey: Final Results and Interpretation. In *Lunar and Planetary Institute Conference Abstracts*, pp. 57–+.

Binzel, R. P., M. Birlan, S. J. Bus, A. W. Harris, A. S. Rivkin, & S. Fornasier (2004, March). Spectral observations for near-Earth objects including potential target 4660 Nereus : Results from Meudon remote observations at the NASA Infrared Telescope Facility (IRTF). *Planet. Space Sci. 52*, 291–296.

Binzel, R. P., S. J. Bus, T. H. Burbine, & J. M. Sunshine (1996, August). Spectral Properties of Near-Earth Asteroids: Evidence for Sources of Ordinary Chondrite Meteorites. *Science 273*, 946–948.

Binzel, R. P., M. J. Gaffey, P. C. Thomas, B. H. Zellner, A. D. Storrs, & E. N. Wells (1997, July). Geologic Mapping of Vesta from 1994 Hubble Space Telescope Images. *Icarus 128*, 95–103.

Binzel, R. P., A. W. Harris, S. J. Bus, & T. H. Burbine (2001, June). Spectral Properties of Near-Earth Objects: Palomar and IRTF Results for 48 Objects Including Spacecraft Targets (9969) Braille and (10302) 1989 ML. *Icarus 151*, 139–149.

Binzel, R. P., D. Lupishko, M. di Martino, R. J. Whiteley, & G. J. Hahn (2002). Physical Properties of Near-Earth Objects. In *Asteroids III*, pp. 255–271.

Binzel, R. P., A. S. Rivkin, J. S. Stuart, A. W. Harris, S. J. Bus, & T. H. Burbine (2004, August). Observed spectral properties of near-Earth objects: results for population distribution, source regions, and space weathering processes. *Icarus 170*, 259–294.

Binzel, R. P. & S. Xu (1993, April). Chips off of asteroid 4 Vesta - Evidence for the parent body of basaltic achondrite meteorites. *Science 260*, 186–191.

Bottke, W. F., D. D. Durda, D. Nesvorný, R. Jedicke, A. Morbidelli, D. Vokrouhlický, & H. Levison (2005, May). The fossilized size distribution of the main asteroid belt. *Icarus 175*, 111–140.

Bottke, W. F., A. Morbidelli, R. Jedicke, J.-M. Petit, H. F. Levison, P. Michel, & T. S. Metcalfe (2002, April). Debiased Orbital and Absolute Magnitude Distribution of the Near-Earth Objects. *Icarus 156*, 399–433.

Britt, D. T., J. F. Bell, H. Haack, & E. R. D. Scott (1992, July). The Reflectance Spectrum of Troilite and the T-Type Asteroids. *Meteoritics 27*, 207–+.

Brunetto, R. & G. Strazzulla (2005, December). Elastic collisions in ion irradiation experiments: A mechanism for space weathering of silicates. *Icarus 179*, 265–273.

Burbine, T. H. & J. F. Bell (1993). How diverse is the asteroid belt? In *Lunar and Planetary Institute Conference Abstracts*, pp. 223–224.

Burbine, T. H. & R. P. Binzel (1994). Asteroid Spectroscopy and Mineralogy. In *IAU Symp. 160: Asteroids, Comets, Meteors 1993*, pp. 255–+.

Burbine, T. H. & R. P. Binzel (2002, October). Small Main-Belt Asteroid Spectroscopic Survey in the Near-Infrared. *Icarus 159*, 468–499.

Burbine, T. H., R. P. Binzel, & S. J. Bus (1997, March). SMASS and SMASSIR - Visible and near-infrared spectral studies of main-belt and near-Earth asteroids. In *Lunar and Planetary Institute Conference Abstracts*, pp. 179–+.

Burbine, T. H., R. P. Binzel, S. J. Bus, P. C. Buchanan, J. L. Hinrichs, A. M. T. Hiroi, & J. M. Sunshine (2000, March). Forging Asteroid-Meteorite Relationships Through Reflectance Spectroscopy. In *Lunar and Planetary Institute Conference Abstracts*, pp. 1844–+.

Burbine, T. H., P. C. Buchanan, R. P. Binzel, S. J. Bus, T. Hiroi, J. L. Hinrichs, A. Meibom, & T. J. McCoy (2001, June). Vesta, Vestoids, and the howardite, eucrite, diogenite group: Relationships and the origin of spectral differences. *Meteoritics and Planetary Science 36*, 761–781.

Burbine, T. H., T. J. McCoy, A. Meibom, B. Gladman, & K. Keil (2002a). Meteoritic Parent Bodies: Their Number and Identification. In *Asteroids III*, pp. 653–667. University of Arizona press.

Bus, S. J. (1999). *Compositional structure in the asteroid belt: Results of a spectroscopic survey*. Ph. D. thesis, Massachusetts Institute of Technology.

Bus, S. J. & R. P. Binzel (2002a, July). Phase II of the Small Main-Belt Asteroid Spectroscopic SurveyA Feature-Based Taxonomy. *Icarus 158*, 146–177.

Bus, S. J. & R. P. Binzel (2002b, July). Phase II of the Small Main-Belt Asteroid Spectroscopic SurveyThe Observations. *Icarus 158*, 106–145.

Carvano, J. M., D. Lazzaro, T. Mothé-Diniz, C. A. Angeli, & M. Florczak (2001, January). Spectroscopic Survey of the Hungaria and Phocaea Dynamical Groups. *Icarus 149*, 173–189.

Cassidy, W. & B. Hapke (1975, July). Effects of darkening processes on surfaces of airless bodies. *Icarus 25*, 371–383.

Cellino, A., V. Zappala, M. di Martino, P. Farinella, & P. Paolicchi (1987, June). Flattening, pole, and albedo features of 4 Vesta from photometric data. *Icarus 70*, 546–565.

Chapman, C. R. (2004, May). Space Weathering of Asteroid Surfaces. *Annual Review of Earth and Planetary Sciences 32*, 539–567.

Chesley, S. R., S. J. Ostro, D. Vokrouhlický, D. Čapek, J. D. Giorgini, M. C. Nolan, J.-L. Margot, A. A. Hine, L. A. M. Benner, & A. B. Chamberlin (2003, December). Direct Detection of the Yarkovsky Effect by Radar Ranging to Asteroid 6489 Golevka. *Science 302*, 1739–1742.

Cloutis, E. A., M. J. Gaffey, T. L. Jackowski, & K. L. Reed (1986). Calibrations of phase abundance, composition, and particle size distribution for olivine-orthopyroxene mixtures from reflectance spectra. *J. Geophys. Res. 91*(10), 641–653.

Cochran, A. L. & E. S. Barker (1984, August). Minor planet 1983TB - A dead comet? *Icarus 59*, 296–300.

Cochran, A. L. & F. Vilas (1998, August). The Changing Spectrum of Vesta: Rotationally Resolved Spectroscopy of Pyroxene on the Surface. *Icarus 134*, 207–212.

Cochran, A. L., F. Vilas, K. S. Jarvis, & M. S. Kelley (2004, February). Investigating the Vesta-vestoid-HED connection. *Icarus 167*, 360–368.

Colina, L. & R. Bohlin (1997, March). Absolute Flux Distributions of Solar Analogs from the UV to the Near-IR. *AJ 113*, 1138–1144.

Conel, J. E. & D. B. Nash (1970). Spectral reflectance and albedo of Apollo 11 lunar samples: Effects of irradiation and vitrification and comparison with telescopic observations. *Geochimica et Cosmochimica Acta Supplement 1*, 2013–+.

Coradini, A., M. Fulchignoni, O. Fanucci, & A. I. Gavrishin (1977). A Fortran V program for a new classification technique; the G-mode central method. *Comput.-Geosci. 3*, 85–105.

de León, J., R. Duffard, J. Licandro, & D. Lazzaro (2004, July). Mineralogical characterization of A-type asteroid (1951) Lick. *A&A 422*, L59–L62.

De Sanctis, M. C., M. Lazzarin, M. A. Barucci, M. T. Capria, & A. Coradini (2000, February). Comet P/Gehrels 3: spectroscopic observations and nucleus models. *A&A 354*, 1086–1090.

Dukes, C. A., R. A. Baragiola, & L. A. McFadden (1999, January). Surface modification of olivine by H^+ and He^+ bombardment. *J. Geophys. Res. 104*, 1865–1872.

Farinella, P. & D. Vokrouhlicky (1999, March). Semimajor axis mobility of asteroidal fragments. *Science 283*, 1507–1510.

Feierberg, M. A., L. A. Lebofsky, & D. J. Tholen (1985, August). The nature of C-class asteroids from 3-micron spectrophotometry. *Icarus 63*, 183–191.

Florczak, M., M. A. Barucci, A. Doressoundiram, D. Lazzaro, C. A. Angeli, & E. Dotto (1998, June). A Visible Spectroscopic Survey of the Flora Clan. *Icarus 133*, 233–246.

Florczak, M., D. Lazzaro, & R. Duffard (2002, September). Discovering New V-Type Asteroids in the Vicinity of 4 Vesta. *Icarus 159*, 178–182.

Florczak, M., D. Lazzaro, T. Mothé-Diniz, C. A. Angeli, & A. S. Betzler (1999, February). A spectroscopic study of the THEMIS family. *A&AS 134*, 463–471.

Folco, L., F. Peri, & F. Pezzotta (2002). The meteorite collection of the Civico Planetario and the Museo Civico di Storia Naurale in Milan, Italy. *Meteoritics & Planetary Science, vol. 37, Supplement, p.95-103 37*, 95–103.

Fornasier, S. & M. Lazzarin (2001, July). E-Type Asteroids: Spectroscopic Investigation on the 0.5μm Absorption Band. *Icarus 152*, 127–133.

Gaffey, M. J. (1997, May). Surface Lithologic Heterogeneity of Asteroid 4 Vesta. *Icarus 127*, 130–157.

Gaffey, M. J. (2001, March). Asteroids: Does Space Weathering Matter? In *Lunar and Planetary Institute Conference Abstracts*, pp. 1587–+.

Gaffey, M. J., J. F. Bell, & D. P. Cruikshank (1989). Reflectance spectroscopy and asteroid surface mineralogy. In *Asteroids II*, pp. 98–127.

Gaffey, M. J., T. H. Burbine, & R. P. Binzel (1993, June). Asteroid spectroscopy - Progress and perspectives. *Meteoritics 28*, 161–187.

Gaffey, M. J., T. H. Burbine, J. L. Piatek, K. L. Reed, D. A. Chaky, J. F. Bell, & R. H. Brown (1993, December). Mineralogical variations within the S-type asteroid class. *Icarus 106*, 573–+.

Gladman, B. J., F. Migliorini, A. Morbidelli, V. Zappala, P. Michel, A. Cellino, C. Froeschle, H. F. Levison, M. Bailey, & M. Duncan (1997). Dynamical lifetimes of objects injected into asteroid belt resonances. *Science 277*, 197–201.

Hanesiak, J. M., D. G. Barber, R. A. De Abreu, & J. J. Yackel (2001). Local and regional albedo observations of arctic first-year sea ice during melt ponding. *J. Geophys. Res. 106*, 1005–1016.

Hapke, B. (2001, May). Space weathering from Mercury to the asteroid belt. *J. Geophys. Res. 106*(15), 10039–10074.

Hapke, B., J. Wagner, A. J. Cohen, & W. Partlow (1978). Reflectance Measurements of Lunar Materials in the Vacuum Ultraviolet. In *Lunar and Planetary Institute Conference Abstracts*, pp. 456–458.

Hardersen, P. S., M. J. Gaffey, & P. A. Abell (2004, January). Mineralogy of Asteroid 1459 Magnya and implications for its origin. *Icarus 167*, 170–177.

Harris, N. W. & M. E. Bailey (1998, July). Dynamical evolution of cometary asteroids. *MNRAS 297*, 1227–1236.

Hiroi, T., J. F. Bell, H. Takeda, & C. M. Pieters (1993, March). Modeling of S-type asteroid spectra using primitive achondrites and iron meteorites. *Icarus 102*, 107–116.

Hiroi, T., R. P. Binzel, J. M. Sunshine, C. M. Pieters, & H. Takeda (1995, June). Grain sizes and mineral compositions of surface regoliths of Vesta-like asteroids. *Icarus 115*, 374–386.

Hiroi, T., A. Kanno, R. Nakamura, M. Abe, M. Ishiguro, S. Hasegawa, S. Miyasaka, T. Sekiguchi, H. Terada, & G. Igarashi (2003, March). The Tagish Lake Meteorite as a Possible Sample from a T or D Type Asteroid. In *Lunar and Planetary Institute Conference Abstracts*, pp. 1425–+.

Hiroi, T. & S. Sasaki (2001, December). Importance of space weathering simulation products in compositional modeling of asteroids: 349 Dembowska and 446 Aeternitas as examples. *Meteoritics and Planetary Science 36*, 1587–1596.

Hiroi, T., F. Vilas, & J. M. Sunshine (1996, January). Discovery and Analysis of Minor Absorption Bands in S-Asteroid Visible Reflectance Spectra. *Icarus 119*, 202–208.

Hiroi, T., M. E. Zolensky, & C. M. Pieters (2001, September). The Tagish Lake Meteorite: A Possible Sample from a D-Type Asteroid. *Science 293*, 2234–2236.

Jedicke, R., D. Nesvorný, R. Whiteley, Ž. Ivezić, & M. Jurić (2004, May). An age-colour relationship for main-belt S-complex asteroids. *Nature 429*, 275–277.

Kelley, M. S., F. Vilas, M. J. Gaffey, & P. A. Abell (2003, September). Quantified mineralogical evidence for a common origin of 1929 Kollaa with 4 Vesta and the HED meteorites. *Icarus 165*, 215–218.

La Spina, A., P. Paolicchi, A. Kryszczyńska, & P. Pravec (2004, March). Retrograde spins of near-Earth asteroids from the Yarkovsky effect. *Nature 428*, 400–401.

Landolt, A. U. (1973, November). UBV photoelectric sequences in the celestial equatorial Selected Areas 92-115. *AJ 78*, 959–+.

Lazzarin, M., M. A. Barucci, & A. Doressoundiram (1996, July). Visible Spectroscopy of Possible Cometary Candidates. *Icarus 122*, 122–127.

Lazzarin, M., M. di Martino, M. A. Barucci, A. Doressoundiram, & M. Florczak (1997, November). Compositional properties of Near-Earth Asteroids: spectroscopic comparison with Ordinary Chondrite Meteorites. *A&A 327*, 388–391.

Lazzarin, M., S. Marchi, M. A. Barucci, M. di Martino, & C. Barbieri (2004, June). Visible and near-infrared spectroscopic investigation of near-Earth objects at ESO: first results. *Icarus 169*, 373–384.

Lazzarin, M., S. Marchi, S. Magrin, & J. Licandro (2005, June). Spectroscopic investigation of near-Earth objects at Telescopio Nazionale Galileo. *MNRAS 359*, 1575–1582.

Lazzaro, D., T. Michtchenko, J. M. Carvano, R. P. Binzel, S. J. Bus, T. H. Burbine, T. Mothé-Diniz, M. Florczak, C. A. Angeli, & A. W. Harris (2000, June). Discovery of a Basaltic Asteroid in the Outer Main Belt. *Science 288*, 2033–2035.

Lazzaro, D., T. Mothé-Diniz, J. M. Carvano, C. A. Angeli, A. S. Betzler, M. Florczak, A. Cellino, M. Di Martino, A. Doressoundiram, M. A. Barucci, E. Dotto, & P. Bendjoya (1999, December). The Eunomia Family: A Visible Spectroscopic Survey. *Icarus 142*, 445–453.

Licandro, J., H. Campins, C. Hergenrother, & L. M. Lara (2003, February). Near-infrared spectroscopy of the nucleus of comet 124P/Mrkos. *A&A 398*, L45–L48.

Licandro, J., F. Ghinassi, & L. Testi (2002, June). Infrared spectroscopy of the largest known trans-Neptunian object 2001 KX_{75}. *A&A 388*, L9–L12.

Licandro, J., J. C. Guerra, H. Campins, M. Di Martino, L. M. Lara, R. Gil-Hutton, & G. P. Tozzi (2002, March). The Surface of Cometary Nulcei Related Minor Icy Bodies. *Earth Moon and Planets 90*, 495–496.

Marchi, S., C. Barbieri, A. Dell'Oro, & P. Paolicchi (2002, January). Hyperion-Iapetus: Collisional relationships. *A&A 381*, 1059–1065.

Marchi, S., R. Brunetto, S. Magrin, M. Lazzarin, & D. Gandolfi (2005, December). Space weathering of near-Earth and main belt silicate-rich asteroids: observations and ion irradiation experiments. *A&A 443*, 769–775.

Marchi, S., A. Dell'Oro, P. Paolicchi, & C. Barbieri (2001, August). Collisional processes and transfer of mass among the planetary satellites. *A&A 374*, 1135–1149.

Marchi, S., M. Lazzarin, & S. Magrin (2004, June). An R-type asteroid within near-Earth objects? *A&A 420*, L5–L8.

Marchi, S., M. Lazzarin, S. Magrin, & C. Barbieri (2003, September). Visible spectroscopy of the two largest known trans-Neptunian objects: Ixion and Quaoar. *A&A 408*, L17–L19.

Marchi, S., M. Lazzarin, P. Paolicchi, & S. Magrin (2005, May). New V-type asteroids in near-Earth space. *Icarus 175*, 170–174.

Marchi, S., P. Paolicchi, M. Lazzarin, & S. Magrin (2006). A general spectral slope–exposure elation for S–type Main Belt and near–Earth asteroids. *AJ*in press.

McSween, H. Y., J. (1999). *Meteorites and Their Parent Planets* (Second ed.). Cambridge University Press.

Michel, P., W. Benz, & D. C. Richardson (2003, February). Disruption of fragmented parent bodies as the origin of asteroid families. *Nature 421*, 608–611.

Michel, P., F. Migliorini, A. Morbidelli, & V. Zappalà (2000, June). The population of Mars-Crossers: Classification and dynamical evolution. *Icarus 145*, 332–347.

Michtchenko, T. A., D. Lazzaro, S. Ferraz-Mello, & F. Roig (2002, August). Origin of the Basaltic Asteroid 1459 Magnya: A Dynamical and Mineralogical Study of the Outer Main Belt. *Icarus 158*, 343–359.

Migliorini, F., P. Michel, A. Morbidelli, D. Nesvorny, & V. Zappala (1998, September). Origin of Multikilometer Earth- and Mars-Crossing Asteroids: A Quantitative Simulation. *Science 281*, 2022–+.

Migliorini, F., A. Morbidelli, V. Zappala, B. J. Gladman, M. E. Bailey, & A. Cellino (1997, November). Vesta fragments from v6 and 3:1 resonances: Implications for V-type NEAs and HED meteorites. *Meteoritics and Planetary Science 32*, 903–916.

Milani, A., M. Carpino, G. Hahn, & A. M. Nobili (1989, April). Dynamics of planet-crossing asteroids - Classes of orbital behavior. *Icarus 78*, 212–269.

Moons, M. & A. Morbidelli (1995, April). Secular resonances inside mean-motion commensurabilities: the 4/1, 3/1, 5/2 and 7/3 cases. *Icarus 114*, 33–.

Morbidelli, A., W. F. Bottke, C. Froeschlé, & P. Michel (2002). Origin and Evolution of Near-Earth Objects. In *Asteroid III*, pp. 409–422. University of Arizona press.

Morbidelli, A. & B. Gladman (1998, September). Orbital and temporal distributions of meteorites originating in the asteroid belt. *Meteoritics and Planetary Science 33*, 999–1016.

Morbidelli, A. & D. Nesvorny (1999, June). Numerous Weak Resonances Drive Asteroids toward Terrestrial Planets Orbits. *Icarus 139*, 295–308.

Moroz, L. V., A. V. Fisenko, L. F. Semjonova, C. M. Pieters, & N. N. Korotaeva (1996, August). Optical Effects of Regolith Processes on S-Asteroids as Simulated by Laser Shots on Ordinary Chondrite and Other Mafic Materials. *Icarus 122*, 366–382.

Moroz, L. V., T. Hiroi, T. V. Shingareva, A. T. Basilevsky, A. V. Fisenko, L. F. Semjonova, & C. M. Pieters (2004, March). Reflectance Spectra of CM2 Chondrite Mighei Irradiated with Pulsed Laser and Implications for Low-Albedo Asteroids and Martian Moons. In *Lunar and Planetary Institute Conference Abstracts*, pp. 1279–+.

Nesvorný, D., R. Jedicke, R. J. Whiteley, & Ž. Ivezić (2005a, September). Corrigendum to "Evidence for asteroid space weathering from the Sloan Digital Sky Survey" [Icarus 173 (2005) 132 152]. *Icarus 177*, 291–291.

Nesvorný, D., R. Jedicke, R. J. Whiteley, & Ž. Ivezić (2005b, January). Evidence for asteroid space weathering from the Sloan Digital Sky Survey. *Icarus 173*, 132–152.

Nikolaeva, O., K. Tobelko, A. Korochantsev, & M. Kreslavsky (1991, June). Reference materials for organic matter of meteorites and asteroids. *Annales Geophysicae 9*, 383–+.

Penco, U., A. dell'Oro, P. Paolicchi, A. Campo Bagatin, A. La Spina, & A. Cellino (2004, October). Yarkovsky depletion and asteroid collisional evolution. *Planet. Space Sci. 52*, 1087–1091.

Pieters, C. M., L. A. Taylor, S. K. Noble, L. P. Keller, B. Hapke, R. V. Morris, C. C. Allen, D. S. McKay, & S. Wentworth (2000, September). Space weathering on airless bodies: Resolving a mystery with lunar samples. *Meteoritics and Planetary Science 35*, 1101–1107.

Pravec, P., P. Kusnirak, & B. Warner (2001, November). 2001 SL_9. *IAU Circ. 7742*, 3–+.

Pravec, P., M. Wolf, & L. Sarounova (1998, May). Occultation/Eclipse Events in Binary Asteroid 1991 VH. *Icarus 133*, 79–88.

Rabinowitz, D. L. (1997, December). Are Main-Belt Asteroids a Sufficient Source for the Earth-Approaching Asteroids? *Icarus 130*, 287–295.

Rivkin, A. S., R. P. Binzel, J. Sunshine, S. J. Bus, T. H. Burbine, & A. Saxena (2004, December). Infrared spectroscopic observations of 69230 Hermes (1937 UB): possible unweathered endmember among ordinary chondrite analogs. *Icarus 172*, 408–414.

Sasaki, S., K. Nakamura, Y. Hamabe, E. Kurahashi, & T. Hiroi (2001, March). Production of iron nanoparticles by laser irradiation in a simulation of lunar-like space weathering. *Nature 410*, 555–557.

Spitale, J. & R. Greenberg (2001, January). Numerical Evaluation of the General Yarkovsky Effect: Effects on Semimajor Axis. *Icarus 149*, 222–234.

Strazzulla, G., E. Dotto, R. Binzel, R. Brunetto, M. A. Barucci, A. Blanco, & V. Orofino (2005, March). Spectral alteration of the Meteorite Epinal (H5) induced by heavy ion irradiation: a simulation of space weathering effects on near-Earth asteroids. *Icarus 174*, 31–35.

Stuart, J. S. & R. P. Binzel (2004, August). Bias-corrected population, size distribution, and impact hazard for the near-Earth objects. *Icarus 170*, 295–311.

Sunshine, J. M., L.-A. McFadden, & C. M. Pieters (1993, September). Reflectance Spectra of the Elephant Moraine A79001 Meteorite: Implications for Remote Sensing of Planetary Bodies. *Icarus 105*, 79–91.

Sunshine, J. M. & C. M. Pieters (1993, May). Estimating modal abundances from the spectra of natural and laboratory pyroxene mixtures using the modified Gaussian model. *J. Geophys. Res. 98*, 9075–9087.

Sunshine, J. M. & C. M. Pieters (1998, June). Determining the composition of olivine from reflectance spectroscopy. *J. Geophys. Res. 103*, 13675–13688.

Sunshine, J. M., C. M. Pieters, & S. F. Pratt (1990, May). Deconvolution of mineral absorption bands - An improved approach. *J. Geophys. Res. 95*, 6955–6966.

Tedesco, E. F., J. G. Williams, D. L. Matson, G. J. Weeder, J. C. Gradie, & L. A. Lebofsky (1989, February). A three-parameter asteroid taxonomy. *AJ 97*, 580–606.

Tholen, D. J. (1984). *Asteroid taxonomy from cluster analysis of Photometry*. Ph. D. thesis, Arizona University, Tucson.

Tholen, D. J. (1989). Asteroid taxonomic classifications. In *Asteroids II*, pp. 1139–1150.

Tholen, D. J. & M. A. Barucci (1989). Asteroid taxonomy. In *Asteroids II*, pp. 298–315.

Thomas, P. C., R. P. Binzel, M. J. Gaffey, B. H. Zellner, A. D. Storrs, & E. Wells (1997, July). Vesta: Spin Pole, Size, and Shape from HST Images. *Icarus 128*, 88–94.

Tsiganis, K., H. Varvoglis, & A. Morbidelli (2003, November). Short-lived asteroids in the 7/3 Kirkwood gap and their relationship to the Koronis and Eos families. *Icarus 166*, 131–140.

Ueda, Y., T. Hiroi, C. M. Pieters, & M. Miyamoto (2002a, March). Changes of Band I Center and Band II/Band I Area Ratio in Reflectance Spectra of Olivine-Pyroxene Mixtures Due to the Space Weathering and Grain Size Effects. In *Lunar and Planetary Institute Conference Abstracts*, pp. 2023–+.

Ueda, Y., T. Hiroi, C. M. Pieters, & M. Miyamoto (2002b, March). Expanding the Modified Gaussian Model to Include the Space Weathering Effects: Estimation of the Weathering Degrees of Pulse-Laser Treated Olivine Samples. In *Lunar and Planetary Institute Conference Abstracts*, pp. 1950–+.

Vilas, F. & B. A. Smith (1985, December). Reflectance spectrophotometry (about 0.5-1.0 micron) of outer-belt asteroids - Implications for primitive, organic solar system material. *Icarus 64*, 503–516.

Weissman, P. R., W. F. Bottke, & H. F. Levison (2002). Evolution of Comets into Asteroids. In *Asteroids III*, pp. 669–686. University of Arizona press.

Wetherill, G. W. (1985, December). Quantitative Calculation of Meteorite Flux from Various Regions of the Inner Asteroid Belt. *Meteoritics 20*, 783–+.

Wetherill, G. W. (1987, September). Dynamical relations between asteroids, meteorites and Apollo-Amor objects. *Royal Society of London Philosophical Transactions Series A 323*, 323–337.

Wetherill, G. W. (1988, October). Where do the Apollo objects come from? *Icarus 76*, 1–18.

Williams, J. G. & J. Faulkner (1981, June). The positions of secular resonance surfaces. *Icarus 46*, 390–399.

Xu, S. (1994). *CCD Photometry and Spectroscopy of Small Main - Asteroids*. Ph. D. thesis, Massachusetts Institute of Technology.

Xu, S., R. P. Binzel, T. H. Burbine, & S. J. Bus (1995, May). Small main-belt asteroid spectroscopic survey: Initial results. *Icarus 115*, 1–35.

Yamada, M., S. Sasaki, A. Fujiwara, T. Hiroi, S. Hasegawa, H. Nagahara, H. Ohashi, H. Ohtake, & H. Yano (1999, March). Simulation of Space Weathering by Nanosecond Pulse Laser Heating and Proton Implantation: Difference of Olivine and Pyroxene Samples. In *Lunar and Planetary Institute Conference Abstracts*, pp. 1566–+.

Yoshikawa, M. (1989, April). A survey of the motions of asteroids in the commensurabilities with Jupiter. *A&A 213*, 436–458.

Zappala, V., A. Cellino, P. Farinella, & Z. Knezevic (1990, December). Asteroid families. I - Identification by hierarchical clustering and reliability assessment. *AJ 100*, 2030–2046.

Zappala, V., I. van Houten-Groeneveld, & C. J. van Houten (1979, February). Rotation period and phase curve of the asteroids 349 Dembowska and 354 Eleonora. *A&AS 35*, 213–221.

Zellner, B., M. Leaka, J. G. Williams, & D. Morrison (1977, December). The E asteroids and the origin of the enstatite achondrites. *Geochim. Cosmochim. Acta 41*, 1759–1767.

Zellner, B., D. J. Tholen, & E. F. Tedesco (1985, March). The eight-color asteroid survey - Results for 589 minor planets. *Icarus 61*, 355–416.

Ziegler, J. F., J. P. Biersack, & U. Littmark (1985). *The Stopping and Range of Ions in Solids*. Pergamon Press.